

Automated Isolation of Circulating Tumor Cells and their Molecular Biological Analysis

D i s s e r t a t i o n

Janis Hendrik Stiefel

Dean: Prof. Dr. Eckhard Thines

Primary Reviewer:

Secondary Reviewer:

Date of the Oral Examination: January 30, 2023

Johannes Gutenberg University Mainz

D77

Primary Supervisor:

Secondary Supervisor:



JOHANNES GUTENBERG
UNIVERSITÄT MAINZ

Automated Isolation of Circulating Tumor Cells and their Molecular Biological Analysis

Cumulative Dissertation

Submitted in Fulfillment to the Requirements for the Degree of
Doctor of Natural Sciences (Dr. rer. nat.)

Faculty of Biology at the Johannes Gutenberg University Mainz

Janis Hendrik Stiefel

*March 12, 1994 in Bruchsal

Mainz, September 2022

Conducted at the
Fraunhofer Institute for Microengineering and Microsystems IMM





In memory of my sister Kassandra.

To my parents
and to my sister Jennifer
and her family.

Abstract

Cancer metastases descend from proliferative circulating tumor cells (CTCs) which disseminate from the primary tumor via blood and lymph vessels. In the last two decades, CTC analysis from blood samples was established for diagnostic and prognostic purposes and therapy monitoring in the course of liquid biopsy. Nonetheless the small number of CTCs compared to billions of blood cells in a patient sample requires sensitive methods to obtain reproducible tumor cell recovery rates. Against this background, the Fraunhofer Institute for Microengineering and Microsystems has recognized the unmet need of standardized CTC isolation and developed automated microfluidic platforms to enrich, detect and isolate single tumor cells from 7.5 mL whole blood. The aim of this thesis was to realize single cell isolation by means of automated immunomagnetic bead enrichment and antibody-based fluorescence detection in a chip-based microfluidic system and the molecular biological characterization of these cells to assay tumor features from liquid biopsy. Therefore, this work compares manual and automated immunomagnetic enrichment in terms of cell recovery in dependency of cell line and input number, bead characteristics, biofunctionalization protocol and blood cell contamination focusing on head and neck squamous cell carcinoma (HNSCC) and metastatic breast cancer. In a prototype enrichment device (IsoMAG), we established an isolation protocol with EpCAM-targeting 1 μm magnetic beads for automated enrichment tested on different epithelial cancer cell lines. White blood cell contamination, usually hampering further downstream analysis of enriched tumor cells, was measured by FACS and minimized to about 1200 cells starting from 7.5 mL blood. In the microfluidic benchtop platform CTCelect, we characterized each process step with two different carcinoma cell lines (MCF-7, SCL-1) demonstrating up to 87 % enrichment, 73 % optical detection and dispensing efficiency. 40 to 56.7 % of cells were recovered after complete isolation from 7.5 mL untreated whole blood. We highlighted the bottlenecks of microfluidic cell isolation in dependency of bead-binding on the cell surface and implemented a gating function for the cytometer subunit to selectively dispense cells instead of autofluorescent objects. In doing so, CTCelect enabled automated dispensing of single circulating tumor cells from HNSCC patient samples, qPCR-based confirmation of tumor-related biomarkers with a simplified one-step protocol and immunostaining using a panel of tumor markers. Additionally, the platform was compared to commercial CTC isolation technologies to highlight advantages and limitations of CTCelect. In conclusion, the achieved findings substantially contribute to the establishment of the platform technology in the applied research field of liquid biopsy.

Zusammenfassung

Krebsmetastasen gehen von proliferativen zirkulierenden Tumorzellen (CTCs) aus, die sich vom Primärtumor über Blut- und Lymphgefäße ausbreiten. In den letzten zwei Jahrzehnten wurde die CTC-Analyse aus Blutproben für diagnostische und prognostische Zwecke sowie zur Therapieüberwachung im Rahmen der Flüssigbiopsie etabliert. Die geringe Anzahl von CTCs im Vergleich zu Milliarden von Blutzellen in einer Patientenprobe erfordert jedoch sensible Methoden, um reproduzierbare Tumorzellgewinnungsraten zu erzielen. Vor diesem Hintergrund hat das Fraunhofer-Institut für Mikrotechnik und Mikrosysteme den dringenden Bedarf an standardisierter CTC-Isolierung erkannt und automatisierte mikrofluidische Plattformen zur Anreicherung, Detektion und Isolierung einzelner Tumorzellen aus 7,5 mL Vollblut entwickelt. Ziel der hier vorgestellten Dissertation war die Realisierung einer Einzelzellisolierung durch eine automatisierte Anreicherung basierend auf immunmagnetischen Partikeln und eine antikörperbasierte Fluoreszenzdetektion in einem Chip-basierten mikrofluidischen System und eine darauffolgende molekularbiologische Charakterisierung dieser Zellen um Tumormerkmale aus Flüssigbiopsien nachzuweisen. Die Arbeit vergleicht daher die manuelle und die automatisierte immunomagnetische Anreicherung hinsichtlich der Zellausbeute in Abhängigkeit von Zelllinie und Inputzahl, Partikeleigenschaften, Biofunktionalisierungsprotokoll und Blutzellkontamination mit Fokus auf Kopf-Hals-Tumoren (HNSCC) und metastasiertem Brustkrebs. In einem Prototyp-Anreicherungsgerät (IsoMAG) wurde ein Isolierungsprotokoll mit effektiven EpCAM-funktionalisierten 1 µm Magnetpartikeln für die automatisierte Anreicherung etabliert, das an verschiedenen epithelialen Krebszelllinien getestet wurde. Die Kontamination mit weißen Blutkörperchen, die eine weitere Analyse der angereicherten Tumorzellen behindert, wurde mittels Durchflusszytometrie gemessen und auf etwa 1200 Zellen aus 7,5 mL Blut minimiert. In der mikrofluidischen Benchtop-Plattform CTCelect wurde jeder Prozessschritt mit zwei verschiedenen Karzinomzelllinien (MCF-7, SCL-1) charakterisiert und dabei eine Anreicherung von bis zu 87 % und eine optische Detektions- und Dispensiereffizienz von 73 % nachgewiesen. 40 bis 56,7 % der Zellen wurden nach vollständiger Isolierung aus 7,5 mL unbehandeltem Vollblut zurückgewonnen. Ferner wurden die Herausforderungen der mikrofluidischen Zellisolierung in Abhängigkeit von der Bindung der Magnetpartikel an die Zelloberfläche aufgezeigt und eine Gating-Funktion für die Zytometer-Untereinheit implementiert, um selektiv Zellen anstelle von autofluoreszierenden Objekten zu dispensieren. Auf diese Weise ermöglichte CTCelect die automatisierte Dispensierung

einzelner zirkulierender Tumorzellen aus HNSCC-Patientenproben, die qPCR-basierte Bestätigung tumor-assoziiertes Biomarker mit einem vereinfachten Ein-Schritt-Protokoll und die bildgebende Antikörperfärbung an einem Panel von Tumormarkern. Darüber hinaus wurde die Plattform mit kommerziellen CTC-Isolierungstechnologien verglichen, um die Vor- und Nachteile von CTCelect aufzuzeigen. Zusammengefasst tragen die erzielten Ergebnisse wesentlich zur Etablierung der Plattformtechnologie in der angewandten Forschung im Bereich der Flüssigbiopsie bei.

Table of Contents

Abstract	I
Zusammenfassung.....	II
Table of Contents	IV
1 Introduction	1
1.1 Circulating Tumor Cells and Metastasis.....	2
1.1.1 Head and Neck Cancer	3
1.1.2 Metastatic Breast Cancer	5
1.2 Tumor Markers in Liquid Biopsy	6
1.3 Methods to Enrich Rare Cells from Body Fluids.....	8
1.3.1 Physical Methods.....	8
1.3.2 Biochemical Methods	9
1.4 Confirmation of Isolated CTCs bona fide	10
1.4.1 Transcriptomic Analysis	10
1.4.2 Immunocytological Approaches.....	11
1.5 Automated Microfluidics for Diagnostic Approaches	11
1.6 Challenges in Automated CTC Isolation	13
1.7 Research Question and Goals of this Project	14
2 Publications	19
2.1 Paper 1.....	21
2.2 Paper 2.....	39
2.3 Paper 3.....	59
3 Discussion and Conclusions.....	77
3.1 Summary.....	77
3.2 Advantages of CTC Analysis	79
3.3 Innovation Management	82
3.4 Future Perspectives.....	83
4 Appendix.....	87
A. Acknowledgements	87
B. Publication notice	88
C. Abbreviations.....	89
D. Supplements and References of the Publications.....	91

Table of Contents

5	References.....	111
6	Curriculum Vitae.....	121

1 Introduction

The viability of multicellular organisms is based on a homeostatic balance between cell growth, proliferation and cell death. Due to frequent copying, hereditary factors and environmental influences, the genome of each cell has a high mutational risk. In most cases, a number of mutations in humans can be neutralized with the aid of programmed cell death (apoptosis) or DNA repair mechanisms. Reaching a critical mutational burden in one cell or in a crucial genomic region, errors in cell fate determination and the re-gain of stem cell properties lead to tumor cell conversion and later to tumor growth (from Latin *tumere* “to be swollen”).

Cancer cells are equipped with two dangerous heritable features: On one hand, they grow and proliferate uncontrollably which finally leads to the actual tumor formation. Tumors are classified “benign” or non-invasive if they are not surpassing the tissue barriers. On the other hand, malignant cancers will invade peripheral tissue or vessels to colonize other body parts [1]. This colonization process is called metastasis. In 1889, the English surgeon Stephen Paget published the seminal “seed and soil” theory [2], where he described for the first time that certain tumor cells (the “seed”) favor certain organs as their “soil”. He concluded that metastases formed only if seed and soil were compatible [3]. The metastatic spread of cancer cells is the most important pathologic aspect as metastasis is responsible for 90 % of cancer-related deaths [4]. Hence the overall survival strongly depends on an early diagnosis. Due to high mortality rates, diagnostic and therapeutic research on metastatic cancer diseases has been a focus topic in medicine for decades. Today, it is accepted in the scientific community that the detachment of circulating tumor cells (CTCs) from the primary tumor and their release in the vascular system play a critical role for the organismic spread of cancer. Methods to isolate CTCs are researched since the middle of the last century [5]. The development of new molecular techniques such as sequencing give additional momentum to the field of liquid biopsy, in particular the analysis of free circulating DNA and circulating tumor cells, CTC stem cells and CTC clusters.

1.1 Circulating Tumor Cells and Metastasis

Cancer is a prevalent cause of death in Western countries. According to the German Federal of Statistics, malignant tumors represent one of the most dangerous diseases in Germany with 230,000 fatal cases each year. The World Health Organization describes cancer as the formation of neoplastic tissue (tumor) due to spontaneous, irreversible, autonomic growth from endogenous tissue [6]. Growing larger than one to two cubic millimeters, tumors can only sustain proliferation with an independent oxygen and nutritional supply. As a result of constant hypoxia, tumor cells induce the “angiogenic switch”, releasing i.e. VEGF (vascular endothelial growth factor) to stimulate vessel sprouting into the tumorous tissue [7]. Mechanic pressure favors the passive detachment of tumor cells into the blood and lymph vessel. In parallel, transcription factors like Snail, Zinc Finger E-Box Binding Homeobox (ZEB) and Twist incite epithelial cancer cells from the solid tumor to transdifferentiate into a mesenchymal phenotype undergoing the so-called epithelial-mesenchymal transition (EMT) [8]. This event is key to the active intravasation of the tumor cells into the vascular system. EMT-like tumor cells lose their structural functional polarity of apical and basolateral domains which allows them to migrate [9].

The fraction of tumor-derived cells in the lymph and blood stream is summarized as circulating tumor cells (CTCs) (Figure 1). Studies showed that CTCs are detectable in 10 to 40 % of breast cancer patients with raising numbers of 40 to 80 % in patients with metastatic tumor burden [10]. In general, one to a thousand CTCs are observed among 10^6 to 10^7 blood cells underlining the urgent need to establish sensitive CTC isolation methods. Most of the CTCs are in fact destined to cell death in the body fluids due to conditions that are not optimal for epithelia-derived cell survival like shear force, oxidative stress and immune cell response. As a result, they might not be viable in the blood circulation for longer than 24 hours [11], which makes them a real-time monitor for therapy response or resistance. Consequently, only a small subpopulation of CTCs contains metastatic precursors [12] with possibly multiple, concurrent resistance mechanisms [13]. Surviving mobile cancer cells passively extravasate in a different tissue. Motile cancer cells adhere at distant capillary beds and are able to transendothelially migrate by mesenchymal-epithelial transition (MET). Either way, these cells enter dormancy or metastasize into a secondary tumor at another location [7,14]. In fact, dormant tumor cells can rest in bone marrow for several years before re-entering the circulatory system [15].

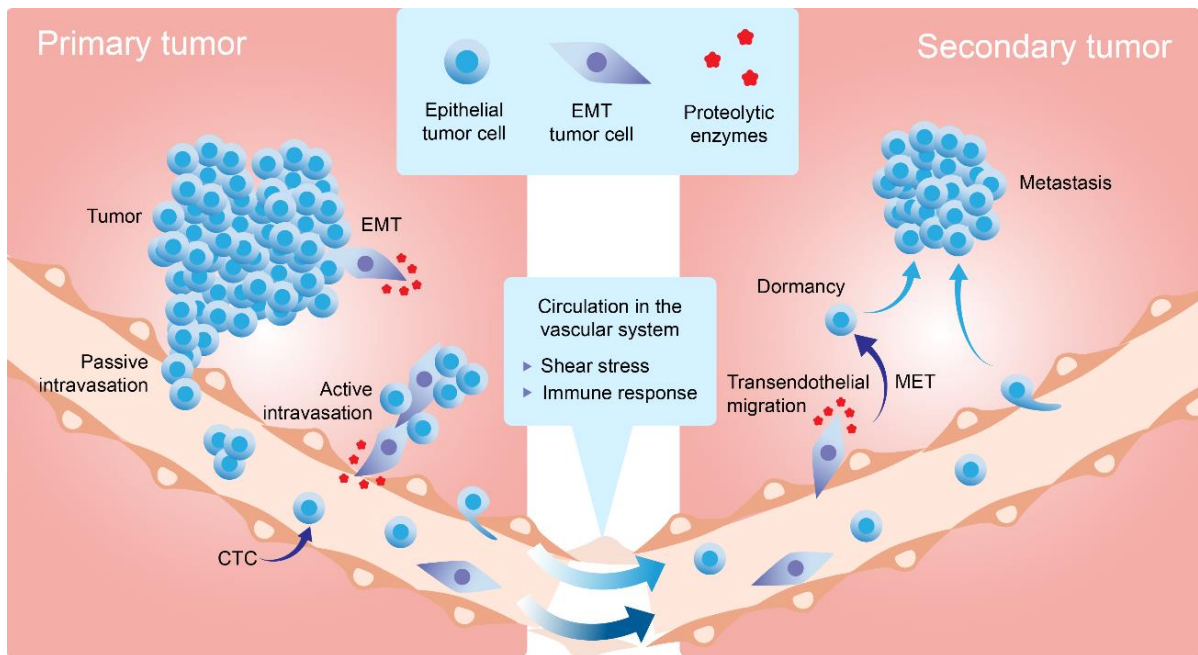


Figure 1: Tumor cells can relocate from the primary tumor in the blood and lymph vessels.

Epithelial tumor cells are transported into the blood and lymph vessels either passively through mechanical pressure or actively in the course of EMT using proteolytic enzymes. In the vascular flow, CTCs are exhibited to biochemical and physical forces which often leads to cell death. The small number of surviving CTCs can enter dormancy or redifferentiate and form metastases.

In recent years, CTC research gained more diagnostic potential in clinical oncology. Various publications state that the biochemical composition of a single CTC subtype as a molecular signature offers information on the tumor origin and possibly even the destination of the cell to suggest a personalized therapy. Cases of CTCs detected in blood years before metastasis have been reported. For example, Ilie et al. published that CTCs were present in 3 % of a COPD patient cohort (chronic obstructive pulmonary disease) without detectable cancerous tissue in the lungs. Following annual computer tomography, lung nodules in CTC positive patients were shown after one to four years, resected and staged as early-stage carcinoma post-surgery [16]. Besides diagnostic profiling, the CTC count in a blood sample was initially established as a prognostic value. Researchers found out that the overall survival drastically decreases above 5 detectable CTCs in a 7.5 mL blood sample [17].

1.1.1 Head and Neck Cancer

At the time of diagnosis, cancer cells in many patients have already disseminated from primary tumor tissue and circulate as CTCs in peripheral blood and lymph vessels or even relocate to neighboring tissues or distant organs. For example in two third of head and neck squamous cell carcinoma (HNSCC) patients, locoregional invasion and adjacent lymph node metastasis is detected within the first diagnosis [18].

HNSCC represents the sixth most malignant tumor worldwide with 650,000 new cancer cases every year [19] and may occur in all (squamous) epithelial tissues and mucous membranes in the head and neck region (Figure 2). Heavy smoking, alcohol consumption, human papillomavirus (HPV) clearance and carcinogenic polymorphisms, especially in immunosuppressed individuals, are favorable dispositions correlating with head and neck cancer development [20].

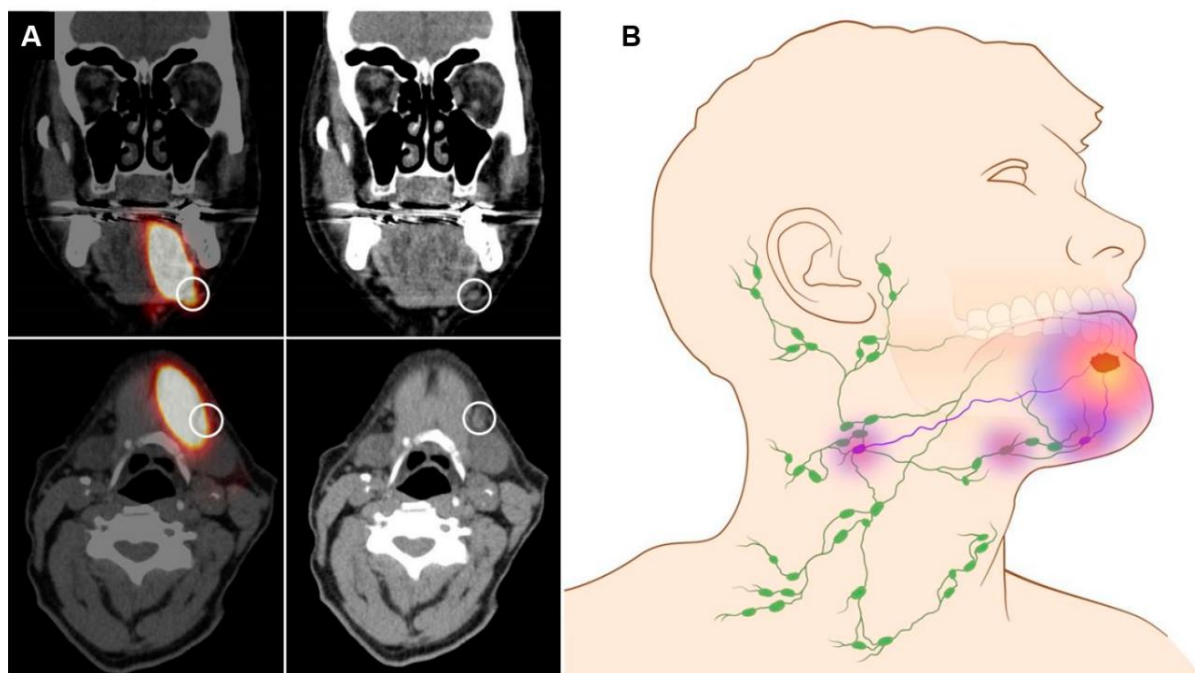


Figure 2: Pathology of Head and Neck Cancer.

(A) SPECT-CT (left) and coronal and axial low-dose CT images (right) of a 72-year-old patient with a cT1N0 floor-of-mouth carcinoma with metastatic sentinel lymph node located in cervical lymph node level Ib (white circle). (B) Schematic illustration of metastatic HNC (©University Medical Center Groningen [21]).

Based on the formation of numerous micrometastases, HNSCC looms a high mortality rate. The 5-year survival rate of patients with distant metastases drastically decreases below 35 % [22]. Furthermore, it is presumed that the presence of micrometastases leads to improved tumor aggressiveness. The metastatic spread is described as a late process in malignant progression but recent studies on breast cancer suggest that the dissemination of primary cancer cells to distant sites might be an early event [23]. Early formation of micrometastases might also play an important role in HNSCC tumorigenesis and progression. The detection of metastasis-driving CTCs in personalized medicine could thus be crucial for higher chances of a cure.

1.1.2 Metastatic Breast Cancer

The German Center for Cancer Registry Data (ZfKD) at the Robert Koch Institute states that on the basis of the current incidence rates, one out of eight women will suffer from breast cancer throughout her life. Further, 16 % of these women will be younger than 50 years at the time of the diagnosis [24]. The mamma carcinoma as the far most frequent cancer in female individuals has, however, a relatively high 10-year survival rate of 83 % when diagnosed early, ideally prior to metastasis, and treated effectively. Stage I breast cancer without sentinel lymph node invasion after biopsy can possibly be cured by surgery and prophylactic hormone therapy. In contrast, metastatic breast cancer (mBC) as a systemic disease invades axillary lymph nodes and later other organs and tissues, such as the bones, lungs, brain or liver and requires harsh therapy administration (Figure 3).

Similar to most cancers, the presence of metastasis-driving CTCs correlates with a poor prognosis of mamma carcinoma. Zhang et al. postulated that the 3-year survival of patients with triple negative breast cancer (TNBC) is significantly higher if there are less than 5 CTCs present in 7.5 mL whole blood prior to surgery [25]. TNBC is a highly invasive form of breast cancer deriving from cells that lost expression of estrogen, progesterone and human epidermal growth factor receptors ESR, PR and HER-2 [26] and is therefore particularly difficult to target without being able to resort to hormone therapy [27]. The hormone receptor status is one of the most important checkpoints in mamma carcinoma diagnostics as clinical guidelines suggest hormone and/or antibody therapy depending on a positive receptor status, replacing or accompanied by radio-chemotherapy.

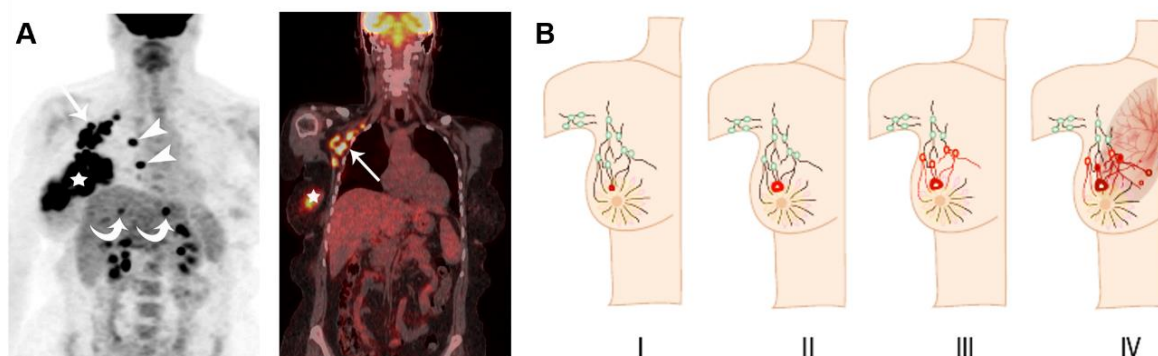


Figure 3: Pathology of metastatic breast cancer.

(A) PET scan of a 52-year-old woman with biopsy-proven right metastatic breast cancer. Maximum-intensity-projection reconstruction of CT-attenuation-corrected PET image shows global hypermetabolic uptake in right breast (star), right subpectoral nodes (arrow), and right internal mammary nodes (arrowheads) and bilobar liver metastases (curved arrows) (left). Coronal PET/CT shows right subpectoral (arrow) and right breast (star) uptake (right) [28]. (B) Staging of breast cancer invasiveness. In stage I, BC occurs in the breast tissue or lymph nodes of the breast in a size of up to 2 cm. Around up to 5 cm growth, the cancer has invaded 1 to 3 axillary lymph nodes in stage II. Or the tumor is larger than 5 cm but has not spread to the axillary lymph nodes. In stage III, the cancer

has spread in 4 to 10 lymph nodes and causes inflammation. In course of further progression to stage IV, the tumor can be any size and the disease has spread to other organs and tissues, such as the bones, lungs, brain, liver, distant lymph nodes, or chest wall [29].

1.2 Tumor Markers in Liquid Biopsy

Following standard procedures, tumor screening and the administration of suitable therapy for a cancer patient requires a tissue biopsy. The U.S. National Cancer Institute (NCI) describes the „biopsy” as the extraction of cells or tissue for a pathological examination. This invasive operation, however, is not always feasible, carries risks in sensitive organs i.e. the brain and implies intensive strains for the patient. Against that, due to the discovery of CTCs in the blood circulation and ultimately the higher risks of operative biopsies, the interest in liquid biopsy has strongly increased. The term “liquid biopsy” summarizes all non- or minimal invasive forms of bio marker characterization in body fluids e.g. blood, urine, cerebrospinal fluid. Tumor markers include CTCs, cell-free or circulating tumor DNA (cf/ctDNA), RNA and tumor-derived exosomes (Figure 4) [30]. Tumor RNA was also shown to be incorporated in platelets making them so-called tumor-educated platelets (TEP). Their pathological relevance is still unclear [31]. In recent years, liquid chromatography-mass spectrometry-based and NMR-based metabolomics have been successfully applied to discover biomarkers for lung, bladder and kidney cancer in urine [32,33].

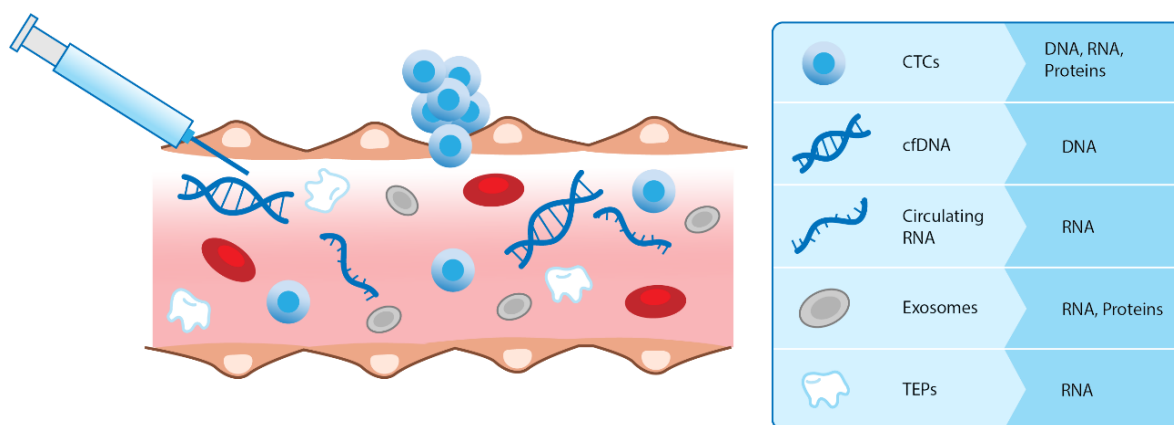


Figure 4: Tumor components and bio marker relevance in whole blood.

CTCs and exosomes are released into the blood stream from solid tumor tissue. Cell-free DNA and RNA come from apoptotic tumor cells. Making use of blood draw, these tumor components can be analyzed on a proteomic, transcriptomic, genetic and (in the case of CTCs) even on a cytobiological level. cfDNA: cell-free DNA; TEPs: tumor-educated platelets.

Several studies concluded that exosomes play an important role in cell-cell communication. Exosomes are 30-100 nm small extracellular vesicles which are secreted by every cell and carry DNA, miRNA, mRNA, proteins and cytokines as cargo [34]. In the same manner, tumor-deregulated nucleic acids can be securely transported from tumor to target cells to

stimulate tumor progression and therapy resistance [35]. miRNA analysis unraveled a correlation of at least four exosomal miRNAs and lung cancer [36]. In addition, the molecular composition of the exosome membrane might indicate the tumor origin and potential medication. Despite the promising results, exosome secretion of healthy leukocytes and endothelial cells raises the background signal hindering the clinical applicability of early detection immensely. Further, clinically practical isolation methods to separate exosomes from blood (centrifugation, filtration) are still missing to exploit exosomes as standardized tumor markers [37]. Similarly, cfDNA is present in both healthy and diseased individuals. Increased levels of cfDNA were detected in metastatic cancer patients [38]. Sequencing of cfDNA can indicate specific genomic alterations, i.e. mutation of onco- and repressor genes, epigenetic changes and gene amplification [39]. Although cfDNA is easily detectable in blood, the application as diagnostic or prognostic parameter is only feasible in certain carcinoma due to strong heterogeneity and tumor taxonomic concentration differences [40]. Additionally, cfDNA analysis requires highly sensitive bio markers to exactly distinguish between healthy and diseased asymptomatic patients. Fernandez-Cuesta et al. showed that a carcinogenic-associated TP53 mutation was present in 11 % of healthy controls making this candidate practically unusable for cfDNA screening [41]. Moreover, radiotherapy leads to an increased level of cfDNA in cancer patient blood which also hampers specific enrichment of tumor-related DNA.

Nevertheless, the presence of tumor markers in body fluids like blood, lymph, urine, cerebrospinal and – in brain cancer even – vitreous fluid offers a broad spectrum for straightforward minimal invasive cancer research [42]. Liquid biopsy could be conducted also in weekly frequencies. Especially the high informative content of CTCs turns them into a promising liquid marker. In contrast to cfDNA analysis, CTC isolation opens up a biotechnological toolbox on RNA, DNA and proteomic levels (Figure 4). Making use of CTCs, contamination with background nucleic acids and proteins as in serum or plasma is strongly minimized. Current expression profiling of mRNA in CTCs from metastatic gastric cancer gave highly interesting new insights into diagnostic properties and personalized therapy adaption. In particular, a majority of gastric CTCs had undergone epithelial-mesenchymal transition (EMT) and indicated the contribution of platelet adhesion toward EMT progression and acquisition of chemoresistance [43].

1.3 Methods to Enrich Rare Cells from Body Fluids

Multi-marker analysis of single CTCs aims to achieve precise drug suitability for personalized medicine. Therefore, CTCs have to be identified, counted, characterized and isolated from a background of billions of blood cells per milliliter blood. Since tumor cells exhibit a broad geno- and phenotypical diversity, there is no universal tumor marker available to target all subtypes of CTCs in an efficient manner [44]. Nonetheless they can be separated from hematopoietic progenitors and blood cells based on physical and biochemical features (Figure 5).

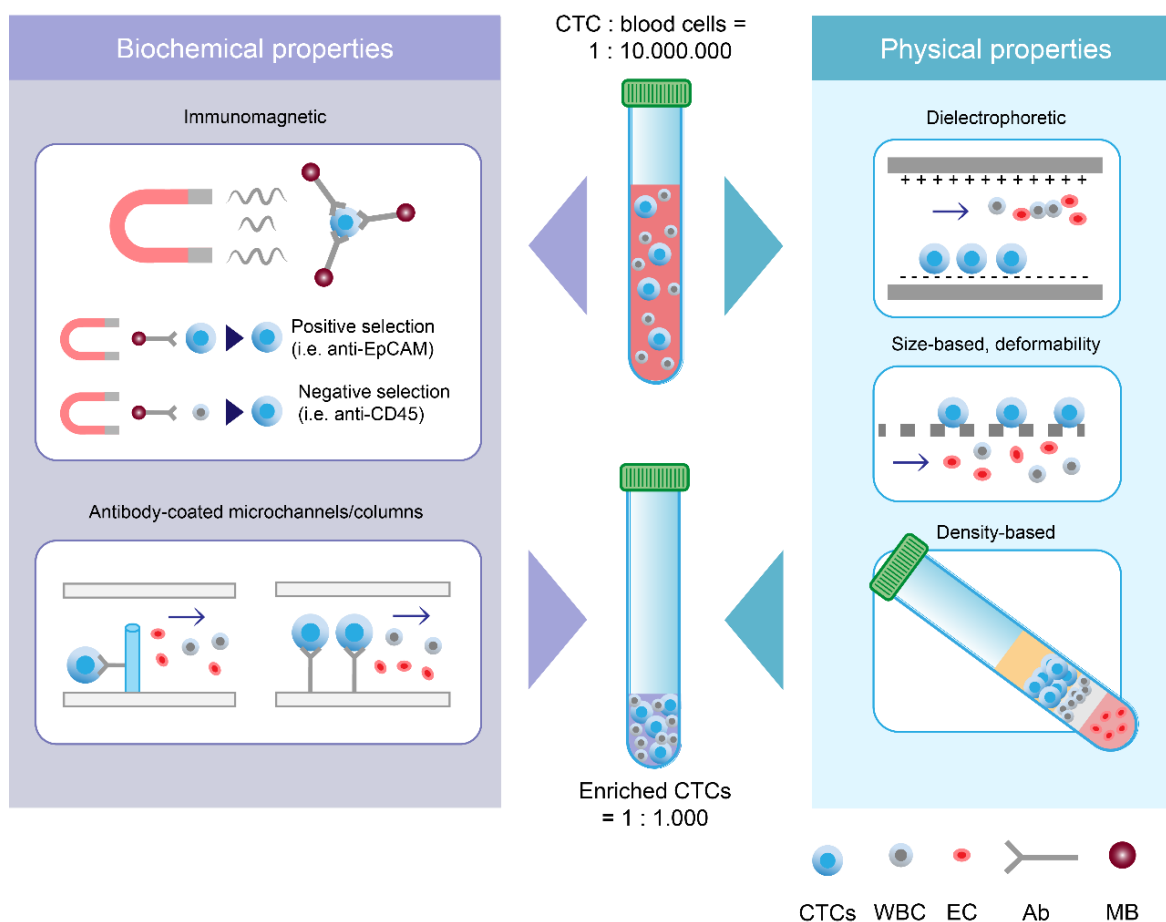


Figure 5: Enrichment methods for circulating tumor cells.

The physical and biochemical properties of CTCs differ from those of blood cells. Based on these features, they can be separated from other cells using immunoselective and electrophoretic methods, sieve technologies and density gradient centrifugation. EC: erythrocyte; Ab: antibody; MB: magnetic bead.

1.3.1 Physical Methods

As displayed on the right side in Figure 5, tumor cells can be separated from blood cells using dielectrophoresis, size-exclusion and membrane filtration, deformability characteristics in a microfluidic chip or by means of density gradient centrifugation [45]. ISET filters (isolation

by size of epithelial cells, RareCell Diagnostics) use an 8 μm mesh membrane to hold back larger, stiffer CTCs and wash out other blood cells. Ficoll, OncoQuick (Greiner Bio-One) can be taken as an example for density gradient media to yield CTCs in the leucocyte phase after centrifugation. The advantages of enrichment based on physical features of cells are clear: The methods do not require immunohistochemical labeling and therefore only have secondary influence on the physiology of the cell. Contrastingly, CTCs are highly heterogeneous and similar in size to mononuclear white blood cells raising the chances of losing them in the background of blood cell contamination [46].

1.3.2 Biochemical Methods

As cancer cells express specific (mostly epithelial) surface antigens, so-called tumor markers that do not appear on leucocytes or mesenchymal cells or vice versa, they can be enriched using biochemical methods. Here, two fundamental immunological principles can be addressed. Tumor cells are either enriched by positive selection with tumor-targeting antibodies or blood cells are depleted with leucocyte targeting antibodies like anti-CD45 (negative selection) (Figure 5 left side).

Immunomagnetic enrichment is based on an antibody-mediated binding between tumor cells and magnetic micro- or nanoparticles and then cell separation by applying a magnetic field afterwards. Positive selection with immunomagnetic enrichment is mostly performed using antibodies targeting epithelial cell adhesion molecules (EpCAM) as 90 % of tumor entities derive from epithelial origin [47]. EpCAMs are transmembrane surface molecules of epithelial cells [48] to mainly form cell-cell contact. EpCAMs are overexpressed on the surface of highly proliferative cells i.e. tumor cells [49].

CellSearch® (Menarini Silicon Biosystems Inc.) is to date the only U.S. Food and Drug Administration approved prognostic method to isolate CTCs from breast, colon and prostate cancer. It is held as the gold standard in the use of positive selection with anti-EpCAM magnetic particles [45]. The system however requires experienced personnel to perform and read out the analysis. Cell fixation is mandatory for intracellular staining in the platform, therefore CellSearch® is predominantly restricted to CTC count measurement as a prognostic value and does not allow for downstream procedures of viable CTCs. This stresses the urgent need for flexible CTC isolation strategies. As shown in Figure 5, functionalization with tumor-targeting antibodies is not limited to magnetic particles but can also be applied to immobilize antibodies on the surface of micro columns or channels. The OncoCEE™ microchip (Biocept, USA) for example is seamed with anti-EpCAM micro columns [50].

On the downside, EpCAM-based methods depend on a strong expression of this antigen and are hence confined by the intrinsic heterogeneity of CTCs. This is most critical in cases of early EMT or late stages of cancer progression due to the loss of EpCAM expression [31]. To capture these CTCs, antibody cocktails could be of assistance. Examples of potential candidates are human epidermal growth factor receptor 2 (HER2), Mucin-1 (MUC1), epidermal growth factor receptor (EGFR), folate-binding protein receptor (TROP-2) and mesenchymal or stem cell targets (c-MET, N-Cadherin, CD318) [51] and V-CAM or integrins.

1.4 Confirmation of Isolated CTCs bona fide

To minimize blood cell contamination in CTC isolates, protein or nucleic acid-based technologies and functional assays require a high specificity. Making use of immunological properties on proteomic levels, CTCs can be detected using membrane-bound and/or cytoplasmic anti-epithelial, anti-mesenchymal, tumor-associated or tissue-specific markers. On the other hand, RT-qPCR, RNA sequencing or cytometric multiplex-bead arrays provide CTC detection on a transcriptomic basis [47].

1.4.1 Transcriptomic Analysis

On the genotypic level, cancer cells exhibit a deregulated gene expression compared to control cells or express unexpected markers of their original epithelial tissue in other parts of the body. Here, nucleic acid-based assays are performed to identify tumor-associated DNA or RNA in the enriched cells using (reverse transcriptase quantitative) polymerase chain reaction ((RT-q)PCR), fluorescence-activated probe particles and fluorescence in-situ hybridization (FISH) [47].

Products of the AdnaTest line (QIAGEN) contain a multiplex PCR to analyze a tumor marker panel from mRNA in CTCs enriched by immunomagnetic separation after RNA isolation and transcription in cDNA (complementary DNA). These kits however often only provide a yes/no result and some of the tested mRNAs e.g. for Muc-1 are also present on activated T cells of the immune system [45]. The prognostic value of the CTC count also cannot be determined clearly as the amount of transcript does not necessarily correlate with the number of cells [52]. Interestingly in this regard, RNA sequencing as an extended technique boosted personalized diagnostics from single gene mutation analysis in the early 2000s, over cancer panel screening in the 2010s to Comprehensive Genomic Profiling (GCP). In parallel since 2001, the cost of DNA sequencing decreased more than 100,000 times from \$100 million

USD per human genome to less than \$600 USD today [53]. For this purpose, a high purity of CTC analytes is necessary and isolation platforms as presented in this thesis can assist.

1.4.2 Immunocytological Approaches

The genotype of a cancer cell impacts the phenotypical translation of presented proteins so that depending on the state and subtype, CTCs display membrane molecules and/or cytoplasmic epithelial, mesenchymal or tumor-associated markers different to other control cells [47]. These antigens can be labeled with fluorophore-coupled antibodies to make them visible in optical systems. CellSearch® and many other CTC isolation platforms use protein-based methods like immunofluorescence analysis for the detection of CTCs after an enrichment step. Cells are stained with nucleus dye 4',6-Diamidin-2-Phenylindol (DAPI), epithelial surface markers EpCAM and cytokeratin (CK) and leucocyte marker CD45 and are then defined as CTCs if DAPI⁺/EpCAM/CK⁺/CD45⁻ and as leucocytes if DAPI⁺/EpCAM/CK⁻/CD45⁺ [50].

Besides biological fluorophores i.e. phycoerythrin (PE), synthetic fluorophores have been developed to realize a more robust photostability, more narrow emission and wider excitation spectra. The 20 nm large semiconductor crystals "QuantumDots" (Thermo Scientific) are an example. Their outer polymer layer can be biofunctionalized with conjugated antibodies, however the surface functionalization requires a two-step protocol and lacks uniformity.

1.5 Automated Microfluidics for Diagnostic Approaches

According to *The Scientist*, at least 5 of the global top 10 innovations in life sciences were based on microfluidic systems in 2020 [54]. As described by Burklund and colleagues: "Microfluidics is an emerging field in diagnostics that allows for extremely precise fluid control and manipulation, enabling rapid and high-throughput sample processing in integrated micro-scale medical systems. These platforms are well-suited for both standard clinical settings and point-of-care applications. The unique features of microfluidics-based platforms make them attractive for early disease diagnosis and real-time monitoring of the disease and therapeutic efficacy" [55]. The most popular application of diagnostic microfluidics is flow cytometry where (fluorescent) cell suspensions are hydrodynamically focused using an outer sheath flow. The cell population of interest is detected on a detector surface using forward and sideward scattered light to measure size and granularity and laser light with optical filters to track fluorescence intensity. For example, different blood cell types like leucocytes, lymphocytes and granulocytes can be distinguished in routine blood work with this method.

Single target cells such as rare CTC populations, however, underlie a certain detection limit with classical flow cytometry and can only be identified and analyzed from pre-enriched cell suspensions using elaborated microfluidic detection. Generally, microfluidic techniques in single cell isolation employ either the principle of marker-based isolation with single cell recognition or marker-free isolation without single cell recognition, which both have their advantages and disadvantages (Figure 6). Marker-dependent methods such as flow cytometry or camera-based immunofluorescence systems require specific labeling but deliver data directly. Marker-free isolations (micro structuration, droplet generation) enrich cells without pre-treatment but deeper analysis of all captured single cells is mandatory.

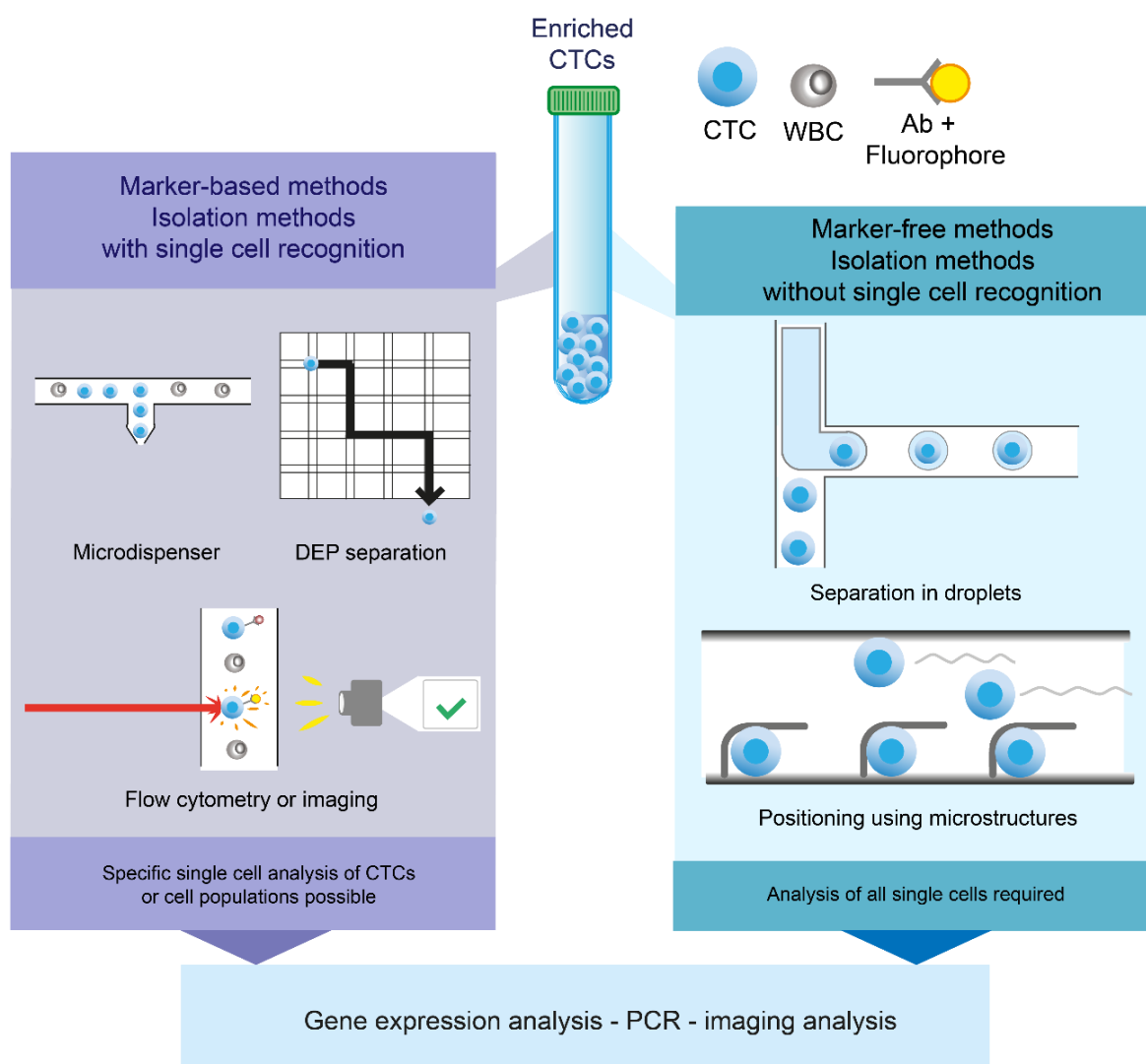


Figure 6: Approaches of microfluidic single cell isolation.

Rare cells in pre-enriched samples can be isolated by means of marker-based and marker-free isolation. Marker-based methods like flow cytometry require specific labeling but allow for direct data of cells of interest. Marker-free isolations using microstructures capture untreated cells but further analysis of all captured single cells is necessary.

1.6 Challenges in Automated CTC Isolation

On one hand, the validation of an optimal therapy based on a conventional tissue biopsy is limited due to the metastatic heterogeneity [56]. On the other hand, the characterization of CTCs via liquid biopsy in the semi-automated FDA-approved CellSearch® system has its own drawbacks. The relatively laborious and cost-intensive analysis can only be conducted by trained personnel and requires cell fixation. To guarantee reproducible results and to efficiently deploy the resources, the development of a fully automated platform to enrich, label, detect and isolate CTCs is worthwhile [57]. The specifications for such a device are as follows:

- Sensitivity: CTCs should also be detectable at low levels.
- Specificity: The purity of the isolated CTCs should be high.
- Viability: The isolation should be as gentle as possible for adequate downstream analysis.
- Throughput: The protocol duration should be as short as possible.
- Automation: A certain automation grade should reduce hands-on time and human error.
- Availability: Systems should be available at clinical facilities, not only at central laboratories, and thus easy to be operated without trained personnel to guarantee short transport distances from-bed-to-bench-to-bed results.

The biggest hurdles to overcome are the diversity of the CTCs and of cancer in general, the rare occurrence of CTCs among millions of blood cells and the rapid degradation of whole blood over time. The pipeline for a successful isolation includes suitable marker identification for the subtype, efficient enrichment and reliable cell staining for fluorescence-based detection. To the last mentioned, the decisive criterion is to gain the highest signal-to-noise ratio possible between CTC signal and the autofluorescence noise of the magnetic particles or contaminating cells. Andree et al. found out that a 1:1.000 proportion of the desired stained cells to the contaminating unstained population leads to a fluorescence overlap of ca. 50 % already as shown in Figure 7 [57]. In this regard, the focus is on the enrichment specificity of CTCs or the depletion of WBCs and a down-scaled sparing use of magnetic particles.

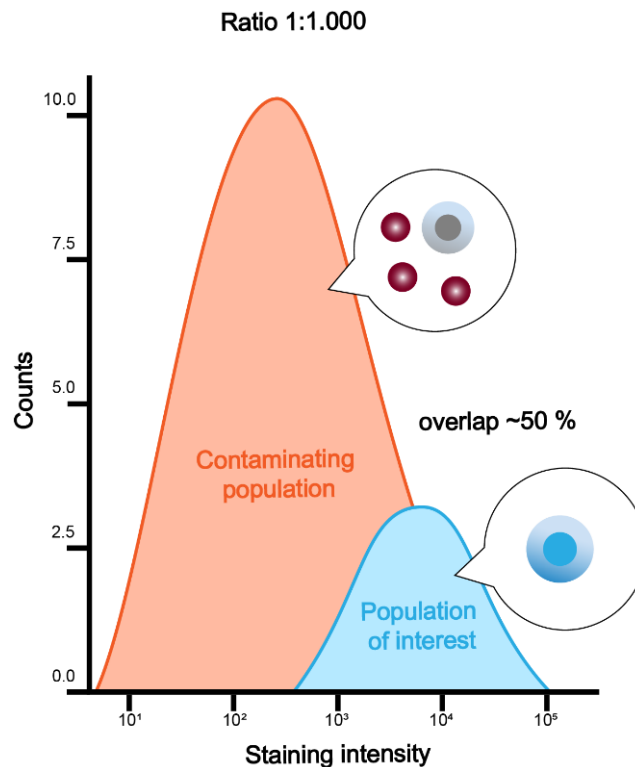


Figure 7: Fluorescence detection of stained and unstained populations in flow cytometry.

The distributions of fluorescence intensities is plotted against the count of a stained (cells of interest) and unstained (contaminating cells, beads etc.) population in a ratio of 1:1.000. The numerical difference leads to a fluorescence overlap of ~50 % (modified acc. to [57]).

1.7 Research Question and Goals of this Project

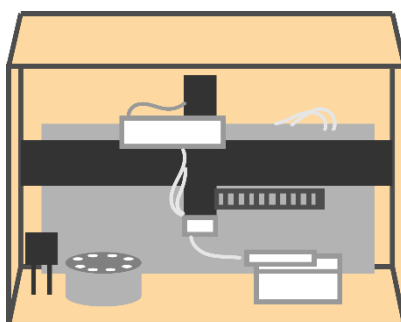
The Fraunhofer Institute for Microengineering and Microsystems (IMM) Mainz has recognized the urgent need for a CTC isolation platform that meets the previously discussed requirements to accelerate microfluidic diagnostics. Since roughly 10 years, it has been the Diagnostics department's goal to elaborate a microfluidic concept for the enrichment, detection and single cell dispensing to finally establish a device for the single cell isolation of CTCs from a 7.5 mL blood sample. In the developmental process, various projects were acquired to determine the exact research need and proof-of-concept. This included platform and software engineering, microfluidic cartridge conception, assay design and establishment, biological validation, optimize respective fluid parameters and finally apply the platform in the (pre)clinical field.

Several prototypes were designed, built and validated. Two of them were fully automated and are subject of this dissertation. The IsoMAG device was developed to automate the immunomagnetic enrichment of CTCs using EpCAM⁺ selection in a tube holder carousel for subsequent blood waste washing with decreasing volumes. This technology was then

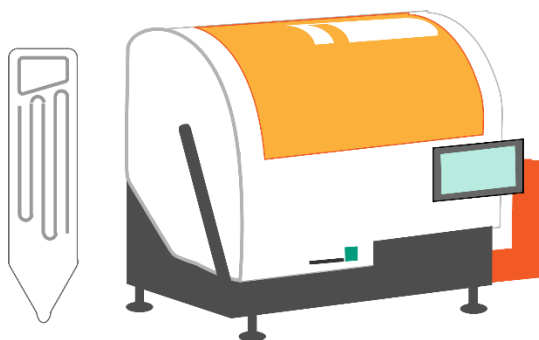
modified resulting in a linear sample holder board and combined with a microfluidic chip system to detect and dispense single CTCs based on Field Programmable Gate Array (FPGA)-supported fluorescence analysis on the CTCelect platform.

In the tubes of the sample holder in the respective IsoMAG and CTCelect module, CTCs are enriched from a 7.5 mL standard blood sample size via immunomagnetic separation (IMS) and transferred in a smaller volume of 300-500 μ L. IMS is performed by means of biotinylated anti-EpCAM coupled streptavidin magnetic particles. Due to the binding affinity of the EpCAM antibody to EpCAM antigens on the cell surface, beads can be bound to cancer cells. Consequently, the cells can be captured and separated from the supernatant by applying magnetic force with an external magnet. Further in the CTCelect platform, the enriched sample is incubated with fluorophore coupled antibodies to label and differentiate them from unspecific background signal (contaminating blood cells and free magnetic particles). Flow cytometric detection of EpCAM⁺ cancer cells takes place in a microfluidic chip where the sample is transferred through a chip funnel at the upper end. The complex chip is designed as a single-use easy-to-produce disposable to avoid cross-contamination and intensive cleaning of the system. The on-chip sample flow is hydrodynamically focused to singularize the fluorescently labeled cells. In case of high fluorescence signals of a cell fitting to the assay's parameter, this cell is dispensed in the cavity of a 96-well plate. Single cell isolation allows for CTC analysis to stratify cancer heterogeneity. Primary CTC culture can be a powerful tool to screen potential cancer targets and to identify personalized therapeutics. These efforts may complement the current diagnostic standard which focuses on the analysis of circulating tumor DNA enabling single cell mutation analysis, expression analysis on RNA level and single cell metabolic analysis [58,59].

Acronym	Process abilities	Principle	Components
IsoMAG	Immunomagnetic enrichment	- Macrofluidics	Benchtop device with <ul style="list-style-type: none"> - Horizontal and vertical axis driving the pipet unit - Magnet arm - Tube holder carousel - External computer



CTCelect	Immunomagnetic enrichment, fluorescence-based cell sorting and single cell dispensing	- Macrofluidics - Microfluidics - Flow control - Hydrodynamic focusing	Benchtop platform with <ul style="list-style-type: none"> - Enrichment module (IsoMAG) - Microfluidic fluorescence-activated cell sorting (μCS) subunit, FPGA supported - Touchscreen - Pipetting robot - Cell sorting - Microfluidic chip
-----------------	---	---	---



The aim of the doctoral project was an in-depth characterization and parameter adaption of the automated process steps, the establishment of a complete assay and the testing of the platform technology from lab-scale with spike-in samples to a (pre)clinical environment using patient samples. Detailed subordinate projects were specified as follows:

1. Comparison and improvement of manual and automated immunomagnetic enrichment in terms of cell recovery in dependency of cell line and input number, particle size, volume, concentration, biofunctionalization protocol and blood cell contamination
2. Feasibility study of antibody staining in the CTCelect platform with different antibodies and fluorophore to enhance signal-to-noise ratio and the transfer to the microfluidic cartridge
3. Investigation on flow properties of cancer cells in the geometrical dimension of the chip with respective parameter settings and fluid composition
4. Developing and proof-of-concept of downstream analysis applications such as immunofluorescence microscopy and PCR-based confirmation of tumor-associated RNAs in single cells
5. Establishing the devices in a clinical setting and determination of their applicability to patient samples
6. Utilizing generated results in publications to multiply scientific visibility.

2 Publications

This section presents the publications for the cumulative dissertation as originally published under peer-review and reprinted with permission from the corresponding publishers. The copyright of the original publications is held by the respective authors.

	Title	Own Contribution
Paper 1	Gribko, A.†; Stiefel, J.†; Liebetanz, L.; Nagel, S.M.; Künzel, J.; Wandrey, M. et al. IsoMAG—An Automated System for the Immunomagnetic Isolation of Squamous Cell Carcinoma-Derived Circulating Tumor Cells. <i>Diagnostics</i> 2021; 11, 2040; (†contributed equally). https://doi.org/10.3390/diagnostics11112040	30 % (shared first authorship) Conceptualization, validation and formal analysis, investigation, data curation, writing, review and editing, visualization.
Paper 2	Stiefel, J.; Freese, C.; Sriram, A.; Alebrand, S.; Srinivas, N.; Sproll, C. et al. Characterization of a novel microfluidic platform for the isolation of rare single cells to enable CTC analysis from head and neck squamous cell carcinoma patients. <i>Eng Life Sci.</i> 2022; 22: 391– 406. https://doi.org/10.1002/elsc.202100133	80 % (first authorship) Conceptualization, methodology, validation and formal analysis, investigation, resources, data curation, writing, review and editing, visualization, project administration, funding acquisition.
Paper 3	Stiefel, J.; Baßler, M.; Wittek, J. et Freese, C. Automated immunomagnetic enrichment and optomicrofluidic detection to isolate breast cancer cells: A proof-of-concept towards PoC therapeutic decision-making. <i>Magnetochemistry</i> 2022; 8(9): 99. https://doi.org/10.3390/magnetochemistry8090099	90 % (first authorship) Conceptualization, methodology, validation and formal analysis, investigation, resources, data curation, writing, review and editing, visualization, project administration, funding acquisition.

2.1 Paper 1



Article

IsoMAG—An Automated System for the Immunomagnetic Isolation of Squamous Cell Carcinoma-Derived Circulating Tumor Cells

Alena Gribko ^{1,†}, Janis Stiefel ^{2,†}, Lana Liebetanz ², Sophie Madeleine Nagel ¹, Julian Künzel ³, Madita Wandrey ¹, Jan Hagemann ¹, Roland H. Stauber ¹, Christian Freese ^{2,*} and Désirée Gül ^{1,*}

- ¹ Department of Otorhinolaryngology, University Medical Center Mainz, Langenbeckstr. 1, 55131 Mainz, Germany; algribko@uni-mainz.de (A.G.); sophiemadeleine.nagel@web.de (S.M.N.); wandrey@uni-mainz.de (M.W.); jan.hagemann@unimedizin-mainz.de (J.H.); rstauber@uni-mainz.de (R.H.S.)
- ² Fraunhofer Institute for Microengineering and Microsystems IMM, Carl-Zeiss-Str. 18-20, 55129 Mainz, Germany; Janis.Stiefel@imm.fraunhofer.de (J.S.); lana-liebetanz@web.de (L.L.)
- ³ Department of Otorhinolaryngology, University Hospital Regensburg, Franz-Josef-Strauß-Allee 11, 93053 Regensburg, Germany; julian.kuenzel@ukr.de
- * Correspondence: Christian.freese@imm.fraunhofer.de (C.F.); guel@uni-mainz.de (D.G.)
- † These authors contributed equally.

Abstract

Detailed information about circulating tumor cells (CTCs) as an indicator of therapy response and cancer metastasis is crucial not only for basic research but also for diagnostics and therapeutic approaches. Here, we showcase a newly developed IsoMAG IMS system with an optimized protocol for fully automated immunomagnetic enrichment of CTCs, also revealing rare CTC subpopulations. Using different squamous cell carcinoma cell lines, we developed an isolation protocol exploiting highly efficient EpCAM-targeting magnetic beads for automated CTC enrichment by the IsoMAG IMS system. By FACS analysis, we analyzed white blood cell contamination usually preventing further downstream analysis of enriched cells. 1 µm magnetic beads with tosyl-activated hydrophobic surface properties were found to be optimal for automated CTC enrichment. More than 86.5 % and 95 % of spiked cancer cells were recovered from both cell culture media or human blood employing our developed protocol. In addition, contamination with white blood cells was minimized to about 1200 cells starting from 7.5 mL blood. Finally, we showed that the system is applicable for HNSCC patient samples and characterized isolated CTCs by immunostaining using a panel of tumor markers. Herein, we demonstrate that the IsoMAG system allows the detection and isolation of CTCs from HNSCC patient blood for disease monitoring in a fully-automated process with a significant leukocyte count reduction. Future developments seek to integrate the IsoMAG IMS system into an automated microfluidic-based isolation workflow to further facilitate single CTC detection also in clinical routine.

Keywords: automation; liquid biopsy; circulating tumor cells; head and neck squamous cell carcinoma; immunomagnetic particle-based detection; metastasis

1. Introduction

Cancer is the second major cause of death in modern society. Besides improved treatment strategies, the development of innovative diagnostics is indispensable for long-term improvement of diagnosis and treatment of cancer patients. The lymph-/hematogenous spread of cancer cells into distant organs and their subsequent growth to overt metastases is the most fatal complication of solid tumors, such as squamous cell carcinoma of the head and neck (HNSCC) [1,2]. Moreover, therapy resistance and associated relapses are common and associated with high patient morbidity [3,4]. The classical view is that metastatic spread is a late process in malignant progression, but today it is accepted that blood circulation and dissemination of primary cancer cells to distant sites is already an early event [5,6].

The fact that these circulating tumor cells (CTCs) are detectable in the peripheral blood of cancer patients months to years after complete removal of the primary tumor in a period called “metastatic cancer dormancy” supports the idea that these cells circulate between metastatic sites [7]. Since their early discovery in the 19th century [8], CTCs have been demonstrated to be clinically recognized and present in the blood circulation of many cancer types including colon [9], lung [10], ovarian [11], breast [12], melanoma [13], prostate [14] and head and neck cancer [15]. Clinical studies present a correlation between the progression of cancer disease and the number of detected CTCs [16,17,18]. A high number of detected CTCs can give information about tumor burden, recurrence and usually represents a poor prognosis. In detail, the determination of CTCs before and after resection also opens up the possibility for monitoring therapeutic response [19] in combination with analyses of circulating tumor DNA (ctDNA) [20]. Hence, the detection and characterization of CTCs as a part of minimal invasive “liquid biopsy” has gained (pre)clinical considerable attention over the last decade [21,22].

However, the capture and detection of CTCs are extremely challenging because of their rarity, the property to move as individual cells or as multi-cellular clumps, and their heterogeneity regarding size and biological and molecular changes during the epithelial-to-mesenchymal transition (EMT) processes. These challenges require the ability to handle a very small number of cells by isolation methods with high efficiency in an acceptable time scale [23]. Various techniques that are based on physical or immunological properties have been developed [24], and different materials with their unique properties according to their

shape, size and surface were applied in this field [25,26,27]. Only a few systems are available on the liquid biopsy market but have been shown to isolate CTCs in a proper way. Thereby, these methods often dictate an exact protocol to the user, taking away application flexibility. In contrast to that, researchers aim for process-adaptable platforms as the disciplines of liquid biopsy expand permanently, concerning various sample types such as tissue-derived single cell suspensions or adjustable sample sizes.

All techniques developed for CTC enrichment have their advantages and disadvantages. In contrast to immunomagnetic separation, physical separation methods (e.g., Parsortix® technology, Angle, Surrey, UK) allow label-free isolation but lack cell distinction due to overlapping sizes of CTCs and white blood cells [28]. A microstructure-based enrichment is limited in throughput and sieve-shaped technologies, error-prone to complex liquids such as whole blood, are consequently at risk of clogging in automated lab solutions. Though it has drawbacks in target selectivity, immunomagnetic enrichment is often the method of choice because it is easily automatable and enables a high sample throughput. Since the establishment of the “Food and Drug Administration” (FDA)-approved CellSearch® system, which is held as the gold standard of automated immunomagnetic enrichment and staining platforms, the sensitivity of CTC detection has markedly improved [29,30]. CellSearch® relies on the expression of the epithelial cell adhesion molecule (EpCAM) for the quantification of CTCs in different tumor types [31]. Although this optical detection method have been used in numerous studies, the cost for instruments (220,000 dollars), sample preparations and analysis are still laborious and relatively high (approx. 1000 dollars/run) [32]. Consequently, such assays did not succeed in establishing in clinical routine as a low-cost diagnostic test. Due to the above-mentioned obstacles, fully automated, easy-to-use platforms will demonstrate future solutions to improve cancer diagnostics and therapies as well as basic scientific knowledge of tumor development.

The Fraunhofer CTSelect unit has been developed to meet the need of such a fully automated, easy-to-use platform for CTC isolation out of 7.5 mL whole blood samples. Herein, we characterized the IsoMAG IMS device as the core unit of such a platform applying fully automated immunomagnetic enrichment of rare cells with flexibly selectable antigen targets. In this proof-of-principle study, we established a robust protocol for the automated isolation of an EpCAM- and CSV (cell surface vimentin)-positive subpopulation of cells with a concomitant reduction of background white blood cells as a prerequisite for implementation of the device into the CTSelect unit allowing downstream analyses on a single cell level. Furthermore, we proved feasibility of the method for two squamous cell carcinoma cell lines and HNSCC patient samples.

2. Materials and Methods

2.1 Cell Lines

The SCL-1 squamous cell carcinoma line was established by Dr. Petra Boukamp (DKFZ, Heidelberg, DE, Germany) [33] and kept in Gibco™ DMEM (low glucose, pyruvate) medium supplemented with 10 % FCS. HNSCCUM-02T squamous cell carcinoma cell line was established by Welkoborsky et al. (UMC Mainz, DE, Germany) [34], and kept in DMEM:F-12 (cc-pro) medium supplemented with 10 % FCS and 1 % L-glutamine. Cell lines were cultured at subconfluence and incubated at 37 °C in a 5 % CO₂ humidified atmosphere. Other cell lines (A431, HEK293T, MV3, BLM) were received from cell line collections (DSMZ, ATCC) and handled as described before [35,36,37].

2.2 Blood Samples

All blood samples were obtained from the University Medical Center Mainz, DE. To quantify leukocyte contamination, whole blood bags (500 mL CompoFlex, Fresenius Kabi, Bad Homburg, Germany) from healthy donors were purchased at the local Blood Transfusion Center. Whole blood from HNSCC patients was collected at the Department of Otorhinolaryngology in compliance with ethical guidelines [38].

2.3 Immobilization of EpCAM Antibodies on Immunomagnetic Beads

Immunomagnetic beads at different sizes and surface properties (Table 1) were purchased at Thermo Fisher Scientific, Darmstadt, DE and coated with biotinylated monoclonal mouse anti-human EpCAM (CD326) antibody 1B7 (20 µg/mL, eBioscience, GB) or anti-human CSV antibody (clone 84-1, Abnova, Taiwan) for 1 h as described by the manual. Free streptavidin binding sites on anti-EpCAM beads were then saturated with a biotin/PBS solution for 30 min. Anti-EpCAM beads were stored at 4 °C for several weeks.

2.4 Manual Cell Isolation by Immunomagnetic Beads

To compare the performance of the IsoMAG IMS unit it was also necessary to establish a standard protocol for manual cell isolation. Cells (SCL-1, HNSCCUM-02T) were released from culture flasks and stained using the CellTrace™ CFSE Cell Proliferation Kit (CFSE) according to the manufacturer's protocol. A defined number of stained single cells were aspirated with a 10 µL pipette from a 1:100 diluted cell suspension in a petri dish and spiked

into 7.5 mL sample volume consisting of cell culture medium, or blood of healthy donors. Next, 100 or 150 μ L (depending on medium or blood) of anti-EpCAM Dynabeads MyOne Streptavidin were added (see Table 1) and incubated for 30 min with slow rotation of the tube. Next, the bead-bound cells were magnetically separated for 10 min by using DynaMag-15 (Invitrogen, Thermo Fisher Scientific, Dreieich, Germany) and resuspended in 5 mL washing buffer. Washing steps and magnetic separation were repeated three times using a decreased incubation time of 5 min and resuspension in washing buffer with decreasing volumes (ranging from 5 mL, 4 mL up to 1 mL).

Table 1. Overview of tested Dynabeads.

Beads	Size	Surface Functionalization
Dynabeads MyOne Streptavidin T1	1 μ m	Tosyl-activated, hydrophobic
Dynabeads MyOne Streptavidin C1	1 μ m	Carboxylic acid, hydrophilic
Dynabeads M-270 Streptavidin	2.8 μ m	Carboxylic acid, hydrophilic
Dynabeads M-280 Streptavidin	2.8 μ m	Tosyl-activated, hydrophobic

2.5 Automated CTC Enrichment Using the IsoMAG Device

For the establishment of a standard protocol using the IsoMAG IMS unit, antibody-coupled beads were added to a 7.5 mL sample volume consisting of cell culture medium, blood of healthy donors or patient blood samples with spiked EpCAM+ SCL-1 or patient-derived HNSCC cells (HNSCCUM-02T). Before initiating the assay in the software, five tubes containing the input sample and washing buffers were placed in the tube holder carousel and a 10 mL pipet tip was put in the holder of the IsoMAG device as described in Table S1. The sample was incubated for 30 min. After incubation, bead-bound CTCs were magnetically separated alternately with several washing steps in decreasing volumes from 5 mL to 1 mL (see Supplementary Table S1 for detailed protocol).

2.6 Characterization of Leukocyte Contamination in IsoMAG Isolates

To quantify analysis-disrupting white blood cell (WBC) contamination in tumor cell isolates, CD45+ cell count after manual and automated IMS was determined by flow cytometry. Therefore, we established a double staining protocol for leukocytes using a CD45-PE antibody targeting the specific surface protein of WBCs (1:50 dilution; Miltenyi Biotec, Bergisch Gladbach, DE, Germany) and nuclear stain RedDot™ (Biotium, Fremont, CA,

USA). Wash buffers were set up in the IsoMAG IMS unit and 150 μ L EpCAM beads were added to 7.5 mL whole blood before initiating the automated protocol. Manual enrichment was performed in parallel. The final samples were separated in a magnet separator, the supernatant was discarded and the bead cell pellet was stained with the above-mentioned solutions. Dual-positive cells [CD45+/RedDot+] were analyzed by FACS using the BD Accuri C6 flow cytometer. Cell counts after IMS were measured in four samples of different healthy donors and the average WBC contamination with standard deviation (SD) was calculated.

2.7 Immunostaining of IsoMAG Isolated CTCs

To assess possible tumor origin of isolated cells, the final 1 mL sample was administered several staining steps. First, isolated cells were stained with fluorescent CD45-FITC antibody (1:1000 dilution) to label leukocytes. Subsequently, the sample was washed three times with PBS in a magnetic separator and transferred to an ibidi 8-well slide (ibidi GmbH, Gräfelfing, Germany) after the last separation step. Cells were centrifuged to the bottom of the slide by a CytoSpin device and fixed in 4% paraformaldehyde for 10 min. After further washing steps, cells were permeabilized (0.1 % Triton X in PBS, 5 min) and stained with nuclear dye Hoechst33342 (1:1000 dilution) for 20 min. Following further washing steps, unspecific binding was blocked for 30 min using 0.5 % BSA in PBS and staining with fluorescent anti-pan-Cytokeratin-PE antibody (1:200 dilution, overnight) was performed.

2.8 Statistical Analysis

Each experiment was repeated at least three times. Data are shown as means with SD and statistical analysis was performed using GraphPad PRISM for Windows (GraphPad Software v9.1.2.226, San Diego, CA, USA, www.graphpad.com, accessed on 13 July 2021). p-values were reported as significant when * $p \leq 0.05$.

3. Results

3.1 Optimization of Biofunctionalized Beads for Cell Enrichment

The selection of magnetic beads and immobilized antibodies on the bead surface are decisive factors in terms of cell-specific enrichment. First, EpCAM-biotin antibodies were immobilized on the streptavidin-biofunctionalized beads. To identify a proper CTC model to characterize IsoMAG, manual immunomagnetic enrichment of various epithelial cancer cell lines, such as cutaneous squamous cell carcinoma cells (SCL-1, SCL-2), and A431 was

performed (Supplementary Figure S1). We determined the highest recovery rates for EpCAM beads using SCL-1 (85 %, $n = 3$) and A431 cells (100 ± 20 %, $n = 3$). As controls, we were also able to isolate melanoma cells (MV3, BLM) targeting melanoma-associated chondroitin sulfate proteoglycan (MCSP), but not HEK293T (Supplementary Figure S1B). Being an appropriate squamous epithelial-derived model close to HNSCC, we therefore chose to proceed with the characterization of IsoMAG using the combination of EpCAM beads and SCL-1 cells. For this cell line, high expression of epithelial marker EpCAM is described. EpCAM mRNA expression in SCL-1 cells was confirmed on a single cell level using RT-qPCR (Supplementary Figure S2).

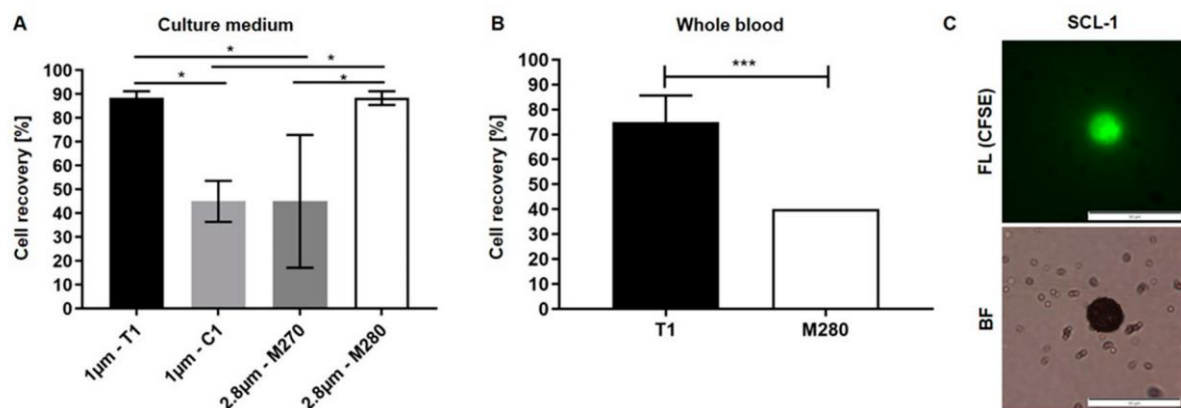


Figure 1. Enrichment of HNSCC cells from cell culture medium (A) and whole blood (B) differs depending on size and type of functionalized magnetic beads. Values are displayed as means of recovered cells using antibody-coupled magnetic beads with specific sizes and surface modifications. Twenty fluorescently labelled SCL-1 cells were spiked into 7.5 mL cell culture medium (A) or 7.5 mL full blood samples (B), and manually enriched by using EpCAM antibody coupled magnetic beads. (A) Welch's t-test, $n = 3$, *: $p < 0.05$ (one-way ANOVA test with Tukey's t-test); (B) Welch's t-test, $n = 6$ (T1), $n = 2$ (M280), ***: $p < 0.002$; (C) recovered, CFSE-stained SCL-1 cells were analyzed by fluorescence microscopy (FL). Corresponding bright-field image (BF) shows beads bound to cell and freely distributed in the medium. Scale bar, 50 μ m.

Since there are numerous commercially available beads with different surface modifications and sizes, the next step was to investigate their potential to enrich EpCAM-positive cells spiked into cell culture medium. In this context, four different types of magnetic beads varying in size and surface properties were tested (Table 1). Therefore, 20 fluorescently labeled SCL-1 cells were spiked into 7.5 mL cell culture medium and functionalized magnetic beads were added. After incubation, these cells were manually enriched with a magnetic separator. We obtained the best recovery rates by using 1 μ m T1 beads and 2.8 μ m M280 beads

(Figure 1A). Using these beads, the cell recovery rate was 88.3 % (± 2.9 % SD) whereas the use of 1 μm C1 or 2.8 μm M270 beads resulted in less than 50 % cell recovery.

Subsequently, the performance of T1 and M280 beads was investigated in blood samples of healthy donors. Again, 20 fluorescently labeled SCL-1 cells were spiked into 7.5 mL blood and were manually enriched using the same protocol. As depicted in Figure 1B, the number of recovered cells is significantly higher using T1 beads compared to M280 beads (75 vs. 40 %). Microscopic analysis of isolated cells in the counting chamber revealed that cells are densely covered by magnetic beads which are also freely distributed in the enrichment medium (Figure 1C).

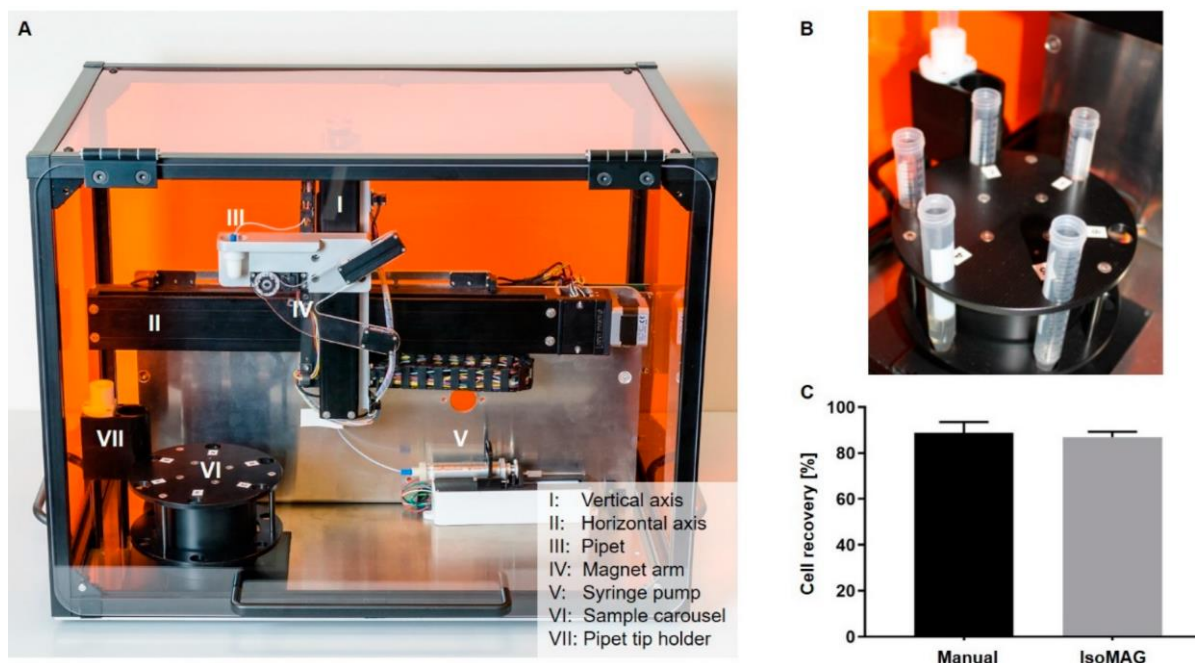


Figure 2. Establishment of automated cell recovery using IsoMAG IMS unit. (A) IsoMAG IMS demonstrator with horizontal and vertical axis driving the pipet unit and magnet arm; (B) the carousel as tube holder for prestorage of sample and wash buffers; (C) 20 fluorescently labelled cells were spiked into 7.5 mL cell culture medium and enriched by using EpCAM antibody coupled T1 (1 μm) magnetic beads. The sample was processed manually or automated using the IsoMAG IMS system. Welch's t-test, $n = 4$, ns: $p > 0.1234$.

Regarding our previous results, T1 beads were chosen for establishment of the automated cell isolation using the IsoMAG IMS demonstrator (Figure 2A). The centerpiece of the benchtop device is a rotatable tube holder carousel with max. 6 reagent slots (Figure 2B). The different positions of the carousel and the 10 mL pipet tip holder to pick up the pipet tip and perform the enrichment are driven by a pipetting robot on a vertical and horizontal axis.

The magnet arm is moveable at a swivel joint to capture bead bound cells and free beads in the pipet tip while reducing the sample volume by discarding the supernatant wash buffers. Macrofluidic sample pipetting is directed pneumatically with a syringe pump. The 7.5 mL starting sample is placed into the first position of the carousel. Positions 2–5 are subsequently filled with washing buffers in a decreasing volume and the assay is initiated in the software on an external computer (for detailed protocol see also Supplementary Table S1).

The results obtained with the IsoMAG IMS unit were directly compared to manually enriched cells with the same batch of magnetic beads. Automated isolation resulted in 86.9 % cell recovery while 88.8 % of the spiked cells could be detected by manual isolation. This means that in our spiking experiments more than 17 out of 20 cells were recovered from a volume of 7.5 mL by both manual enrichment and the fully automated protocol without significant difference. Statistical analysis of recovery rates showed a slightly lower SD of 2.4 % (n = 4) after automated isolation compared to manual enrichment (4.8 % SD; n = 4), indicating a reproducible automation.

3.2 Reduction of Blood Cell Contamination

Besides a robust protocol and an easy-to-handle automated system, it is crucial to reduce the number of “background” WBCs to enable high quality downstream analyses. In preliminary work we already established the basic isolation process, including optimization of necessary washing steps (data not shown). In this study, the automated assay was characterized regarding washing buffers to minimize the unspecific carryover of dual-positive leukocytes [CD45+/RedDot+]. Samples were analyzed by FACS to determine WBC contamination. Gates were set with CD45-PE/RedDot™-stained blood dilution as positive control and stained beads as negative control. The results presented in Figure 3A show that the number of leukocytes after the automated isolation process was about 1200 cells.

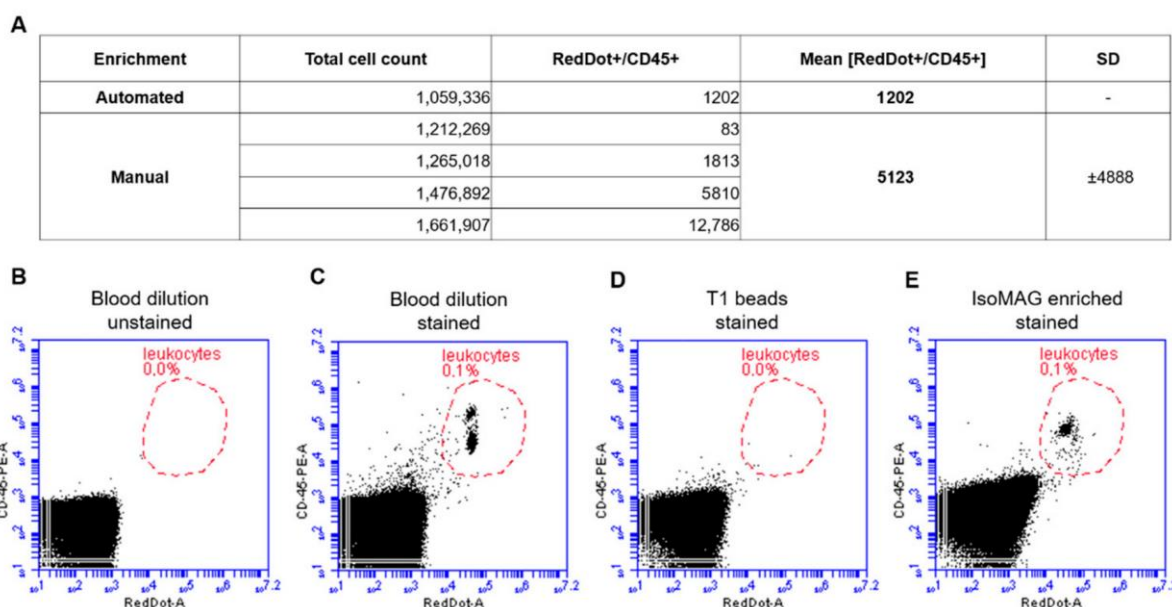


Figure 3. Automated immunomagnetic enrichment procedure exhibits a significantly lower amount of leukocyte contamination compared to manual cell isolation. (A) Summary of enrichment processes and quantification of leukocyte contamination. (B–E) After the automated enrichment process, cells were stained with CD45-PE antibody and nucleic staining reagent RedDot™. Blood dilution (1:1000) shows a dual-positive cell population (B,C). After the enrichment process, this gating was used to quantify the leukocyte contamination (E) while showing no staining of the free beads themselves (D).

Comparable results were achieved after manual enrichment (5123 dual-positive cells). However, we observed a broad scattering of WBC counts with a standard deviation of almost 4900 cells in manually enriched samples. Thus, an automated protocol has been developed considering both a high efficiency of cell recovery as well as a low rate of WBC contamination.

3.3 Automated Enrichment of Head and Neck Cancer Cells

We applied the method to a second cancer entity originating from squamous cell tissue with an epithelial, EpCAM-positive phenotype as proof-of-principle. Thus, enrichment experiments were also performed with an epithelial cell line model derived from head and neck squamous cell carcinoma (HNSCCUM-02T). HNSCCUM-02T cells show high EpCAM expression allowing enrichment with our system (Supplementary Figure S3A).

Automated enrichment (spike-in) experiments with HNSCCUM-02T cells were conducted as described before and demonstrated applicability of the IsoMAG IMS unit using blood

samples, both from healthy donors and patient blood (Figure 4 and Figure 5). In total, 95 % (± 15) of spiked cells were recovered (Figure 4A), quantified by fluorescence microscopy after intracellular staining of epithelial tumor marker pan-cytokeratin (pan-CK) [39] and CD45 (Figure 4B). Isolated tumor cells were identified by expression of cytokeratin [Hoechst+/CD45-/panCK+] and could be differentiated from CD45-positive leukocytes [Hoechst+/CD45+/panCK-] appearing at low frequency after enrichment.

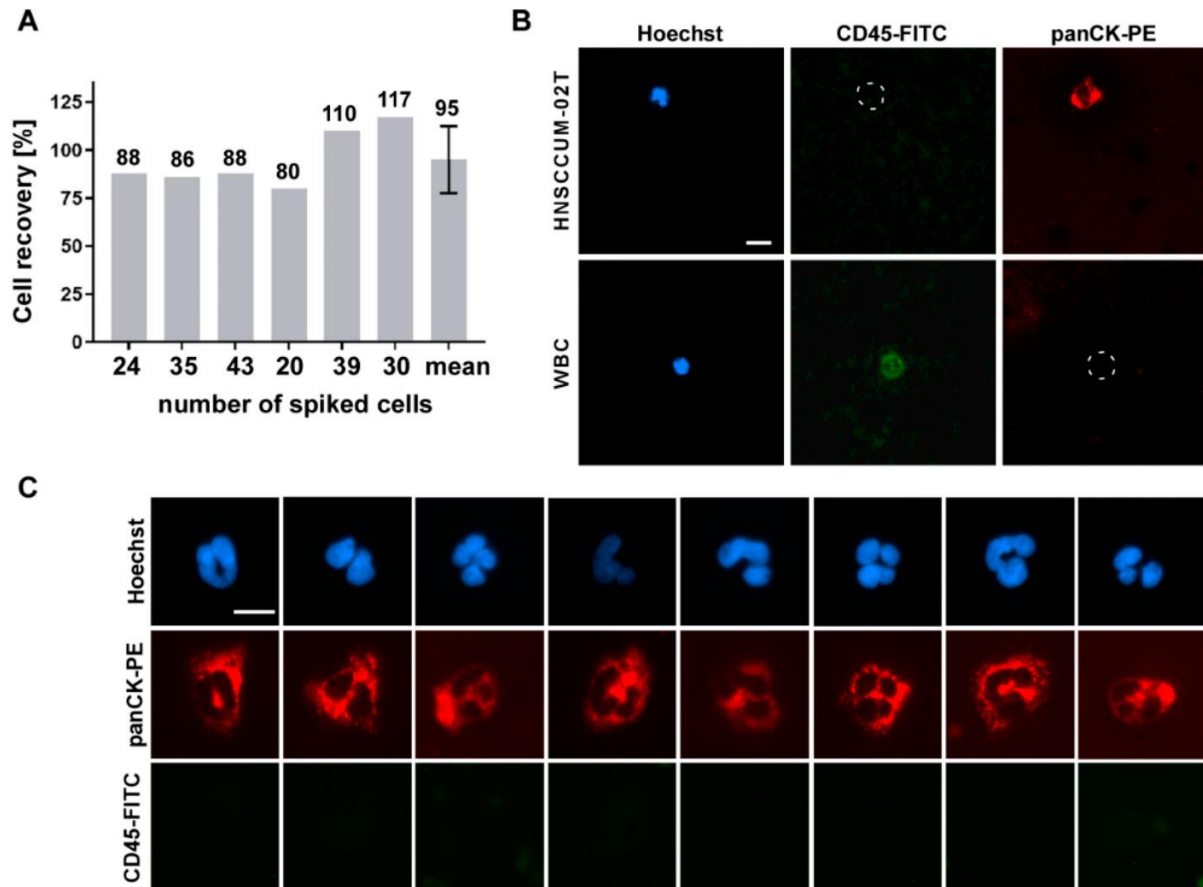


Figure 4. Cell isolation by the IsoMAG System resulted in high recovery rates for head and neck cancer cells. (A) Different numbers of HNSCCUM-02T cells were spiked in blood samples and enriched by EpCAM-coupled T1-beads using the IsoMAG unit. (B) For cell counting, recovered cells were stained with Hoechst dye, cytokeratin (panCK-PE) and CD45-FITC antibodies and quantified by fluorescence microscopy. [Hoechst+/CD45-/panCK+] cells were classified as HNSCCUM-02T cells, [Hoechst+/CD45+/panCK-] cells as leukocytes (WBC). Scale bar, 10 μ m. (C) Examples of cells enriched by CSV-coupled T1-beads. Cells were stained as described in (B). Scale bar, 10 μ m.

As dynamic EMT and MET processes seem to modulate primary tumors, metastases and CTCs disease- and patient-dependently, detection systems allowing the use of variable

CTC/cancer markers are highly desirable. To underline the advantage and full flexibility of our device to also isolate cells by using variable cancer markers, we here targeted cell-surface vimentin (CSV) as an additional proof-of-concept example. As shown in Figure 4C, we performed spike-in experiments using engineered CSV-coupled immunomagnetic beads to isolate HNSCCUM-02T cancer cells from human blood. Expression of CSV was verified by Western blot analysis and immunofluorescent staining (Supplementary Figure S3C,D). Importantly, automated isolation of spiked HNSCCUM-02T cells using CSV-coupled beads also resulted in high recovery rates of $\pm 95\%$ (Figure 4C).

3.4 CTC Screening Using Blood of HNSCC Patients

Finally, three HNSCC patients were screened for CTCs applying our established protocol for the IsoMAG IMS system. The results shown in Figure 5 impressively demonstrate the clinical applicability of the system. All cells positive for cytokeratin but negative for CD45 expression [Hoechst+/CD45-/panCK+] were counted and classified as potential CTCs (Figure 5B). Here, we were able to isolate 74 to 93 potential CTCs with an epithelial-like character from patients suffering from different head–neck tumor subtypes (hypo- and oropharynx cancers with lymph node metastasis, see Figure 5A). We also captured preliminary data on isolation of CTCs out of patient blood using a combination of EpCAM and CSV beads (Supplementary Figure S4). However, these results obtained from a small and heterogeneous group of patients are preliminary and have to be confirmed by larger studies and further analysis methods, e.g., sequencing.

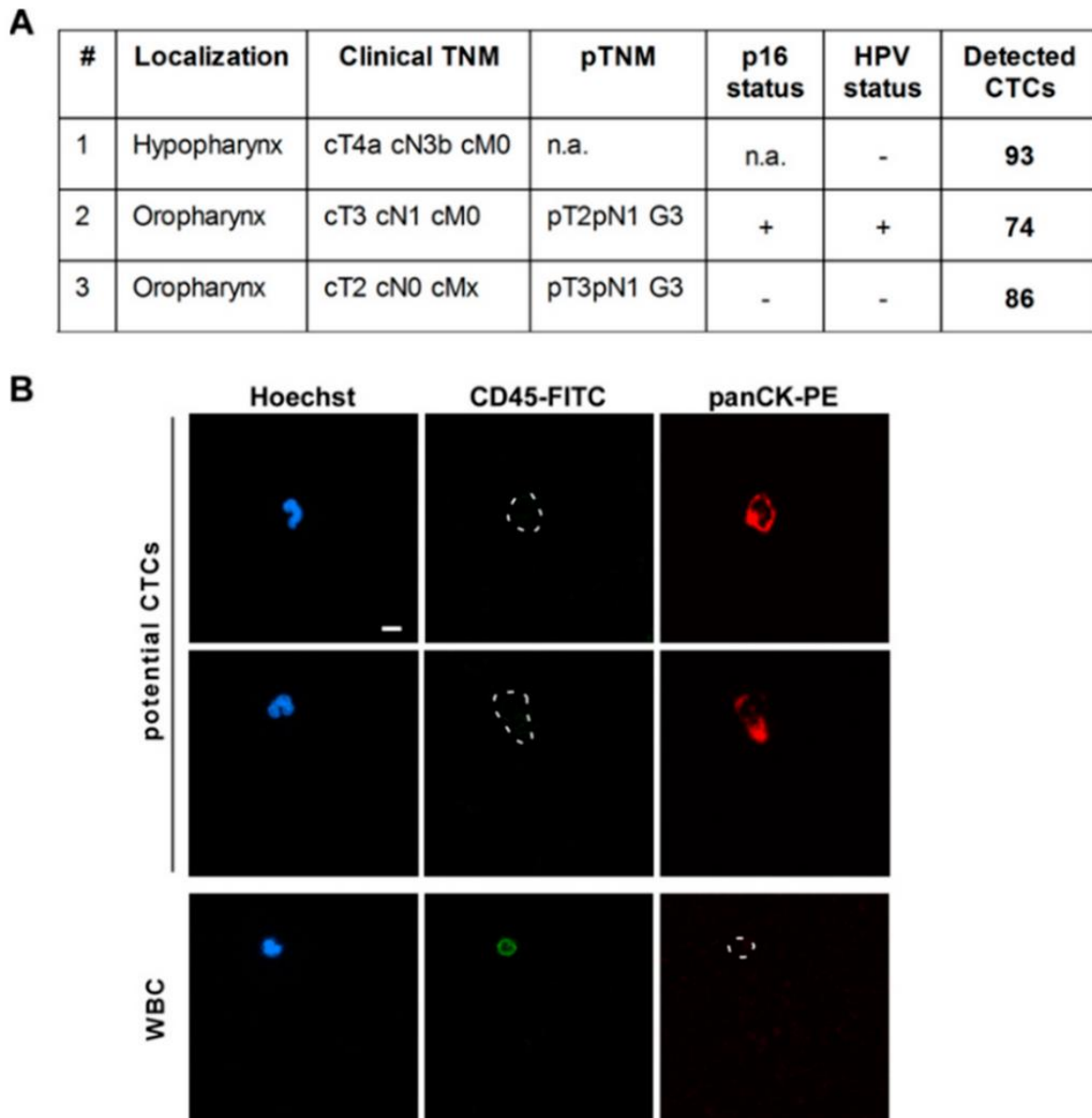


Figure 5. Potential circulating tumor cells (CTCs) could be enriched from head and neck cancer patient blood. (A) Clinical parameters and numbers of detected CTCs for three patients suffering from hypo- or oropharyngeal cancers including lymph node metastases. (B) 7.5 mL of patient blood was mixed with EpCAM-coupled T1 beads and placed into the IsoMAG unit for automatic enrichment of CTCs. For cell counting, enriched cells were stained with Hoechst dye, cytokeratin (panCK-PE), and CD45-FITC antibodies and quantified by fluorescence microscopy. [Hoechst+/CD45-/panCK+] cells were classified as potential CTCs, [Hoechst+/CD45+/panCK-] cells as leukocytes (WBC). Scale bar, 10 μ m.

4. Discussion

Personalized cancer therapy will benefit from analysis of single solid and circulating tumor cells in the future. In order to develop a fully automated system for the enrichment and

isolation of single tumor cells, the reduction in sample volume plays a pivotal role. Thus, excellent performance is required for the enrichment step depending on the developed system but also on the developed protocol.

In the present study, we successfully established a robust protocol for the automated isolation of CTCs by the IsoMAG IMS device, a core unit of the CTCelect platform. As a first step, we developed a suitable CTC model system to establish the protocol for squamous cell carcinoma. Although we also achieved high recovery rates for the epithelial A431 cells, we decided to use SCL-1 and HNSCCUM-02T cell lines as squamous epithelial-derived models close to HNSCC. Of note, we are aware of variable EpCAM expression in “primary CTCs” versus established cancer cell lines. However, for the development and comparison of CTC selection procedures and devices, CTC models with defined EpCAM levels are mandatory. Using this model, we demonstrated improved performance of 1 μm tosyl-activated, hydrophobic magnetic beads (T1) which thus were chosen for our final protocol. In addition to their advantageous characteristics for automated applications, such as a low sedimentation rate and faster reaction kinetics compared to M-280/M-270 beads, our results are in line with other studies showing improved capture efficiency and specificity of 1 μm T1 beads for magnetic cell detection [40,41].

Downstream analyses of isolated cells by fluorescence microscopy not only confirmed expression of relevant cancer markers, but also revealed tight binding of magnetic beads to the cell surface (see also Figure 1C). Regarding the size of the used T1 beads (1 μm) and an average diameter of CTCs between 10–12 μm [28], the surface of a cancer cell could theoretically be covered with 300–450 magnetic beads suggesting severe consequences for cell integrity and viability. However, we observed that isolated CTCs are not completely covered with beads, and preliminary studies revealed that re-attachment and cultivation of isolated cells is not excluded, albeit very challenging (see Supplementary Figure S5). Here, additional washing and bead detachment steps, as well as careful adjustments of cell cultivation, such as the use of preconditioned medium and collagen-coated slides, are necessary to receive viable and proliferating cells. Due to the highly versatile construction and design of the device, it is possible to implement such additional purification steps to the automated IsoMAG protocol. Moreover, the biocompatibility of micro/nanocarriers may be affected by biomolecule corona formation [26,42,43]. It is accepted that when micro/nanocarriers enter physiological environments, proteins and other biomolecules bind to their surfaces, leading to the rapid formation of a biomolecule corona [44]. The corona may be critically co-defining the biological, medical, biotechnological and pathophysiological

identity of micro/nanocarriers, although the mechanistic details have not been resolved in detail [45,46].

As an additional relevant factor, reduction of background white blood cells is mandatory for the establishment of a reliable protocol allowing downstream single-cell analysis. In summary, our study shows that using the optimized protocol for IsoMAG tumor cells from patient samples can be enriched and detected in a semi-automated process combined with a reduction of white blood cells (WBC) starting from a large volume (7.5 mL). The broad scattering of WBC counts we observed could depend on a naturally different blood cell count between healthy individuals. It is conceivable that the WBC count could be a hindrance to nucleic acid-based downstream applications at this point due to enforced background noise. A purity of at least 50 % is recommended for proper genomic analysis, whereas in our small patient screening, a vast percentage of total output cells was WBCs. On an average, we were able to isolate 84 potential CTCs from three patient samples, while EpCAM-based enrichment entailed a bycatch of ~1200 WBCs. Nevertheless, the relatively low number of 10^3 WBCs (compared to 10^7 WBCs/mL in healthy adults) enabled immunofluorescent assessment of the patient isolates and marker-based distinction between potential CTCs and WBCs to deliver a ready-to-use assay in an otorhinolaryngology lab environment. In comparison, a similar WBC bycatch of over 800 cells/sample was described for CellSearch® [47], whereas size-based Parsortix® delivers purity grades ranging from 29–97 % depending on the study [48,49].

To address downstream analysis, subsequent microfluidic cell sorting of the IsoMAG isolates, manual cell picking or aspiration technologies such as the ALS CellCelector™ are appropriate tools to improve signal-to-noise ratio for transcriptomic analysis. We already started implementing IsoMAG in an in-house developed microfluidic single-cell-sorting workflow resulting in a purity of ≥ 75 % (Supplementary Figure S6). By aspirating only dispensed droplets that contain fluorescent cells for RNA isolation, we obtained promising PCR results detecting even small numbers of EpCAM+ tumor cells with low WBC background signal. These findings underline that (immunomagnetic) pre-enrichment of the CTCs by IsoMAG is an indispensable prerequisite for microfluidic cell sorting and downstream CTC analysis.

Interestingly, during protocol establishment we observed cell recovery rates of >100 %. This was likely due to false positive panCK or false negative CD45 staining which has been optimized during establishment. However, our automated protocol combines both a high efficiency of cell recovery as well as a low rate of WBC contamination.

Furthermore, in the presented study we could also show that the established method is adaptable to the detection of EpCAM-, as well as CSV-positive subpopulation of CTCs. Typically, immunomagnetic cell isolation devices use epithelial markers, mostly EpCAM, for CTC detection neglecting the fact that cancer cells undergo morphological changes during epithelial-to-mesenchymal transition (EMT) and the reverse process (MET). Importantly EMT/MET which takes place during entry and transport in the blood stream is accompanied by up- and downregulation of surface markers used for CTC detection, such as EpCAM, N-/E-Cadherine, and cell-surface vimentin [50]. Thus, in contrast to other commercial systems we are able to capture cells exhibiting not only epithelial, but also mesenchymal and/or an intermediate phenotype. Preliminary data combining beads targeting EpCAM as wells as CSV for automated cell enrichment were also promising but have to be confirmed in larger studies to assess the added value of using multiple markers for HNSCC.

In our small patient screening study, we were able to isolate 74 to 93 potential CTCs with the optimized protocol. Previous studies applying different methods for CTCs detection in HNSCC revealed a broad range of enumerated cells. Whereas Grisanti et al. detected 0-2 CTCs in 16-40 % of the patients using the CellSearch® platform [51], manual enumeration of immunofluorescent stained cells resulted in higher CTC numbers (0–37 CTCs/1000 PBMC) [18]. Despite the broad ranges of detected CTCs, the obtained results of our IsoMAG IMS unit are in the order of previous studies combined with low numbers of leukocyte contamination. We could also observe a slight tendency for an increasing CTC number in T4 staged tumors compared to T1–3 as described previously [16,18]. Of course, these results have to be interpreted with caution because the small number of patients does not allow reliable assessment. This observation and the fact that a high mortality rate of HNSCC patients correlates to late diagnosis show the necessity of an early and reliable detection method of CTCs. Semi-automated detection of CTCs such as IsoMAG has the potential to be related as a standardized part of liquid biopsy with the advantages of real-time personalized analysis in combination with non-invasiveness and individual prognostic therapy [15].

Taken together, there are several findings of this study underlining the advantages of the IsoMAG device compared to other immunomagnetic isolation methods. Whereas CellSearch® is marketed relying only on epithelial targeting of preserved cells in the CELLTRACKS® AUTOPREP® System and requires centrifugation [52], the IsoMAG protocol allows highly flexible targeting of viable CTCs without blood pre-processing. Implementation into the CTCelect workflow in future will allow downstream single-cell analysis and cell cultivation. The general major advantage of automated cell isolation in contrast to manual

enrichment consists of standardizing protocols and preventing human errors while reducing costs and hands-on time. Commercial magnetic cell separation devices, i.e., an autoMACS® Separator (Miltenyi Biotec, Bergisch Gladbach, Germany) were strongly improved over the last few years but were mostly marketed to isolate abundant cell populations, rather than rare cells such as CTCs. With regard to the long-term goal of a low-cost diagnostic test, IsoMAG was characterized with in-house functionalized EpCAM beads minimizing material expenses to 35 EUR per 7.5 mL blood compared to 102 EUR for Miltenyi StraightFrom® Whole Blood CD326 MicroBeads. Conclusively, the overall aim of our study is the implementation of IsoMAG IMS unit as a core unit of the CTCelect for the fully automated isolation of single CTCs without sample preparation. Due to urgently needed low cost minimally invasive diagnostics methods in the clinical routine, allowing the sensitive and reliable detection of tumor components in patients' blood, the establishment of our IsoMAG IMS unit of CTCelect also represents a technology for single cell isolation and comprehensive downstream "omics"-based analyses. Such approaches will deepen our understanding of CTC pathobiology, a prerequisite for improved treatments and management of cancer patients in the future.

5. Conclusions

Here, the automated IsoMAG IMS unit was thoroughly characterized as a reliable, economic, and straightforward technology for automated and reproducible CTC detection and enrichment. In addition, the IsoMAG IMS system was shown to allow the use of variable cancer/CTC markers, such as cell surface vimentin. Its flexibility can be tailored to the user's specific needs for various malignancies and/or cell types. Future developments aim to combine immunomagnetic separation with microfluidic devices to further improve the power of automated immunomagnetic cell isolation devices for research and the clinics.

2.2 Paper 2

Received: 14 October 2021 | Revised: 14 December 2021 | Accepted: 24 December 2021

DOI: 10.1002/elsc.202100133

Engineering

in Life Sciences

RESEARCH ARTICLE

Characterization of a novel microfluidic platform for the isolation of rare single cells to enable CTC analysis from head and neck squamous cell carcinoma patients

Janis Stiefel¹ | Christian Freese¹ | Ashwin Sriram² | Sabine Alebrand¹ |
Nalini Srinivas² | Christoph Sproll³ | Madita Wandrey⁴ | Désirée Gül⁴ |
Jan Hagemann⁴ | Jürgen C. Becker² | Michael Baßler¹

¹Fraunhofer Institute for Microengineering and Microsystems IMM, Mainz, Germany

²Translational Skin Cancer Research, DKTK Partner Site Essen/Düsseldorf, West German Cancer Center, Dermatology, University Duisburg-Essen, Essen, Germany; German Cancer Research Center (DKFZ), Heidelberg, Germany

³Clinic for Oral and Maxillofacial Surgery, Düsseldorf University Hospital, Heinrich-Heine-University, Düsseldorf, Germany

⁴Department of Otorhinolaryngology/ENT, University Medical Center, Mainz, Germany

Abstract

Detailed examination of tumor components is leading-edge to establish personalized cancer therapy. Accompanying research on cell-free DNA, the cell count of circulating tumor cells (CTCs) in patient blood is seen as a crucial prognostic factor. The potential of CTC analysis is further not limited to the determination of the overall survival rate but sheds light on understanding inter- and intratumoral heterogeneity. In this regard, commercial CTC isolation devices combining an efficient enrichment of rare cells with a droplet deposition of single cells for downstream analysis are highly appreciated. The Liquid biopsy platform CTCelect was developed to realize a fully-automated enrichment and single cell dispensing of CTCs from whole blood without pre-processing. We characterized each process step with two different carcinoma cell lines demonstrating up to 87 % enrichment (n = 10) with EpCAM coupled immunomagnetic beads, 73 % optical detection and dispensing efficiency (n = 5). 40 to 56.7 % of cells were recovered after complete isolation from 7.5 mL untreated whole blood (n = 6). In this study, CTCelect enabled automated dispensing of single circulating tumor cells from HNSCC patient samples, qPCR-based confirmation of tumor-related biomarkers and immunostaining. Finally, the platform was compared to commercial CTC isolation technologies to highlight advantages and limitations of CTCelect. This system offers new possibilities for single cell screening in cancer diagnostics, individual therapy approaches and real-time monitoring.

1. Introduction

In the field of liquid biopsy, research on circulating tumor DNA (ctDNA) combined with the detection and analysis of circulating tumor cells (CTCs) has developed into an auspicious minimal invasive tool for the early detection in personalized medicine for tumor patients [1]. Due to the fact that CTCs play an important role in cancer metastasis as the main cause of tumor death, the number of CTCs in a blood sample is considered an independent prognostic factor for the overall survival [2]. In addition to the CTC count particularly on the hunt for the primary tumor in early stage cancer, CTC analysis refines the selection, adaptation and even development of therapies. Although the overall principle of complex metastasis, from the intravasation of CTCs into the circulatory system, arrest and extravasation through vascular walls into distant tissues to the final proliferation of cells to micrometastases, is understood, future intensive study on CTCs and their subtypes will result in much deeper knowledge of these multifaceted processes. Recent studies show that the characterization of CTCs and their subpopulations, that is, disseminated tumor cells (DTC), metastasis-initiating cells and even dual-positive cells (CD45+/EpCAM+) helps to understand the metastatic behavior of tumors and to deduce prognostic predictions and diagnostic statements [3, 4].

When developing isolation technologies for these cells, their rarity in a blood sample is the biggest hurdle to overcome. Besides billions of healthy blood cells, only one to hundreds tumor-associated cells can be found per mL blood [1]. Systems that are able to enrich CTCs from blood well-balanced between sensitivity and specificity, are therefore highly appreciated. In addition to the enrichment, such systems should exhibit a high capture efficiency, high isolation purity, and ideally the ability to handle a high sample volume in the shortest time possible [5].

Available techniques are based on two major principles: physical methods such as filtration and density dependent techniques or biochemical immuno-affinity dependent methods using ligand-surface interactions with bound antibodies or antibody-bound magnetic beads for the enrichment of CTCs.

The CellSearch system (Menarini Silicon Biosystems) uses magnetic beads that are biofunctionalized against epitopes of tumor-associated EpCAM (Epithelial cell adhesion molecule) to enrich CTCs from patient blood [6, 7]. It has been established to correlate the number of isolated EpCAM+ cells in a blood sample with the overall survival prediction of breast cancer, metastatic colorectal cancer and prostate cancer patients [8-10].

Nevertheless, CTC research in other cancer entities like head and neck squamous cell carcinoma (HNSCC) remains comparably stagnant. With an annual incidence of almost a million new cases and 450,000 deaths worldwide, HNSCC ranks however the fifth most common cancer [11]. Besides carcinogenic polymorph dispositions, smoking, alcohol abuse, and an infection with human papillomavirus correlate with head and neck cancers [12]. In two third of HNSCC patients, initial diagnosis of the primary tumor goes hand in hand with the discovery of adjacent metastatic lymph nodes [13]. Increased mortality is associated with the abundant presence of micrometastases, whereas the 5-year survival rate of patients with distant metastatic sites sinks below 35 % [14]. HNSCC cells that undergo epithelial-mesenchymal transition (EMT) deregulate epithelial characteristics like cell adhesion and enhance invasive migration. EMT is a dynamic reversible process correlating with the development of stem cell properties and fostering metastasis. This fact stresses the importance of an in-depth understanding of metastatic metabolisms, including the heterogeneity of disease-driving CTCs, to pave the way for innovative therapeutics.

PRACTICAL APPLICATION

Still today standardized therapeutic guidelines like relatively broadband chemotherapy are followed depending on the primary tumor entity neglecting the metastatic profile of systemic cancer. On the downside, disseminated and circulating tumor cells of many cancers show intratumoral heterogeneity and cause disease relapse years after surgery. Hence, easy-to-use platforms, like the show-cased CTCelect device, to isolate these rare cells in a completely automated way and analyze them on a single cell level will be of high significance as predictive measures for therapeutic success to accompany cancer treatment. The microfluidic chip-based cell sorting unit was implemented into a one-step device for user-friendly handling. Studies with the system could therefore directly provide new insights both in therapy monitoring as clinical application and in basic research of tumor biology to unravel metastatic processes.

The aim of the present work was to characterize a fully-automated system in detail which is customizable for any tumor type with a reliable capture rate and CTC purity facilitating access to molecular diagnostics. The presented CTCelect system combines immunomagnetic enrichment from 7.5 mL whole blood, microfluidic fluorescence-activated cell sorting (μ CS) and single cell dispensing through a microfluidic disposable cartridge independently of the tumor entity (Figure 1) in one fully-automated benchtop device. This study aimed to evaluate the functionality and the diverse applicability of CTCelect by means of cutaneous squamous cell carcinoma and mamma carcinoma cell line models and to present data of dispensed single tumor cells from HNSCC patient blood.

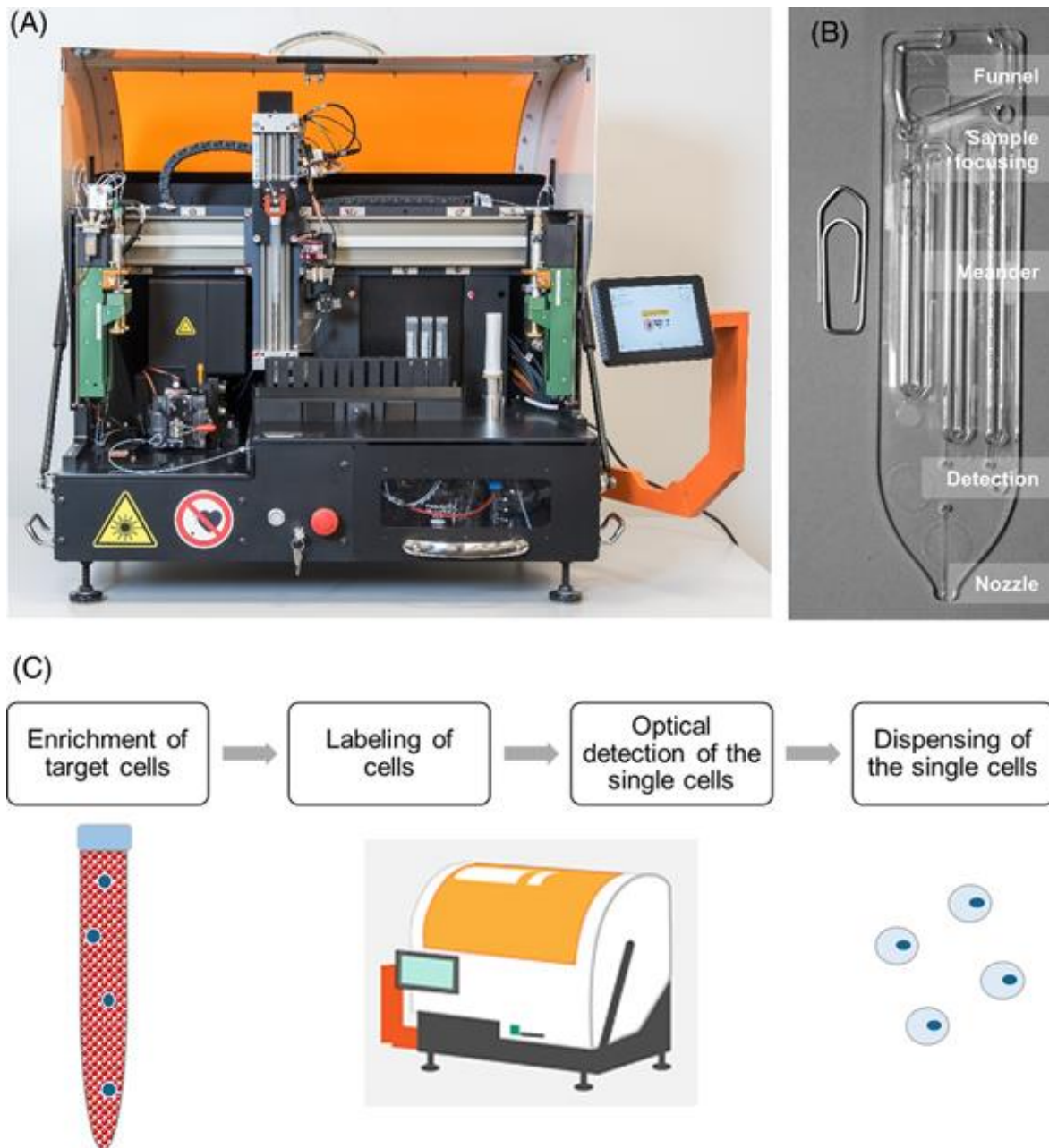


Figure 1. CTCelect system, microfluidic chip and process conception. (A) The benchtop device consists of an immunomagnetic enrichment module (right-sided) and a microfluidic fluorescence-activated cell sorting (μ CS) subunit (left-sided). The fully-automated isolation process is user-controlled via touchscreen. Sample handling and transfer is managed by a pipetting robot. (B) The CTCelect chip is placed in the chip holder of the cell sorting subunit and disposed after isolation. The chip consists of a reservoir funnel for the cell suspension, a hydrodynamic focusing channel, a detection zone and a nozzle for cell dispensing. (C) CTCelect concept for single cell dispensing from 7.5 mL samples.

2. Materials and Methods

If not otherwise indicated, reagents and supplements were purchased at Thermo Fisher Scientific, Darmstadt, DE.

2.1 Cell lines

MCF-7 breast cancer cells were purchased from AdnaGen (Langenhagen, DE) and cultured in RPMI1640 medium with L-glutamine (Capricorn Scientific, Ebsdorfergrund, DE) supplemented with 10 % fetal calf serum (FCS; Merck, Darmstadt, DE). The SCL-1 squamous cell carcinoma line was kindly provided by Dr. Petra Boukamp (DKFZ, Heidelberg, DE) [15] and cultured in Gibco DMEM (low glucose, pyruvate) medium supplemented with 10 % FCS. Cell lines were split at subconfluence and incubated at 37°C in a humidified atmosphere in the presence of 5 % CO₂.

2.2 Blood samples

Whole blood bags from healthy donors were obtained from the local Blood Transfusion Center (University Medical Center Mainz, DE) in 500 mL CompoFlex blood bags (Fresenius Kabi, Bad Homburg, DE) with CPD-1 anticoagulant and stored at room temperature for a maximum of three days. Patient samples were collected at the Tumor Center of Western Germany (University Hospital Essen, DE) from a HNSCC patient with increasing metastasis in adjacent lymph nodes (pTNM staging: pT2pN3b), at the Department of Otorhinolaryngology/ENT, (University Medical Center Mainz, DE; pTNM staging n.a.) and processed within 24 h after blood draw. Informed consent was obtained from the patients and approved by the ethical committee vote at the Medical Faculty of the Heinrich-Heine-University Düsseldorf (ref.no. 3090; 2016) and by the local ethics committee in Mainz (ref.no. 837.485.15 (10253); 2016).

2.3 Immobilization of biotinylated antibodies on streptavidin coupled magnetic microbeads

The immunomagnetic separation (IMS) of CTCs from whole blood required tumor-specific coating of immunomagnetic beads with biotinylated monoclonal mouse anti-human EpCAM (CD326; 20 µg/mL) antibody 1B7. Various beads with different sizes ranging from 1 to 4.5 µm diameter and different surface properties (tosyl-activated, hydrophobic; carboxylic acid, hydrophilic) were tested with SCL-1 cells in our preliminary work and the herein used

Invitrogen Dynabeads MyOne Streptavidin T1 (10 mg/mL) with a binding capacity of 400 pmol biotinylated peptides per mg beads enabled the best recovery rates in our setting. These microbeads indicate a low sedimentation rate and high binding capacity due to their small diameter and are hence ideal for automated enrichment. EpCAM antibody was immobilized on the bead surface with an extended incubation time of 1 hour. After immobilization, magnetic beads were added a saturated biotin/PBS solution for 30 min with gentle rotation of the tube to block free streptavidin binding sites and prevent clumping. After an additional washing step, anti-EpCAM magnetic beads (hereinafter abbreviated as EpCAM beads) were stored in PBS/0.1 % BSA at 4 °C for several weeks.

2.4 Determination of CTCelect recovery rates of cultured tumor cells

To evaluate the CTCelect enrichment efficacy, recovery rates of cultured tumor cells after automated IMS from medium and whole blood were determined. Robust cancer cell models were required and MCF-7 and SCL-1 cells are a suitable candidate for immunomagnetic enrichment to prevalidate the functionality of the platform. We tested both cell lines to have high EpCAM expression (see Supporting Information S1). Cells were stained using the CellTrace CFSE Cell Proliferation Kit (CFSE) according to the manufacturer instructions. 15 mL sized ROTILABO centrifuge tubes without rim (Carl Roth, Karlsruhe, DE) are most suitable for the tube holder of CTCelect and were used in all the experiments. Culture medium or whole blood from healthy donors was aliquoted in volumes of 7.55 mL medium or 7.5 mL blood and spiked with different numbers of stained tumor cells, respectively (tube I). 100 µl EpCAM beads (1 mg) were added to medium samples, blood samples contained 150 µl EpCAM beads (1.5 mg), both resulting in a total volume of 7.65 mL and a final beads concentration of 0.13 - 0.2 mg/mL. Subsequently, tubes II, III and IV were prepared with 5 mL buffer 1 (PBS/20 % FCS, 2 mM EDTA) and two tubes (V-VI) were filled with 0.5 mL buffer 2 (PBS/0.1 % BSA, 2 mM EDTA).

To start the automated enrichment, tubes I-VI and a 10 mL pipet tip were placed in the holders of the CTCelect device as described in Table 1 and the process was initiated on the touchscreen. Before moving on to the next tube, each washing step was alternated with magnetic capture of bead-bound tumor cells and residual beads in the pipet tip (see Supp. S2). The processed samples were manually separated in a magnet separator for evaluation purposes. Supernatant buffer was discarded and the bead cell pellet was resuspended in 50 µl PBS. CTC counts were determined in a Neubauer counting chamber using fluorescence microscopy.

Table 1. Automation process of the complete CTCelect single cell isolation

Process	Location	Volume [mL]	Contents	Description (Duration)
IMS	Tube I	7.65	Spiked medium/whole blood; immuno-magnetic beads	Incubation (30 min) with gentle mixing
Washing	Tube II	5	Buffer 1	Wash off beads-cell complexes; leukocyte reduction
	Tube III	5		
	Tube IV	5		
Staining	Tube V	0.3	Buffer 2	Ab staining, volume reduction
Transfer	Tube VI	0.3	Transfer buffer	Transfer to <i>CTCelect</i> chip
Reservoir	Tube VII	0.5	Transfer buffer	Overlay on residual sample
μ CS	<i>CTCelect</i> chip	0.25 max	Transfer buffer/PBS	Laser-based detection; Single cell dispensing

2.5 Automated CTCelect single cell isolation of cultured tumor cells and CTCs from patient blood

Fully-automated CTCelect single cell isolation was evaluated with cultured tumor cells from medium and whole blood (2.5.a). The automated workflow is depicted in Figure 1C. Further, potential CTCs from HNSCC patient blood were isolated by means of the CTCelect single cell dispensing unit after manual pre-enrichment using detachable beads (2.5.b) and complete isolation (2.5.c). Experiments were performed at different sites in Germany which was easily manageable because both sites have their own CTCelect device to address time-sensitivity. In total, the team built three devices.

- a. The functionality of the developed assay was confirmed with spike-in experiments using intracellular CFSE dye. 20 CFSE pre-stained tumor cells were added to 7.55 mL medium or 7.5 mL whole blood from healthy donors.
- b. To confirm epithelial/pEMT origin of HNSCC cells from patient blood, single cell dispensing was investigated after manual pre-enrichment from peripheral blood using detachable Invitrogen™ CELLection™ Epithelial Enrich anti-CD326 and -CD51, -CD61, -CD106 immunomagnetic beads (Miltenyi Biotec, Bergisch Gladbach, DE) combined with phycoerythrin-coupled monoclonal CD326 and CD51 antibody (EpCAM-PE Ab/Integrin α -V-PE Ab; both Biolegend, Koblenz, DE). Pre-enrichment was performed manually to detach the beads from the cells. The respective research group has access

to downstream NGS technologies that is, Nanostring, 10x Genomics that require bead-free cells after single cell dispensing.

- c. Complete single cell isolation was verified with 7.5 mL actual patient blood with EpCAM-PE Ab 1B7 (1:30 in buffer 2). Single cell isolation was performed as described in Table 1 and outlined in Figure 2A.

The enriched and labeled sample was then transferred to the disposable CTCelect chip with a final volume of 300 μ L in the chip reservoir. Similar to a conventional flow cytometer, the CTCelect cell detection is based on the principle of hydrodynamic focusing and optical fluorescence detection (Figure 2B). Microfluidic handling of the chip was managed with a system of two syringes directing sample and sheath flow. The sample flow consisted of a self-formulated transfer buffer, while sheath flow and dispenser were supplied with PBS. The maximum sample volume (250 μ l) was loaded in the chip meander and μ CS was initiated by the CTCelect software for the first measurement. Fluorescent cells were dispensed in the cavities of a 96-well plate if matching the given real-time peak analysis criteria of the fluorescence detection algorithm. Subsequently, 500 μ L transfer buffer was pipetted from tube VII to the chip funnel to overlay the residual 50 μ L sample and to avoid air bubble formation in the chip channels. The rest of the sample was then loaded in the chip for a second measurement cycle. Dispensed single cell droplets on the 96-well plate were evaluated using fluorescence microscopy (10x objective) in the FITC and TRITC channel or RT-qPCR.

2.6 Characterization of blood cell contamination in CTC enriched samples

Especially on single cell level, white blood cell (WBC) contamination in tumor cell isolates complicates molecular downstream analyses. The number of CD45+ WBCs after IMS was determined by flow cytometry. Wash buffers were prepared and placed in the tube holder of the CTCelect device as described in Table 1 and 150 μ L EpCAM beads were added to 7.5 mL whole blood before initiating automated IMS. The final sample was separated in a magnet separator. The supernatant was discarded and the bead cell pellet was stained with CD45-FITC Ab solution (diluted 1:5 in buffer 2; BD Biosciences, Franklin Lakes, USA). Flow cytometry was performed using the BD Accuri C6 flow cytometer. Gates were set with CD45-FITC stained beads as negative control and peripheral blood mononuclear cells (PBMCs) from a buffy coat as positive control (see Supp. S3). CD45+ cell counts after IMS were obtained from two samples of different healthy donors and the average WBC contamination with standard deviation (SD) was calculated.

2.7 Single cell RT-qPCR of isolated CTCs

To confirm the CTC/DTC transcriptomic character in the single cell isolates from HNSCC patient blood, two-step real time quantitative PCR (RT-qPCR) of target RNAs for EpCAM, Integrin α -V and Stratifin was performed. β -actin (RPLP0) served as housekeeping RNA control. RNA was extracted from dispensed droplets immediately after CTCselect isolation using a single cell RNA purification kit (GenElute, Merck, DE) and reverse transcribed with the Invitrogen SuperScript double stranded cDNA synthesis kit. qPCR was conducted in triplicates (Invitrogen™ SYBR Green PCR Master Mix) on a single cell cDNA per well in a 384 well cycler (BioRad CFX384 Touch Real-Time PCR Detection System, Feldkirchen, DE) and individual threshold cycle values (CT) were obtained. Relative mRNA expression was calculated using the Δ CT method. Primer sequences are available upon request.

2.8 Immunostaining of isolated CTCs

CTCselect single cell isolates were pooled together to assess tumor origin of the isolated cells using immunostaining. The sample was stained with fluorescent CD45-FITC antibody (1:1000; BD Biosciences, Franklin Lakes, USA) to label leukocytes. Subsequently, the sample was resuspended in EndoPrime medium (Capricorn Scientific, Ebsdorfergrund, DE) and transferred to an ibidi 8-well slide to set overnight. Cells were centrifuged to the bottom of the slide by a CytoSpin device (300 x g, 10 min) and fixed by using 4 % paraformaldehyde for 15 minutes. After further washing steps, cells were permeabilized (0.1 % Triton X in PBS, 5 minutes) and stained with nuclear dye Hoechst33342 (1:1000) for 20 min. Alternated with several washing steps, unspecific binding was blocked for 30 min using 0.5 % BSA in PBS and the sample was incubated with polyclonal anti-Zonula occludens-1 primary antibody 40–2200 (ZO-1; 1:200, 1 h) and anti-rabbit Alexa Fluor 633 secondary antibody (1:500, 1h).

2.9 Statistical analyses

Each experiment was repeated at least three times. Data is depicted as means with SD and statistical analysis was done using GraphPad PRISM 8.2.0 for Windows (GraphPad Software, San Diego, California USA, www.graphpad.com). P values of two-tailed unpaired t-tests were reported as not significant (ns) when $P^{ns} > 0.05$ and as significant when $P^* \leq 0.05$.

3. Results

3.1 CTSelect enrichment performance

The functionality of the CTSelect enrichment unit was investigated by spike-in experiments with different tumor cell lines in culture medium. 7.55 mL medium aliquots were spiked with 10, 25, and 50 CFSE-stained breast cancer cells (MCF-7) or squamous cell carcinoma cells (SCL-1). EpCAM beads were added and the samples were processed in the CTSelect enrichment unit with the above described protocol (Table 1). After evaluating the device functionality in culture medium, comparable experiments were performed in 7.5 mL whole blood from healthy donors. Following the protocol, all buffers were placed in the device and the enrichment assay was started. Samples were automatically enriched and washed from blood components, subsequently (Figure 3D).

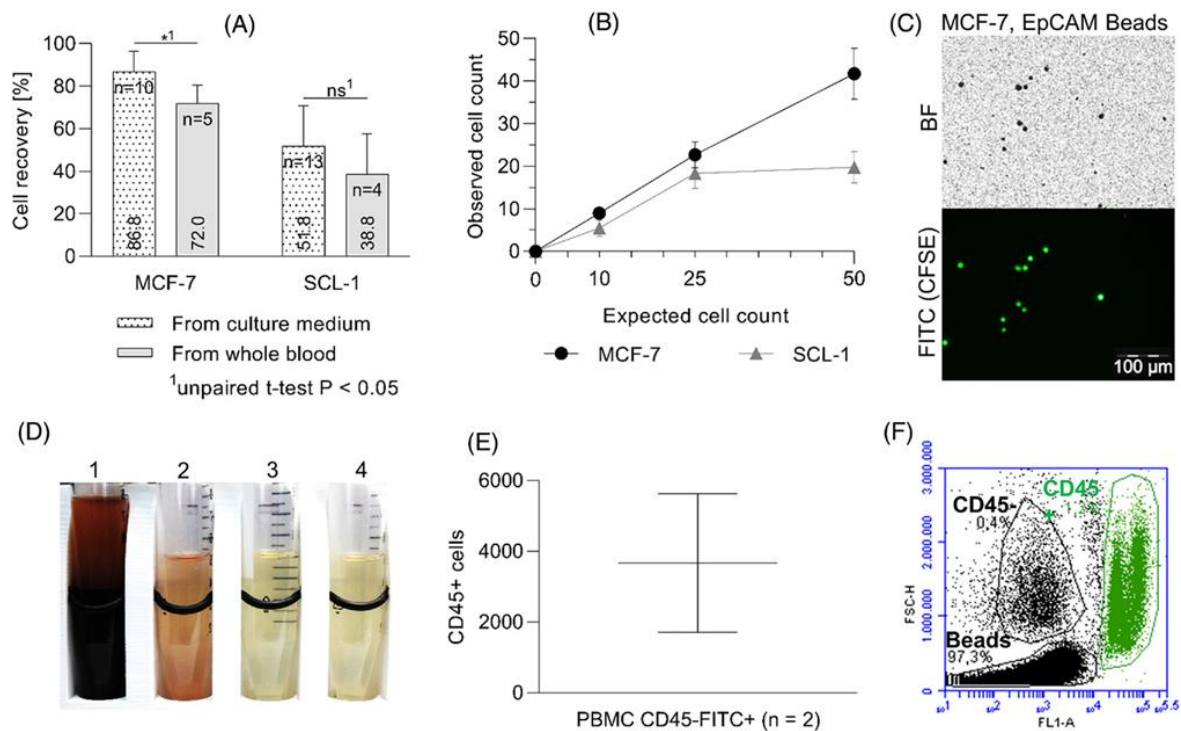


Figure 3. CTSelect enrichment performance. (A) Recovery rates of MCF-7 and SCL-1 cells after automated IMS from culture medium (black dotted) and whole blood (gray). 10 to 50 cells were spiked into the samples, respectively. Cells were stained with CFSE and enriched with 1 μ m EpCAM Beads. Recovery rates of all experiments were averaged and are shown as means with SD and statistical analysis using a two-tailed unpaired t-test $P < 0.05$. (B) Observed MCF-7 (black circles) and SCL-1 (gray triangles) cell counts after CTSelect enrichment from medium were plotted as means with SD against the expected cell count ($n \geq 3$). (C) Bright field (BF) and fluorescence microscopy of CFSE stained and EpCAM bead-bound single MCF-7 cells (scale bar: 100 μ m). (D) Blood residues (1) and wash buffers with blood component waste (2-4) of subsequent CTSelect enrichment process steps in

a magnetic separator. In this case almost no loss of sample/beads occurred. Otherwise, beads would be visible as brown accumulations on the backside of the tube. (E) Cell count of CD45+ blood cell contamination after CTCselect enrichment with EpCAM beads from 7.5 mL donor blood. Contamination was determined via flow cytometry with CD45-FITC Ab staining. (F) Flow cytometry data of a 7.5 mL blood sample after CTCselect enrichment. The scatter plot shows green fluorescence (FL1) on the x-axis against forward scatter (FSC) particle size on the y-axis. Populations of beads, CD45- and CD45+ cells (green) are distinguished in circles.

Cell counts after CTCselect enrichment were determined visually using fluorescence microscopy. Intact cells were identified as round-shaped, green fluorescing objects with a bead-bound surface (Figure 3C). MCF-7 cells were automatically enriched with an $86.8 \pm 9.7\%$ recovery rate from medium and with $72 \pm 8.4\%$ from whole blood, hence the enrichment efficacy from blood was lower than from culture medium with only minor significance ($P^* = 0.0122$).

Further, $51.8 \pm 18.9\%$ of SCL-1 cells were recaptured from medium and $38.8 \pm 18.9\%$ from donor blood after automated IMS with EpCAM beads, meaning enrichment efficacy between blood and medium was not significantly different ($P^{ns} = 0.2437$). The mean recovery rates of all experiments are shown in dependency of the cell line, respectively (Figure 3A). Observed cell counts after CTCselect enrichment from medium were plotted against the expected cell count of 10, 25 and 50 spiked cells and summarized in Figure 3B. Recovery rates of MCF-7 cells showed a nearly linear correlation, independently of the expected cell count between 10 to 50 cells. Up to 25 expected cells, automated recovery of SCL-1 cells followed a similar stable linearity but resulted in a flattened curve at an expected cell count above 25 cells input. Less than half of 50 spiked SCL-1 cells could be automatically enriched with EpCAM beads.

As blood cell contamination is a disruptive factor for CTC downstream molecular analyzes, the reduction of CD45+ PBMCs in CTC enriched samples was determined additionally. Therefore, processed blood samples were stained with CD45-FITC Ab after automated CTCselect enrichment from 7.5 mL donor whole blood. On average, 3,665 counts of PBMCs were measured in a total volume of 300 μ L via flow cytometry (Figure 3E-F; population indicated in green). Comparing to the CD45+ cell count in blood sample #1 ($19 \cdot 10^6$ CD45+ cells; data not shown), the number of CD45+ cells was significantly reduced using the CTCselect enrichment.

3.2 Automated single cell isolation from culture medium and donor blood

Complete automated single cell isolation was evaluated by means of spike-in experiments of 20 MCF-7 and SCL-1 cells in culture medium and whole blood from healthy donors. CTCelect device functionality was confirmed using CFSE staining according to Table 1. Regarding the MCF-7 cell line model with CFSE dye, 58.3 ± 15.3 % of single cells were counted after isolation from culture medium and 56.7 ± 19 % were detected after isolation from whole blood with comparable recovery efficiency. With the same experimental setup, SCL-1 cells were automatically isolated at rates of 56.7 ± 18.9 % (medium) and 40.0 ± 5.0 % (whole blood) recovery (Figure 4A). No significant differences in enrichment efficiencies between 'from medium' or 'from donor blood' is seen for both SCL-1 ($P^{\text{ns}} = 0.1807$) and MCF-7 cells ($P^{\text{ns}} = 0.8870$).

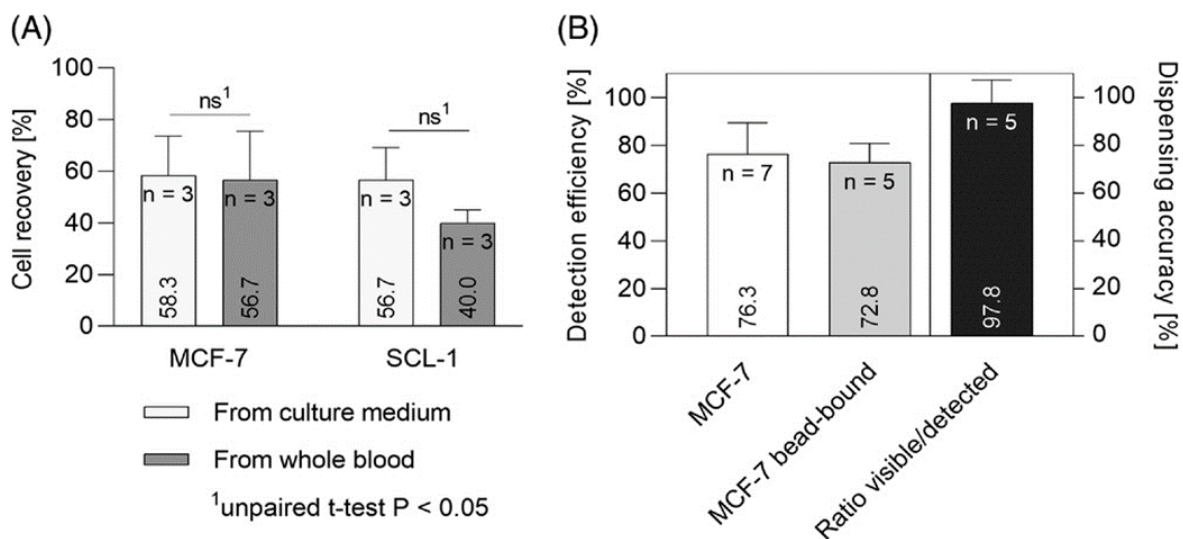


Figure 4. CTCElect single cell detection, dispensing and isolation from 7.5 mL samples. (A) Recovery rates of MCF-7 and SCL-1 cells after automated single cell isolation from culture medium (light gray) and whole blood (dark gray). 20 CFSE stained cells were spiked into 7.5 mL samples and incubated with $1 \mu\text{m}$ EpCAM beads. Pre-enriched cells were automatically singularized and dispensed in droplets after μCS in the CTCElect chip. Recovery rates of all experiments were determined with fluorescence microscopy of the droplets and are displayed as means \pm SD (ns; two-tailed unpaired t-test $P < 0.05$). **(B)** Detection efficiency and dispensing accuracy of CTCElect μCS . 50 CFSE stained, unbound and bead-bound MCF-7 cells were directly spiked in the CTCElect chip for single cell isolation. Droplets were microscopically screened for single cells and detection efficiency was averaged by the observed cell count in dependency of the spiked cell number. Dispensing accuracy was calculated dividing the actual number of visible cells in the droplets by the number of events detected by the software.

More specifically detailed, the detection efficiency and dispensing accuracy of the peak analysis software and microfluidic dispensing through the chip was investigated (Figure 4B), Direct processing of CFSE stained MCF-7 cells led to visible detection of 76.3 % unbound cells and 72.8 % bead-bound cells without significant difference. Furthermore, a very high dispensing accuracy of 97.8 % was determined as the ratio between visible bead-bound cells in the droplets and the detected events in the software, respectively. The microfluidic parameters and flow properties of single cells were intensively studied in our preliminary work to set the dispensing criteria (data not shown).

3.3 Verification of epithelial/pEMT origin of HNSCC cells from patient blood

Tumor-specific single cell dispensing was investigated in peripheral blood of HNSCC patients. According to method 2.5 b), manual immunomagnetic enrichment was performed with EpCAM beads for pre-EMT CTCs and Integrin α -V, CD61, CD106 beads for partial/post-EMT CTCs. Pre-enriched samples were then detached from the beads and labeled with either EpCAM-PE or Integrin α -V-PE staining (Figure 5A). In this patient, 30 EpCAM+ CTCs and 20 CD51+ CTCs were detected in 7.5 mL blood with fluorescence microscopy, respectively. Pre-enriched and labeled samples were pipetted in the CTCelect chip and then automatically processed for single cell isolation in droplets (Figure 5B).

The successful single CTC isolation from patient blood by means of the microfluidic CTCelect unit was confirmed using RT-qPCR. 11 epithelial-like and 13 mesenchymal/pEMT-like CTCs were isolated and singly dispensed from the pre-enriched 7.5 mL blood samples of the same HNSCC patient (Figure 5B). RT-qPCR was performed to detect target RNAs encoding EpCAM, Integrin α -V, Stratifin and β -actin as positive control. CT values for each well were determined and relative mRNA expression was normalized to β -actin (Figure 5C).

Samples with a CT < 40 for β -actin were identified as “positive” (droplet contained a cell) and samples with a CT < 40 for β -actin and at least one of the other three markers as “CTC-positive” (droplet contained a potential CTC). False-positive results were identified via melt curve analysis and excluded from the calculations. In this regard, 100 % of the dispensed droplets were CTC-positive, since all of the 11 epithelial-like and 13 mesenchymal-like CTCelect samples had a CT < 40 for β -actin, EpCAM and Stratifin RNA at comparable levels. Additionally, all of the mesenchymal-like CTCs were positive for CD51 RNA with sample A01 showing the highest an 8-fold level of CD51 compared to β -actin. In contrast, only 4 epithelial-like CTCs (A03, 04, 10, 11) contained detectable CD51-related nucleic acid and A11 even exhibited higher CD51 than EpCAM RNA. The 13 mesenchymal/pEMT-like

CTCs also significantly contained EpCAM RNA of at least 4-fold greater than the housekeeping RNA.

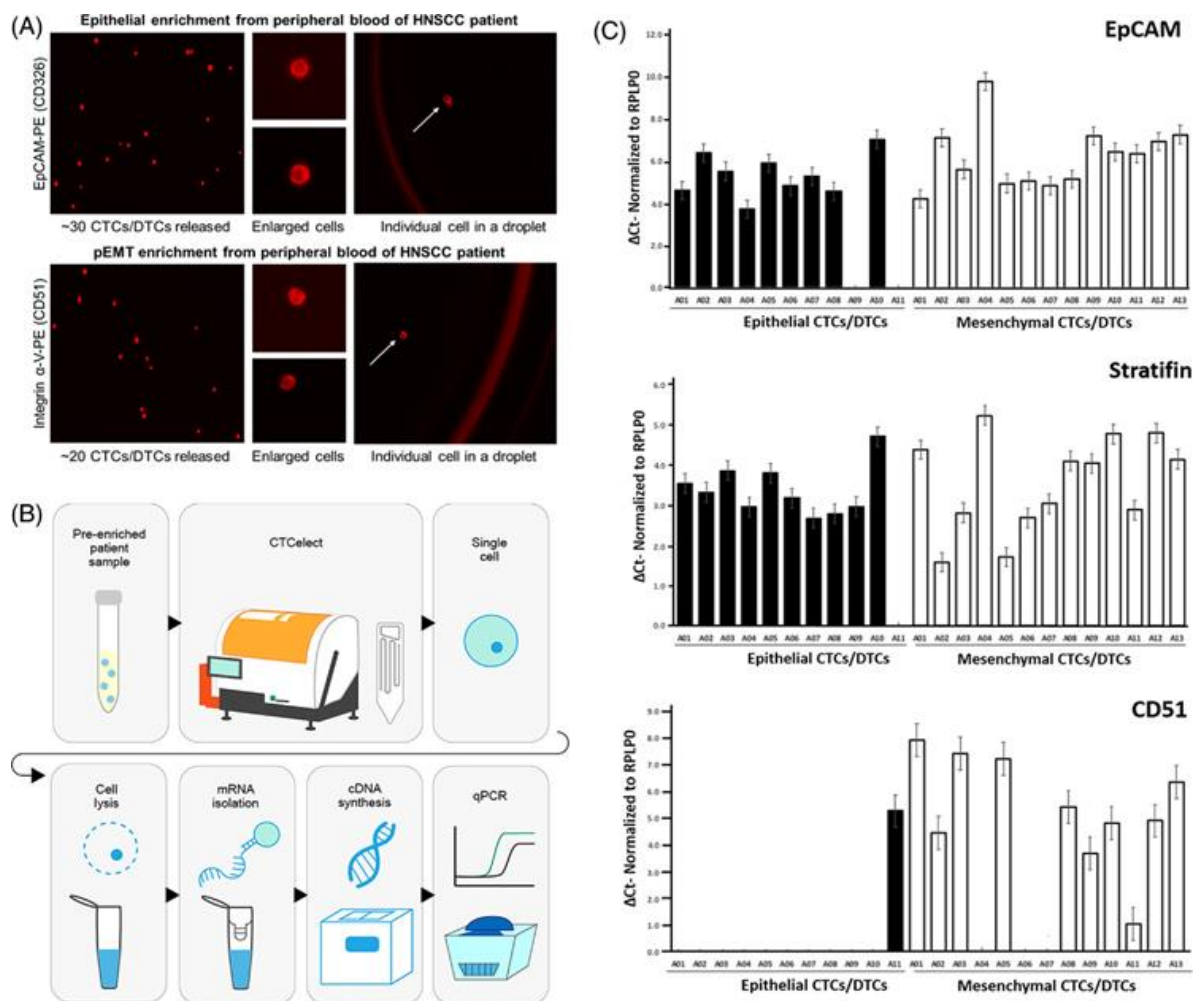


Figure 5. RT-qPCR of CTC isolates after CTSelect single cell dispensing from pre-enriched HNSCC patient blood. (A) Immunofluorescent staining of potential pre-enriched CTCs/DTCs from HNSCC patient blood. Pre-EMT CTCs were enriched with EpCAM beads and stained with EpCAM-PE Ab from a 7.5 mL blood sample (left top). Integrin α -V, CD61, CD106 beads and Integrin-PE staining was used for partial/post-EMT CTCs (left bottom). Cells were released from the beads by DNase I cleavage. The pre-enriched samples were pipetted in the microfluidic cartridge of CTSelect and beads-free CTCs were then single cell isolated in droplets by means of the CTSelect μ CS subunit. The set of images on the right side shows potential single CTCs in droplets highlighted with white arrows and the droplet outlines. (B) Workflow of single cell RT-qPCR. (C) Relative mRNA expression encoding EpCAM, Stratifin and CD51 normalized to β -actin (RPLP0) by RT-qPCR in epithelial and mesenchymal CTCs. Single cell total RNA was extracted from dispensed droplets and reverse transcribed into cDNA. cDNA was aliquoted and qPCR was conducted with one cDNA aliquot per well amplifying target nucleic acids respectively for EpCAM, CD51, Stratifin and β -actin as positive control of epithelial-like CTCs (pre-EMT enrichment) and mesenchymal-like CTCs (pEMT enrichment).

Relative expression was calculated from triplicates using the Δ CT method and is displayed as means with SD.

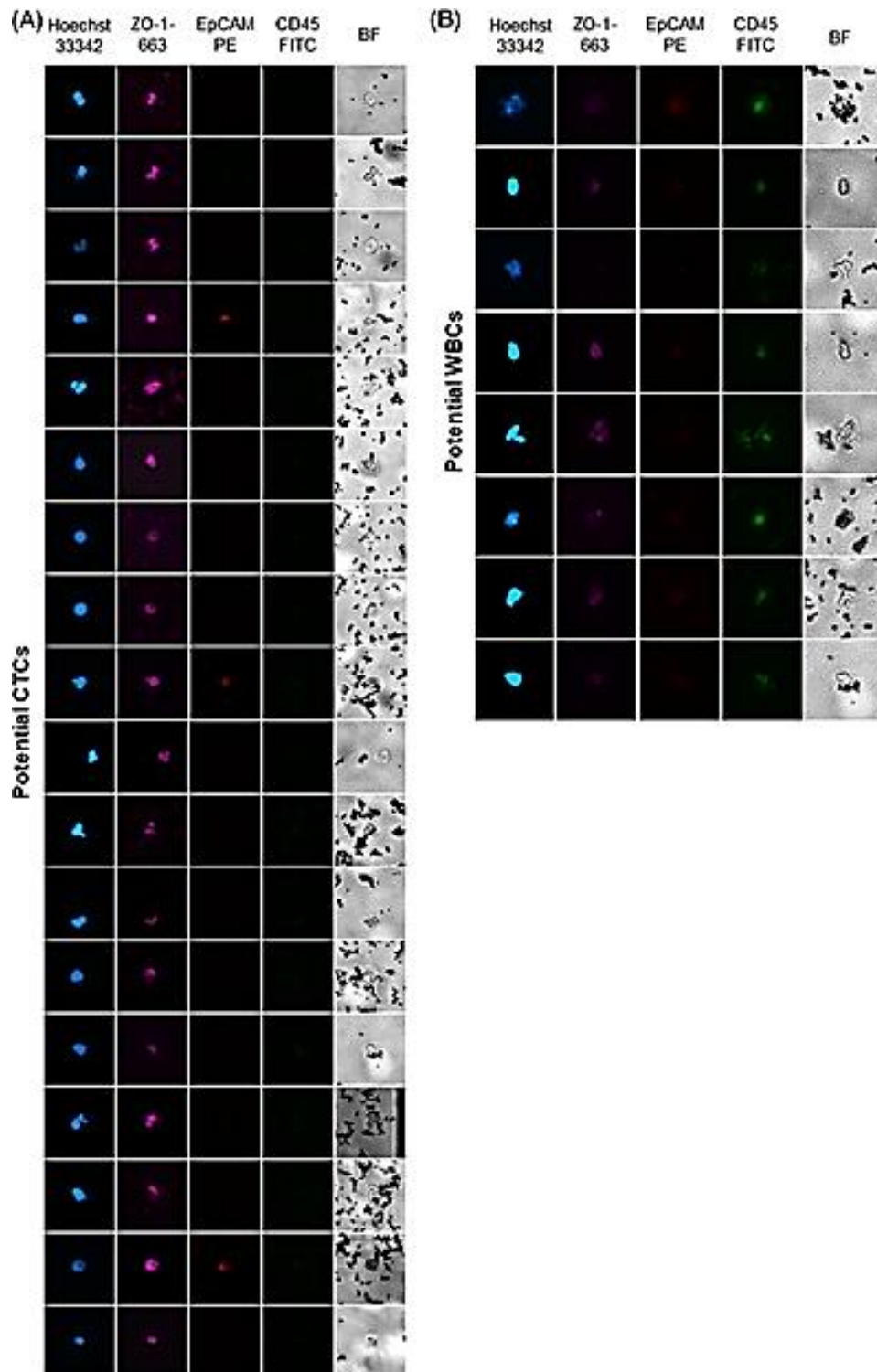


Figure 6. Immunostaining of potential CTCs and WBCs after CTSelect isolation. Dispensed cells were pooled together and subsequently stained with cell core dye Hoechst33342 (blue), ZO-1 as epithelial marker (magenta) and CD45 as WBC marker (green). Residual EpCAM staining from

CTCelect isolation is displayed in red. Cells were identified as **(A)** potential CTCs if Hoechst+/ZO-1+/CD45- and **(B)** as WBCs if Hoechst+/CD45+.

Following method 2.5 c), completely automated CTC isolation from 7.5 mL HNSCC patient blood was performed. The dispensed droplets were pooled and stained using Hoechst33342 cell core staining, ZO-1 as epithelial marker for potential CTCs and CD45 as negative control for contaminating WBCs. 18 potential isolated CTCs and 9 contaminating WBCs could be detected using fluorescence microscopy (Figure 6).

4. Discussion

From the patient's point of view, single CTC isolation from peripheral blood is the least invasive procedure to evaluate tumor heterogeneity based on epigenomic, genetic or transcriptional markers and is therefore more time effective and reproducible than assays drawn from primary tumor tissue. This study covered a profound biological validation of the design, biotechnological effort and engineering concept of the CTCelect platform for automated single cell isolation from whole blood. CTCelect helps to identify, enrich, isolate and analyze CTCs and their subpopulations. Many researchers suggested that the precise characterization of CTCs will facilitate estimating both metastization patterns and outcome, driving clinical decision-making and surveillance strategies [16].

For these purposes, the subunits of the system were separately tested and evaluated. Concerning cell enrichment, CTCelect provided recovery rates from medium of 68 - 100 % in breast cancer single cells and 28 % to 88 % in cultured squamous cell carcinoma cells. Further, 65 % to 85 % of MCF-7 cells and 20 % to 55 % of SCL-1 cells could be enriched from 7.5 mL whole blood from healthy donors (Figure 3). In comparison, Chudziak and colleagues determined 69.5 % enrichment efficiency of spiked lung cancer cells in their marker-free CTC enrichment device Parsortix although it has to be mentioned that the sample input only ranged from 0.5 to 4 mL volume [17]. We extensively characterized the enrichment sub-unit in our previous study before it was implemented in the overall CTCelect platform [18]. Similar to manual enrichment, there was no significant loss of cells due to vibrational disruption or tube surface adhesion. The enriched cells were accurately detected using fluorescent microscopy. More detailed, decreased enrichment efficiency by 15 % (MCF-7) and 13 % (SCL-1) in donor blood compared to culture medium was noted. As it has previously been postulated that the magnetic susceptibility in blood is significantly less negative than in aqueous solutions like medium [19, 20], we consequently hypothesize a

generally lower magnetic force attracting immunomagnetic beads in whole blood. In addition, a steric competition with the abundant blood cell background could possibly prevent a proportion of the target CTCs from binding beads and being magnetized. Another important aspect influencing cell recovery rates is that cell deformability, viscoelasticity, and stability (density of actin filaments etc.) could play a role for robustness against shear stress in automated pipetting and these characteristics will be different among various cell types. Comparing the two cell lines, MCF-7 cells were detected at higher rates than SCL-1 cells. The density of antigens blocking phagocytosis could be higher on the cell surface of MCF-7 cells and therefore be more favorable for spike-in experiments. Breast cancer-associated HER2 and lymphoma-related CD47 exhibit a “please don't eat me” signal to macrophages [21, 22]. Besides that, Figure 3B showed that when the number of spiked SCL-1 cells is higher than 25, there is an inconsistency between observed and expected cell count. This however does not suggest that the platform is not efficient in recovering larger numbers of CTCs as according to the results, the enrichment efficiency of MCF-7 cells followed a linear trend at higher expected cell counts. In our recently published work, we screened several melanoma and carcinoma cell lines (MV3, SCL-1, SCL-2, BLM, patient-derived HNC cells) and targets (MCSP, EpCAM, cell surface vimentin) to find a suitable candidate for the testing of microfluidic platforms. The enrichment fluctuation appeared frequently depending on the cell line and the sample volume also in manual enrichment. Further, we observed a similarly efficient cell line-dependent recovery rate at even higher cell counts of 1000 cells for that is, A431 cells using the same beads [18]. The practicability of spike-in experiments to test novel CTC platforms, in cell line models without evolutionary pressure in vitro combined with intracellular synthetic dyes, remains discussable and limits the study design. Nevertheless, these prevalidations are inevitable to investigate the proof-of-concept and invented design of the device. In this context, it has to be centered that the actual CTC count in a cancer patient has a multifactorial nature and therefore represents a dynamic measure with discrepancies.

For a successful singularization of the CTCs in the microfluidic cartridge and a high purity of the single cell dispensing it is also important to reduce the amount of WBC contamination during immunomagnetic enrichment. Thus, the automated enrichment process was characterized in terms of leukocyte by-catch. Enriched samples of 7.5 mL whole blood from healthy donors were labeled with WBC marker CD45-FITC and roughly 3.700 CD45 positive PBMC were detected via flow cytometry (Figure 3E). Healthy adults normally have a wide range of 3 - 10 million leukocytes per mL blood [23], which concludes a by-catch reduction of $1:10^5$ by means of CTCelect enrichment. Other devices like marker-dependent CellSearch® or Isoflux™ and label-free ScreenCell™ or ClearCell showed similar contaminations of 10^2 – 10^4 blood cells while authors also discussed a patient-dependent discontinuity in leukocyte

by-catch using Parsortix [17, 24]. Their approaches often provide a final sample pooled with WBCs while subsequent marker-based single cell detection in CTCelect further purifies the CTC fraction for compatible molecular analysis.

Combined enrichment with single cell detection and dispensing in one assay resulted in only minor cell losses with recovery rates of almost 60 % for both MCF-7 and SCL-1 cells from culture medium in the model system. Even from 7.5 mL whole blood, single cells were isolated at a probability of 57 % (MCF-7) and 40 % (SCL-1) (Figure 4A). The determined recovery rates from untreated whole blood at a high purity grade of less than 10 % probability to dispense a WBC with a CTC [25] showcases a fine parameter balance of CTCelect compared to other CTC isolation microdevices (Table 2).

Table 2. Comparison between CTCelect and different CTC isolation technologies.¹

	CTCelect	DEPArray	CellSearch	Sievwel	Parsortix
Sample type	Whole blood, cell suspension	Cell suspension	Whole blood, leucapheresis	Cell suspension	Whole blood, cell suspension
Automated isolation of viable cells	Yes	yes	no	manually	Yes
Automated optical counting	Yes	setup	Yes	Yes	No
Isolation method	Marker	Electrophoresis, marker	Marker	Marker, size	Size, compressibility
Single cell dispensing	yes	yes	No	CellCelector	No
Isolation efficiency	Enrichment 38.8% to 72 % Dispensing 72.8 % Isolation 40% to 56.7 %	99.7 % ^{a)}	93 % ^{c)} 81 % ^{d)}	n. a.	98 % ^{g)} > 80 % (7.5 mL blood) ^{h)} 30% to 70 % (1 mL blood) ^{h)} 37 % ⁱ⁾
Purity (WBC contamination)	66 - 90 %	100 % ^{a)}	800 WBCs/sample ^{e)}	n. a.	97 % ^{g)} 29 % ^{h)}
Throughput	4*10 ¹¹ cells/chip ² ; 96 wells (3.3 mL/h)	10-10,000 cells/chip ^{b)}	n. a.	370,000 cells/chip ^{d)}	n. a.
Working volume	0.3–10 mL	n. a.	7.5 mL	0.5–2 mL/chip	10 mL
Cycle duration	2.25 h	2 - 3 h	n. a.	n. a.	n. a.

¹ No claim to be exhaustive.

^{a)} Di Trapani et al. 2018. Cytometry. Part A, 93(12), 1260–1266.

^{b)} <http://www.siliconbiosystems.com/depararray-technology-faqs>.

^{c)} https://documents.cellsearchctc.com/pdf/e631600006/e631600006_EN.pdf.

^{d)} Riethdorf et al. 2007. Clin Cancer Res 13(3), 920–928.

^{e)} Sieuwerts et al. 2009. Breast Cancer Res Treat 118, 455.

^{f)} <https://www.sievwel.com/product-information>.

^{g)} Ciccioi et al. 2021. ANGLE plc AACR 2021 Virtual Meeting. <https://angleplc.com/wp-content/uploads/EMT-assay-poster-AACR-2021-final.pdf> [2021-09-10].

^{h)} Chudziak et al. 2014. CRUK – Manchester, NCRI conference 2014. <https://angleplc.com/wp-content/uploads/CRUK-Manchester-poster-1.pdf> [2021-09-10].

¹⁾ Gorges et al. 2014. The University Medical Center Hamburg-Eppendorf (UKE), ACTC Conference. https://angleplc.com/wp-content/uploads/Angle_Hamburg_MC_poster_ebook-2.pdf [2021-09-10].

² *Not dispensable. Current limitation: 96-well plate; drive duration of object table: 500 ms.*

For example, studies on devices using hydrodynamics, size-based filtration or dielectrophoresis showed indeed cell recovery rates of 70 % to 85 % but were only able to process approximately 1 mL/h or lacked CTC isolate purity [5]. In fact, at a flowrate of $2.25 \cdot 10^{-15}$ L/s and 5 ms nozzle-emptying time, it is theoretically possible to detect, but not dispense, 200 events per second and $4 \cdot 10^{13}$ cells/chip in 500 μ L. The current dispensing limitation is the 500 ms drive time of the object table and the 96-well plate format. CTCelect manages a moderate sample throughput of 3.3 mL/h with the current run time of around 2.3 h and 7.5 mL input volume. Additionally, most of the available systems require either sample transfer between different devices or blood pre-processing like density gradient centrifugation for buffy coats. Pre-enriched samples or yielded mononuclear phases of blood to specify the respective research needs can also be sampled in the herein discussed platform. To our knowledge, the possibility to use whole blood samples for automated single cell dispensing of rare cells in only one marker-based device to make them available for corresponding analyzes stands alone.

The workflow for downstream single cell RT-qPCR was simplified to immediate single cell lysis on the well plate. Direct reverse transcription in the cavities of the well plate coming from the device as well as the assay implementation to release detachable beads in the enrichment unit are subjects of future work. This evaluation however included the earliest results of the CTCelect device towards isolating single CTCs from a patient with metastatic head and neck squamous cell carcinoma in a clinical environment. In these patient samples, 30 EpCAM+ CTCs and 20 CD51+ CTCs were detected via fluorescence microscopy (Figure 5A). Microfluidic cell singularization enabled single cell RT-qPCR and allowed a distinction in 11 pre- and 13 pEMT CTC subtypes on the basis of different tumor-related markers (Figure 5C). Hence our findings evidence the potential of CTCelect to depict cancer plasticity. IVD companies, that is, QIAGEN N.V., offer non-automated CTC isolation/PCR platforms to characterize common tumor entities such as lung, prostate and breast cancer, but not for HNSCC diagnostics. Further, CTC liquid biopsy in HNSCC could elucidate crucial information on early assessment of treatment measures and effectiveness with respect to the detection of micrometastases at the initial diagnosis, complementing well-established ctDNA characterizations. Moulriere et al. recently detected chromosomal mutations of solid tumors in the blood by whole genome copy number variation analysis [26]. Encompassing studies on ctDNA and CTC characterizations have been carried out [27] but, especially in head and

neck cancers, the respective literature landscape is sparsely settled and to be addressed in the future with the suggested data.

It is obvious that immuno-biochemical techniques targeting antigens like EpCAM are not infallible for all tumor entities or heterogeneous CTC populations, especially CTCs undergoing epithelial-mesenchymal transition (EMT) which is closely linked to invasive metastasis. Against that, mixtures of antibodies like integrin subtypes, cell surface vimentin or stem cell markers are of assistance to improve the enrichment of partial/post-EMT mesenchymal-like CTCs. Besides these affinity-based techniques to enrich and isolate CTCs, the physical methods base on distinction in cell size, density or even plasticity. Due to the fact that CTCs are a heterogeneous population in blood, they have some characteristics in common with healthy mononuclear blood cells. Thus, methods based on filtration, centrifugation or size exclusion may not be used for a standard clinical test system. Further, it is important to mention that there are other obstacles, i.e. the purity of the CTC fraction, before realizing subsequent applications such as single cell sequencing or copy number variation studies.

The certainly limited patient screening in this study clearly demonstrated the feasibility of downstream applications. The platform enabled fully-automated CTC isolation from HNSCC patient blood and immunofluorescent identification of 18 potential CTCs for proof-of-concept (Figure 6). Several researchers have stated that the presence of CTCs in the blood is of prognostic relevance for overall and progression-free survival in patients with head and neck cancer [28] and that HNSCC exhibits early stage micrometastatic sites and severe intra-tumoral heterogeneity which is closely linked to poor disease outcome. In this context, an important advantage of CTC/DTC isolation over imaging technologies is that minimal residual disease (MRD), for example DTC micrometastases, are undetectable by the latter. Especially bone marrow is intensively studied as a reservoir for dormant DTCs with the capacity to re-enter the circulatory system and trigger MRD in distant tissues [29]. It is easily plausible to broaden the applicability of the CTCelect device to process liquid biopsies from bone marrow or dissolved lymph node resections. All of these aspect stress the necessity of an improved cell biological understanding to foremost provide a good care for HNSCC patients. High-resolution of cell heterogeneity, metastatic invasiveness and evolutionary pressure on cancer cells is key to precision medicine. To conclude, the presented results demonstrate the robust technical performance of CTCelect and its feasibility as a novel tool for liquid biopsy to make CTCs available for corresponding examinations on a single cell level with respect to head and neck squamous cell carcinoma.

2.3 Paper 3



Article

Automated Immunomagnetic Enrichment and Optomicrofluidic Detection to Isolate Breast Cancer Cells: A Proof-of-Concept towards PoC Therapeutic Decision-Making

Janis Stiefel ^{*}, Michael Baßler , Jörn Wittek and Christian Freese

Diagnostics, Fraunhofer Institute for Microengineering and Microsystems IMM, Carl-Zeiss-Straße 18–20, 55129 Mainz, Germany

* Correspondence: janis.stiefel@imm.fraunhofer.de

Abstract

In breast cancer research, immunomagnetic enrichment of circulating tumor cells (CTCs) from body fluids has impressively evolved over the last decades. However, there is growing interest in further singularizing these pre-enriched rare cells to decrease signal-to-noise ratio for downstream molecular analysis, e.g., to distinguish between hormone receptor-associated tumor subtypes. This can be done by a combinatory principle to link magnetic cell separation with flow cytometry and single cell dispensing. We have recently introduced an automated benchtop platform with a microfluidic disposable cartridge to immunomagnetically enrich, fluorescence-based detect and dispense single cells from biological samples. Herein, we showcase the fine-tuning of microfluidic cell isolation in dependency of bead-binding on the cell surface. We implemented a gating function for the cytometer subunit of the benchtop platform to selectively dispense cells instead of autofluorescent objects. Finally, we developed a simplified qPCR protocol without RNA purification targeting breast cancer-relevant progesterone and estrogen receptor, Muc-1, Her-2, EpCAM and CXCR4 transcripts. In conclusion, the presented results markedly demonstrate a future diagnostic and therapy-accompanying semi-automated workflow using immunomagnetic enrichment, fluorescence-based isolation and dispensing of circulating tumor cells to achieve tumor subtyping by means of rapid, simple and immediate molecular biological examination of single cells.

1. Introduction

The characterization of rare cells has become a major topic in applied research since addressing personalized medicinal approaches is seen as the future to oppose complex pathologies. For example, the enrichment, detection and isolation of circulating tumor cells (CTCs) reveals crucial information on prognostic [1], diagnostic [2] and even therapeutic aspects [3] that can support treatment decision-making in oncology. It is known that CTCs detach from the primary epithelial tumor tissue and intravasate into the cardiovascular system to foster secondary tumor formation as disease-driving precursor at another site [4].

For malignant neoplasia of the breast tissue in particular, liquid biopsy of biomarkers such as cell-free circulating tumor DNA (ctDNA), exosomes and CTCs has attracted immense interest in the scientific community. Based on the current incidence, one out of eight women will be diagnosed with breast cancer throughout her life. Moreover, one in six of these women will be younger than 50 years at the time of the diagnosis. Although breast cancer is by far the most common solid tumor type in females, it has a relatively high 10-year survival rate of 83 % when diagnosed at early stage, ideally prior to metastasis, and treated appropriately [5]. Comparable to most cancers, the systemic spread of secondary tumors (metastasis) is the major cause of death due to multi-organ failure or opportunistic infections in metastatic breast cancer.

Since the hormone receptor status and surface antigen distribution among different subtypes of breast cancer occupy a critical role for disease invasiveness, tumor burden and therapy decision, the characterization of CTC biomarker features at the point-of-care (PoC) has become a subject of intense research. An association of CTCs with poor prognosis due to metastasis could already be shown in breast cancer as well as in various other cancers. More detailed, the 3-year survival of patients with triple negative breast cancer (TNBC) is significantly higher at prior-surgery CTC counts below 5 cells in 7.5 mL whole blood [6]. TNBC is highly invasive due to cancer cells that lost expression of estrogen, progesterone and human epidermal growth factor receptors ESR, PGR and HER-2 [7] and is hence especially difficult to tackle without hormone therapy with a strong tendency to therapy-resistant metastization [8].

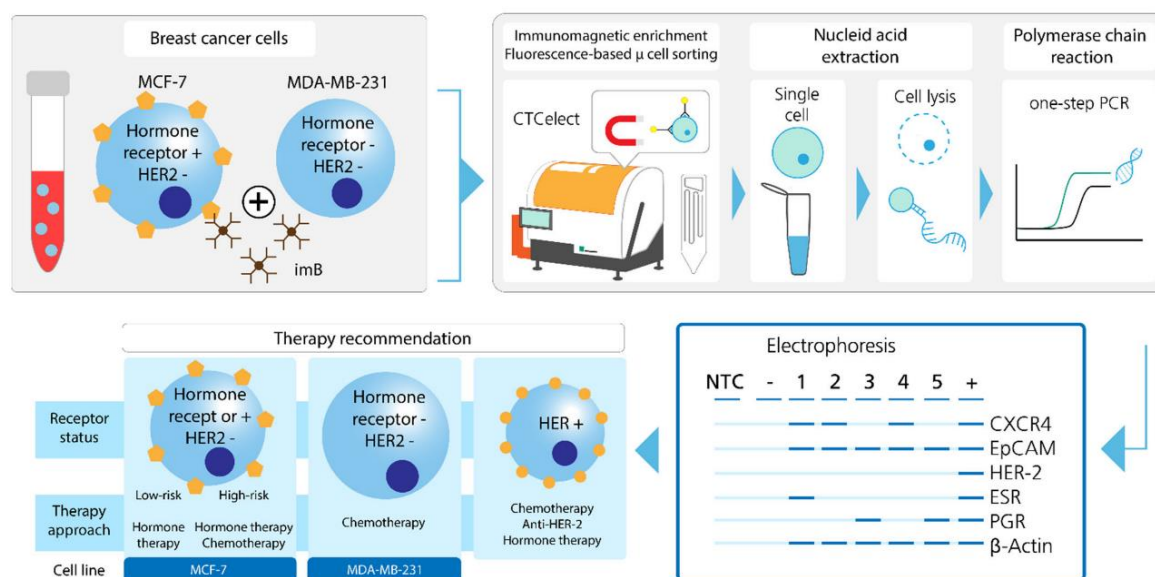


Figure 1: Automated isolation workflow of single tumor cells for the molecular analysis of different cancer-associated markers and their diagnostic and therapeutic potential. After enrichment with immunomagnetic beads (imB) and fluorescence-based microfluidic cell sorting of cancer cells from a 7.5 mL sample, single cell RNA is analyzed using RT-PCR and electrophoresis. In dependency of different markers, tumor subtypes and respective therapy approaches can be potentially derived.

Besides size exclusion, magnetic cell separation has become a key technique for the isolation of CTC subpopulations from biological suspensions like blood and leucapheresis products. However, improvement in selectivity, yield, and sensitivity of the separation protocols with cost reduction and standardization is still needed to fully implement magnetic cell separation in breast cancer diagnostics or therapeutic decision-making. Magnetic cell separation of CTCs from complex body fluids like whole blood often results in high background signal of white blood cell contamination (1:1000) hampering downstream molecular analysis. Interdisciplinary research to combine immunomagnetic separation, microfluidic cell sorting and system engineering in biological validation can tackle the challenge to lower the signal-to-noise ratio. We developed an automated benchtop platform (CTCelect) for the single cell isolation of CTCs using immunomagnetic enrichment, chip-based microfluidic cell sorting and single cell dispensing in droplets on a 96-well plate to overcome these current limitations. The device was characterized in-depth and optimized in our previous works [9,10]. The platform consists of an immunomagnetic enrichment module and a microfluidic fluorescence-activated cell sorting subunit with a disposable cartridge (see Supplementary Figure S1). Fluid control and sample transfer is managed by a pipetting robot and syringe pumps. Epithelial cell adhesion molecule (EpCAM)-positive selection of tumor

cells from a 7.5 mL sample with subsequent depletion of leukocytes takes place in the enrichment module of the device. The enriched and stained sample is then transferred to the cell sorting subunit into the microfluidic chip for detection and single cell dispensing in microliter droplets.

In this study, we investigated the flow properties of magnetic bead-bound cells in the microfluidic demonstrator and highlight the bottlenecks of immunomagnetic microfluidic cell separation respectively. Additionally, we showcase a proof-of-concept for a simplified detection and distinction of hormone-related tumor markers in single hormone receptor-positive and triple-negative breast cancer cells developing a protocol for combining automated cell enrichment, detection and dispensing with one-step PCR analyses (Figure 1). These results contribute to sharpen the overall picture of an individual cancer pathology and to pave the way towards additional therapy suggestions from liquid biopsy.

2. Results

2.1. Impacts of immunomagnetic bead-binding on flow properties and fluorescence signal of single cells in a microfluidic cartridge

To minimize bead sedimentation in the microfluidic chip during the time course of microfluidic isolation, different sample buffers were tested. For the following experiments, uniform 1.0 μm diameter superparamagnetic beads were functionalized with EpCAM antibodies.

The sedimentation of beads in phosphate buffered saline (PBS) and in viscous sugar (alcohol)-based buffers in different concentrations was visually documented over 30 min (Figure 2A). Finally, we chose a polysaccharide solution at the lowest possible concentration (0.125 %) without visible sedimentation for the subsequent experiments, herein after referred as “transfer buffer (TB)”. Previously, increased bead sedimentation in the chip funnel and in the curves of the meander structures of the cartridge was observed using PBS as sample flow. By switching to TB, beads stayed in suspension and did not sink onto the lower meander walls (Figure 2B).

The location of EpCAM bead-bound, CFSE stained cells was identified with fluorescence microscopy after complete CTCselect isolation to investigate cell loss in the chip or recovery on the well plate depending on different sample buffers (Figure 2C). Due to the process of automated immunomagnetic enrichment of cells using a pipetting module [10], it was first investigated whether cells remain in the 10 mL pipet tip. On average, almost no cells were lost in the pipet tip in both settings (PBS: 0; TB: <1). Cell loss in the chip channels could be reduced by 78 % using TB (9 vs. 2 cells), while fluorescence detection and visibility of

dispensed cells on the well plate was increased 4.6-fold and 3.2-fold, respectively. While improving the flow characteristics of cells in the microfluidic cartridge, TB was not affecting the dispensing of droplets. The cartridge nozzle was designed to enable droplet generation without satellite droplets allowing precise cell dispensing with TB (Figure 2D).

The fluorescence signals and flow characteristics of bead-bound and bead-free breast cancer cells (MCF-7) in the microfluidic cartridge of the CTCelect platform were investigated. To guarantee an efficient CTC isolation, the influence of bead-binding to cells and their impact on fluorescent detection was determined. New parameters of detection were defined accordingly. The fluorescence signal of labeled cells is obtained in the platform by Silicon photomultipliers (SiPM) detectors in relative fluorescence units (RFU; arbitrary units [a.u.]). CFSE stained cells were incubated with beads and then loaded in the chip reservoir with different concentrations of free beads. We observed a decrease in fluorescence intensity of CFSE stained bead-bound cells depending on the presence of excess free beads (0 or 1×) in the detection channel (Figure 3B).

In addition, we observed a decrease in the fluorescence intensity when cells were previously enriched in the CTCelect platform. Previous automated enrichment lowered the fluorescence intensity drastically but still surpassed the 200–350 a.u. fluorescence threshold for dispensing. Interestingly, the fluorescence signal was not severely differentiating between 0.125×, 0.25×, 0.5× and 1× free beads concentrations (Figure 3A). The velocity of bead-bound cells could be calculated based on our detection method. Contrastingly to the fluorescence signals, the velocity profiles of the different samples after the complete isolation process (437 mm/s) compared to detection only (436 mm/s) did not differ significantly (Figure 3C) The speed window range to trigger dispensing was consequently narrowed down to objects with a velocity of 300–500 mm/s. Real-time fluorescence peak detection and algorithm-based analysis to measure the velocity of the bead-bound target cells allows to determine the delay-time for dispensing. The software demands an absolute path length value in meters to correct the distance between measurement point and dispensing nozzle. We empirically evaluated a path length = -0.011 m to obtain the highest recovery rates of visible cells in the dispensed droplets (Figure 3D).

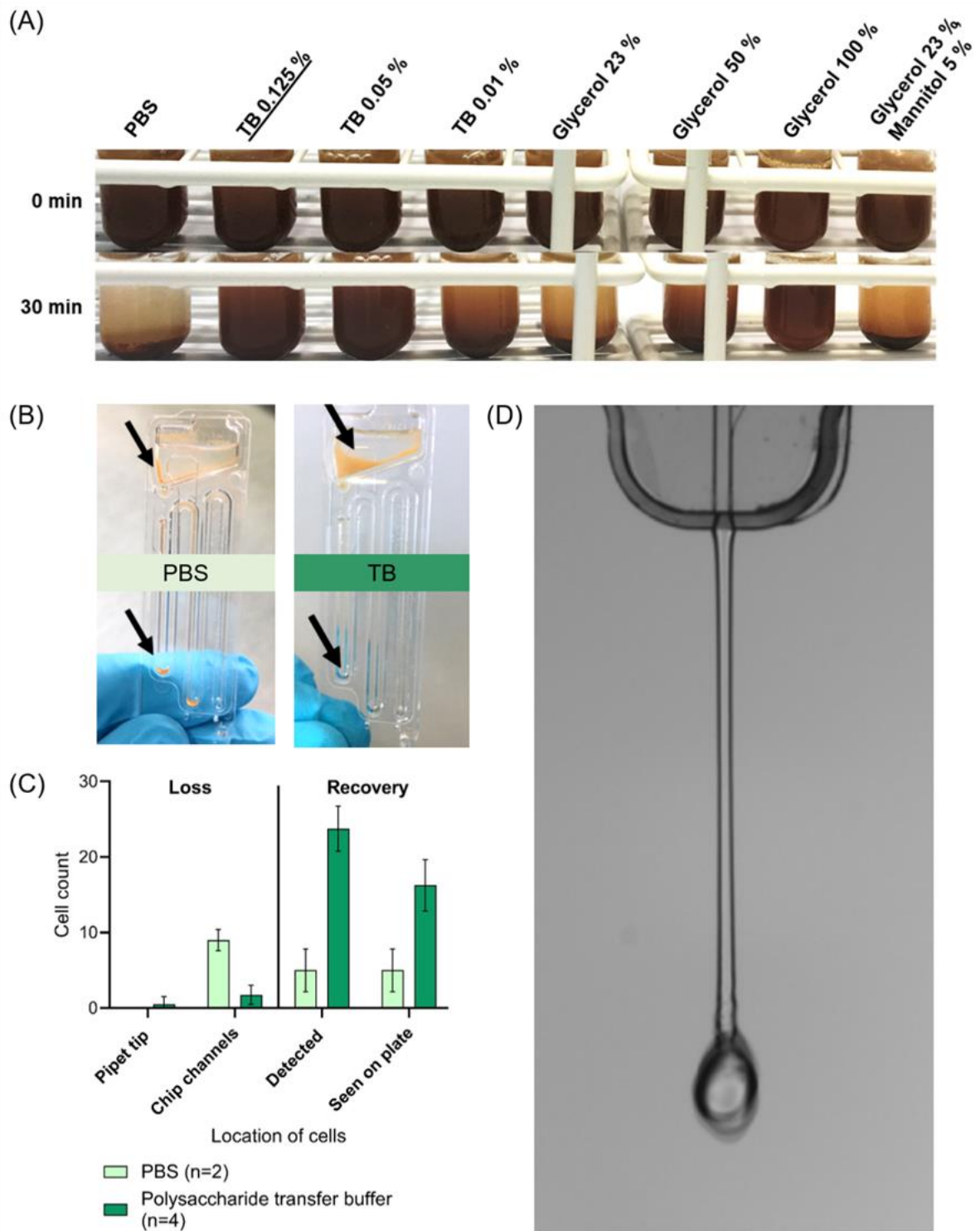


Figure 2: Influence of flow buffer composition on magnetic microbeads in microfluidic systems. (A) Bead sedimentation test was performed with $5 \times 10^9/\text{mL}$ $1 \mu\text{m}$ beads in different solutions of phosphate buffered saline (PBS), polysaccharide transfer buffer (TB), glycerol and mannitol. The visual sedimentation was documented after 30 min. (B) The use of 0.125 % TB strongly reduced bead sedimentation in the chip funnel and the meander structures of the microfluidic cartridge

compared to PBS which also significantly increased cell recovery (**C**) after automated isolation of MCF-7 cells (5 ± 2.8 vs 16.2 ± 3.4). (**D**) Precise dispensing of a droplet out of the chip nozzle.

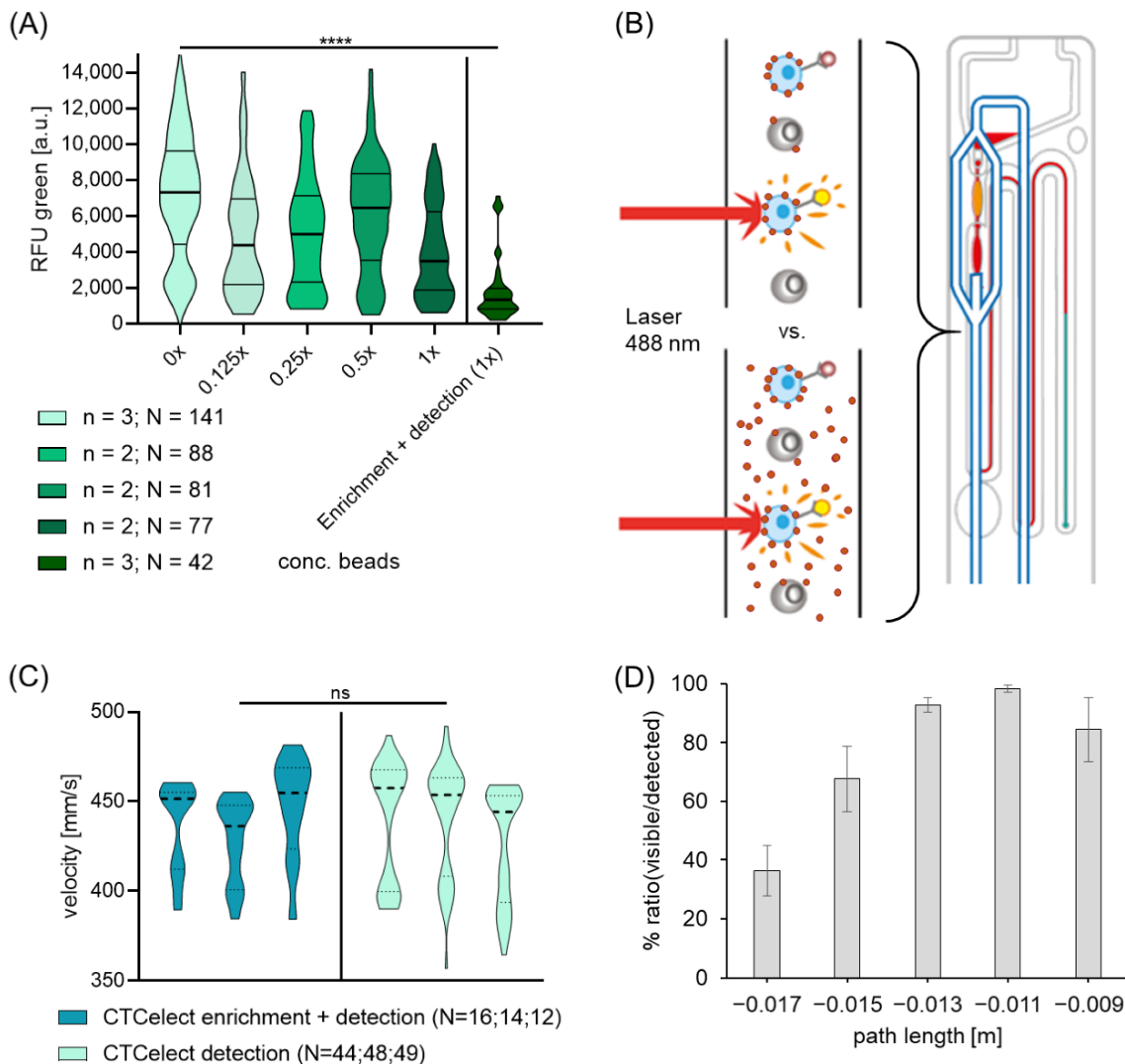


Figure 3: Characterization of fluorescence and flow properties of bead-bound single cells.

(**A**) The relative fluorescence intensity of CFSE stained bead-bound MCF-7 cells (in RFU) was recorded with our microfluidic flow cytometry subunit in dependency of free beads in the channel (x-axis) and previous automated enrichment. Relative fluorescence is presented as violin plot with median and first and third quantile (one-way anova, with Tukey's multiple comparisons test, **** $p < 0.0001$). (**B**) Explanatory illustration of single cell detection in the microfluidic cartridge with or without free beads. (**C**) The velocity of bead-bound single cells was measured in the detection channel of the chip and compared between manual bead incubation (436 mm/s) and previous automated immunomagnetic enrichment (437 mm/s). Velocity is given as violin plot with median and first and third quantile (paired t-test, $p^{ns} = 0.88$). (**D**) Empirical determination of ideal path length correction to time the dispensing trigger. The set path length correction is displayed against the ratio between software detected and visible cells after dispensing.

2.2. Optimization of optomicrofluidic cell detection with immunomagnetic bead-dependent signal-to-noise ratio

The effects of PE-conjugated antibody staining in combination with bead enrichment was characterized in the microfluidic chip. To verify staining intensity, MCF-7 cells were spiked-in whole blood and immunomagnetically enriched using a manual magnetic separator. We used EpCAM-PE as a classical marker for epithelial tumor cells in liquid biopsy and Hoechst33342 to label DNA in all cells. The final sample was visually assessed by fluorescence microscopy and flow cytometry. EpCAM⁺ MCF-7 cells were distinguishable from blood cells due to a visible red staining (Figure 4A). Interestingly, we observed a strong autofluorescence signal of free beads and/or blood components in the background (red smear). This contaminating population was also easily detectable in the flow cytometer as numerous counts with intensities below $RF_{FL2} < 10^4$ a.u. (Figure 4B) compared to the flow cytometry results of EpCAM-PE stained MCF-7 cells without beads and blood contamination (see Supplementary Figure S2).

The antibody staining was then characterized in the microfluidic platform. Fluorescence signals in green- and red-sensitive channels of unbound and bead-bound MCF-7 cells after EpCAM-, CD144-, CD84-, CD63-PE versus EpCAM-PE staining only was then measured in the CTCelect detection unit. We recorded a slightly higher red fluorescence signal using the antibody mix on unbound cells in the benchtop platform (Figure 4C) and comparable fluorescence (7.4×10^5 vs. 7×10^5 a.u.) in a conventional flow cytometry system (see Supplementary Figure S2). When combining with previous immunomagnetic enrichment, this effect however vanished and an advantage of mixing different PE-conjugated antibodies could not be confirmed with our detection unit at low cell numbers (Figure 4D).

Taking these results into consideration, the autofluorescence spectrum of unstained (brown dots) and EpCAM-PE-stained free beads (black dots) was measured as shown in Figure 4E and an increased fluorescence signal balanced in both the red and green detector channels ($y = x$) was detected. Bead-bound, EpCAM-PE stained MCF-7 cells could be distinguished from free beads by higher red fluorescence (yellow squares). Consequently, we developed a gating function following a linear equation $y = mx + b$ to differentiate the cell population from the beads population. The function was used to identify bead-bound EpCAM-stained from free beads in different sample (pink triangles). This feature was subsequently implemented in the software to dispense only cells at a higher likelihood rather than contaminating autofluorescent objects (mostly beads). The term $y = 3.7x + 130$ for example was well-suited for our optomicrofluidic setting.

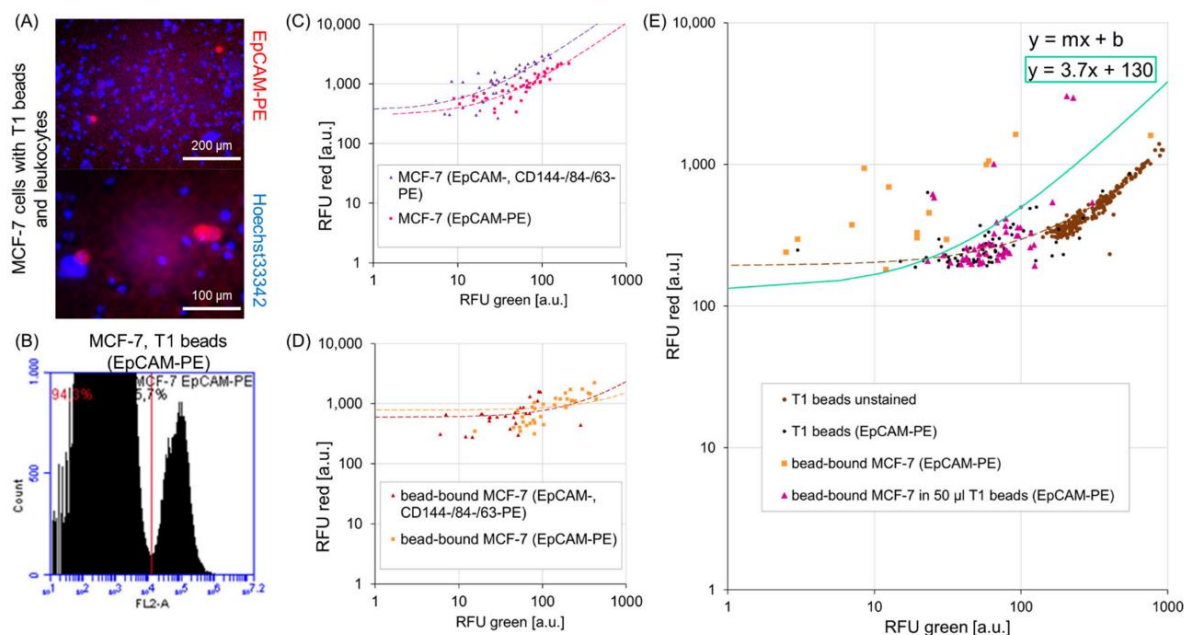


Figure 4: Selective optomicrofluidic detection of antibody stained bead-bound MCF-7 cells.

(A) Immunofluorescence staining of beads-enriched MCF-7 cells spiked in whole blood. Epithelial marker EpCAM-PE (red) was used and DNA was stained with Hoechst33342 (blue). Therefore MCF-7 cells are identified as EpCAM+/Hoechst+ while leukocytes are EpCAM-/Hoechst+. Elevated red background signal indicates autofluorescence of excess free beads. (B) Relative fluorescence intensity (FL2) of sample A in flow cytometry. Objects with higher RFFL2 $> 10^4$ a.u. (red line) are counted as cells. The remaining counts at RFFL2 $< 10^4$ a.u. are defined as contaminating background signal from autofluorescent free beads or blood components. Fluorescence intensities in green- and red-sensitive channels of unbound (C) and bead-bound (D) MCF-7 cells after EpCAM-, CD144-, CD84-, CD63-PE versus EpCAM-PE staining only was then measured in the CTCelect detection unit. (E) Various fluorescence measurements of unstained and EpCAM-PE stained beads and MCF-7 cells in the CTCelect demonstrator. A chromatic criterion for gating following $y = mx + b$ was introduced to distinguish between beads and cell population.

2.3. Establishment of a rapid protocol to assay cancer-related mRNAs in beads-enriched single cells

For the swift classification of isolated single cancer cells, a protocol for a simplified RNA isolation using chemical lysis and one-step qPCR was optimized and established as a downstream process in combination with the CTCelect platform. First, our two-step qPCR protocol was characterized using a commercial column-based RNA isolation kit to confirm fluorescence signals at low cell number. Therefore, we picked single cells from a cell suspension in a petri dish and directly lysed one, 20 and 40 cells per spin column. We observed an increase in relative fluorescence intensity in clear correlation with the cell

number for both EpCAM and β -actin expression as expected (Figure 5A). To investigate the influence of the cell detachment process in single cells on RNA yield compared to adherent cells under culture conditions, we seeded single cells in a 96-well plate as a control (“cultured”) and isolated the total RNA from one well according to Yaron et al. [11]. The amplification curves for EpCAM indicated a decreased RNA yield in replicates of picked single cells ($C_T = 37.5 \pm 1.6$) in comparison to cultured single cells ($C_T = 34.3 \pm 1.5$). Melt curve analysis was done to confirm the specificity of amplicates (see Supplementary Figure S3).

To now simplify and shorten the protocol, a guanidine salt-free lysis buffer (LB) to chemically lyse the single cells without RNA purification and a one-step qPCR kit was introduced and compared to conventional RNA isolation and two-step qPCR results (Figure 5B). Though a slight significance in amplification decrease (* $p = 0.02$) between using two- or one-step qPCR occurred (green vs. dark blue), the advantages and easiness of the one-step analysis was prioritized. Previously, the one-step protocol was modified by prolonging reverse transcription to 20 min and the extension time to 10 s to improve the reaction. Single cell qPCR after CTSelect dispensing led to lower C_T values compared to directly lysing a single cell from a petri dish (picked; grey).

For a higher clinical relevance at low CTC frequencies, PCR-based confirmation of hormone-related tumor markers was established after CTSelect isolation. For that, 20 CFSE stained MCF-7 cells were immunomagnetically enriched and dispensed automatically in the same well. After cell lysis, RNA isolates were split 1:4 to test for the expression of (1) progesterone (PGR), and (2) estrogen (ESR) and (3) CD45 as a negative control. Additionally, (4) the multiplex BreastCancer Detect Adnatest (QIAGEN) for GA733-2, Muc-1 and Her-2 as well as β -actin housekeeping expression was performed according to the manual, modified by column-free chemical lysis using LB. PCR products were detected using gel electrophoresis and automated electrophoresis with the Agilent Bioanalyzer (Figure 5C,E). PGR and ESR expression could be confirmed, while the Adnatest was only positive for the actin housekeeping RNA in our experimental setting.

For the future distinction between high-risk triple negative and hormone receptor positive breast cancer cells, we established the same PGR and ESR mRNA PCR test extended by EpCAM, β -actin and CXCR4 mRNA detection in MDA-MB-231 cells (Figure 5D). As expected, both MCF-7 and MDA-MB-231 cells were positive for epithelial EpCAM, CXCR4 and β -actin expression, whereas MCF-7 cells were hormone receptor positive (ESR⁺/PGR⁺/HER-2⁻) and MDA-MB-231 cells were triple negative (ESR⁻/PGR⁻/HER-2⁻).

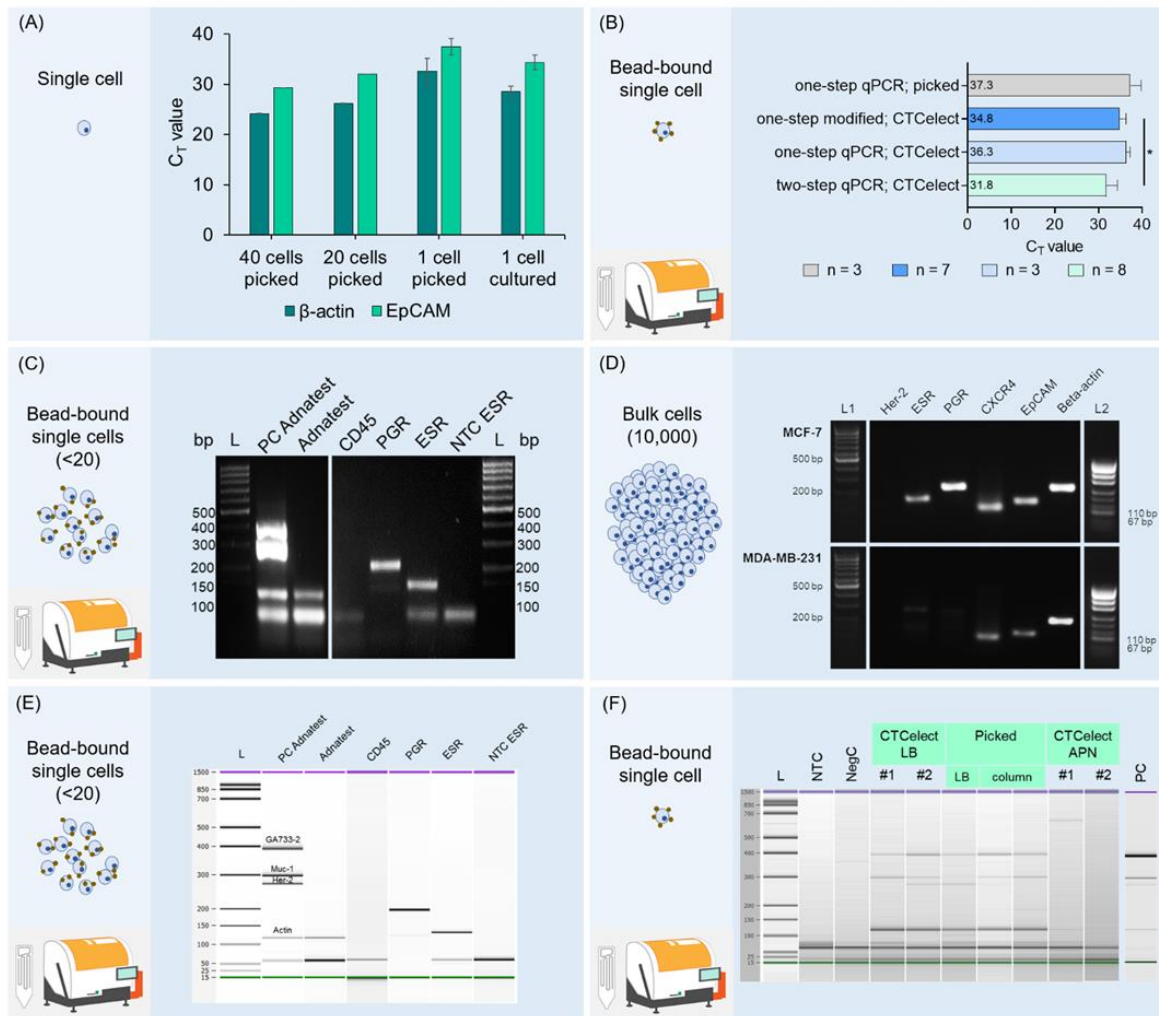


Figure 5: Establishment of simplified tumor marker-relevant PCRs from bead-bound single cells. (A) qPCR results after a two-step protocol using mRNA from 1, 20 and 40 MCF-7 cells with column-based RNA purification. (B) Comparison of C_T values between one- and two-step protocols for RT-qPCR targeting β -actin from one single cell each after CTSelect isolation. C_T values of “one-step modified; CTSelect” and “two-step qPCR; CTSelect” were significantly different (unpaired t-test, * $p \leq 0.05$). An optimized one-step qPCR protocol was established and used for the following tests. Namely, electrophoresis of PCR products targeting Adnatest, and CD45 (159 bp) as negative control from RNA of <20 MCF-7 cells after CTSelect isolation was performed in agarose gel (C) and with the Agilent Bioanalyzer (E) using the new established modified one-step qPCR protocol. (D) Gel electrophoresis to establish a test to distinguish hormone receptor positive/Her-2⁻ MCF-7 and hormone receptor negative/Her-2⁻ MDA-MB-231 cells in one-step PCR without RNA purification; HER-2 108 bp, ESR 129 bp, PGR 194 bp, CXCR4 60 bp, EpCAM 136 bp, β -actin 176 bp. (F) Bioanalyzer electrophoresis of Adnatest PCRs from MCF-7 single cell RNA after complete CTSelect isolation process. The different RNA extraction methods (guanidine salt-free lysis buffer (LB), RNeasy column, APN kit) are indicated above the lanes, respectively; actin 120 bp, HER-2 265 bp, Muc-1 299 bp, GA733-2 395 bp).

Beyond that, a second set of experiments using undiluted RNA isolates and two-step PCR for the multiplex BreastCancer Detect Adnatest was performed to potentially gain better signals (Figure 5F). With this setting, not only β -actin but also epithelial cancer-related GA733-2 and Muc-1 expression could be confirmed in single cells after CTCelect isolation or being picked from a petri dish with or without RNA purification (LB). Low levels of Her-2 mRNA were found in three single cells. Contrastingly, there was no amplification from single cells after CTCelect isolation using the AllPrep DNA/mRNA Nano kit (APN; QIAGEN) in our case.

3. Discussion

CTCs are systemic tumor components and hence are of high clinical value, not only to access minimal-invasive tumor components but also to correlate the cell count with disease staging and monitor treatment efficacy as personalized measure. An additional benefit of isolating CTCs from liquid samples is that the molecular profile is obtained from relevant single tumor cells that include all information on RNA and DNA level and is not highly diluted in the blood-like cell-free tumor DNA. Thus, the isolation of single tumor cells can be of great advantage for personalized therapies. However, current isolation methods are error-prone, laborious and cost intensive precluding CTC analysis for larger patient cohorts. Immunomagnetic separation is widely used to pre-enrich target CTCs from body fluids. We can use this pre-enrichment step in combination with an automated microfluidic detection and dispensing process to further purify the cells of interest from contaminating blood cells. Thus, the immunomagnetic enrichment step requires accuracy, specificity and adaptability to the needs of the microfluidic detection and dispensing step. By doing that, we are able to combine both processes in one automated benchtop device. In previous publications, the advantages and disadvantages of our process were qualitatively compared to existing methods [9,10].

We knew that certain obstacles arise by introducing relatively dense magnetic particles in microfluidic systems. The aim of this study was to adapt the immunomagnetic enrichment and handling of the pre-enriched cell-bead suspension. Even though 1 μ m magnetic beads have a relatively low sedimentation rate which makes them useable for automated isolations, they still gravitate after a certain period of time, especially in low-density aqueous solutions. This is this reason why we formulated a polysaccharide buffer that prevented visible bead sedimentation for at least 30 min (Figure 2A) enabling improved sample flow and

consequently the overall recovery rate of the isolated cells. Effects of fluid inertia and viscosity on the settling of particles in a viscous buffer are described in detail in the literature [12,13]. Glycerol as an agent to prevent the sinking of beads was only successful using a 100 % concentrated solution in our investigations. Studies report an already significant cytotoxic influence on mammalian cell volume due to osmotic pressure and decreased viability in 3.5 % concentrated glycerol [14], excluding this solution as potential transfer buffer for microfluidic CTC isolation.

In addition, when working with high proportions of excess magnetic beads, a few effects hamper fluorescence-based cell detection. For example, Andree et al. showed that in flow cytometry an unstained population overlaps with the fluorescence signal of a target cell population due to uneven probability distributions. A ratio of 1:1000 between a wanted (stained) and an unwanted (unstained) population already led to an overlap of 48.9 % in fluorescence intensity [15]. On one hand, they block epitopes for antibody staining and quench the fluorescence on the cell surface (see Supplementary Figure S2). On the other hand, beads exhibit a certain autofluorescence at 488 nm excitation as shown on the microscopic image in Figure 4A and described, i.e., by Roth et al. [16]. If not mixed properly or due to suboptimal buffers, beads may form agglomerates and falsify the detection process. We observed these influences in our experiments and adjusted the parameters accordingly to provide fluorescence-based single cell dispensing. These effects are more severe using antibody staining which generally emits lower fluorescence than synthetic dyes and relies on EpCAM expression only. In the literature, it was stated that a cocktail of fluorescent-labelled antibodies could improve the detection of cells [17]. With our detection set-up, we could not confirm a clear advantage of using a mixture of PE-conjugated antibodies to enhance fluorescence intensity of bead bound cells. For this purpose we developed a gating function that was implemented in the CTCelect software. We managed a distinction between the autofluorescent beads population and the fluorescent cell population to selectively trigger cell dispensing (Figure 4E).

Finally, molecular analysis of isolated tumor cells was optimized and accelerated by means of one-step qPCR to detect hormone-related breast cancer-associated targets. We found that under the same conditions, the efficacy of the one-step PCR method is not as high as that of the two-step method. Nevertheless, it was possible to successfully display the hormone receptor status of hormone receptor positive, Her-2⁻ MCF-7 cells (as defined by [18,19]) on a single cell level with one-step PCR after complete CTCelect enrichment, detection and dispensing (Figure 5C,E). Additionally, a comparable concept was developed for triple negative MDA-MB-231 cells which will be further investigated in the future (Figure

5D). Eventually, it should be the user's choice to perform one- or two-step PCR depending on time constraints, transcriptomic frequency and target number. Multiplexing in single cell PCR is undoubtedly limited by low sample input, lysis buffer dilution and RNA degradation. The 4-fold multiplexing Adnatest was not applicable using 1:4 diluted unpurified RNA from <20 cells (Figure 5C,E). In comparison with column-based nucleic acid extraction, chemical lysis also risks potential sample loss by inefficient pipetting. However, by keeping lysis buffer volumes low and therefore RNA concentrations high, an assay of up to 3 cancer- or hormone-associated targets from one cell was realized (Figure 5E).

From a clinical point of view, the hormone receptor status is a key checkpoint in breast cancer diagnostics as hospital guidelines suggest hormone and/or antibody therapy depending on a positive receptor status, replacing or accompanied by radio-chemotherapy. Without axillary lymph node infiltration, stage I breast cancer has high curative chances by mastectomic resection and prophylactic hormone therapy only. In the opposite viewpoint, metastatic breast cancer is characterized by lymph node, bone, lung, brain or liver invasion and the respective therapy contains harsh radiation and cytotoxic chemical agents with severe side-effects for the patient. Not least because of that, personalized and, above all, correct therapy administration has become a major topic in basic and clinical research. Alix-Panabières and Pantel have impressively reviewed that CTC characterization can provide answers to these in-depth questions [20]. The isolation of ctDNA for Next Generation Sequencing is exploited and extensively evolved to monitor cancer dynamics [21]. Improved single tumor cell isolation as shown in the present study might be useful to overcome limitations in the clinical use of these methodologies due to standardization in automation and lowered costs. In theory, it is also possible to use the residual blood sample for ctDNA analysis after the pre-enrichment of CTCs with the workflow of the CTCelect benchtop system or separate the plasma from the cell phase beforehand. This would enable a parallel isolation of ctDNA and CTCs to provide encompassing diagnostics from the same sample in a clinical setting or for central laboratories. Although magnetic cell separation is a straightforward, combinable and automatable technique, commercial bead systems mostly use batch analysis (PCR) for tumor markers. The herein presented combination-of-combinations principle could reduce background signal for detailed examination of molecular tumor features.

To conclude, our improved protocol to directly isolate and amplify single cell RNA allows for a swift single CTC analysis resulting from immunomagnetic enrichment in combination with microfluidic dispensing, highlighting the potential for future therapeutic decision-making.

4. Materials and Methods

If not otherwise specified, reagents and supplements were purchased at Thermo Fisher Scientific, Darmstadt, DE.

4.1. Cell lines and blood samples

The MCF-7 cell line was purchased from AdnaGen (Langenhagen, Germany) and cultured in RPMI1640 medium with L-Glutamine (Capricorn Scientific, Ebsdorfergrund, Germany) supplemented with 10 % fetal calf serum (FCS; Merck, Darmstadt, Germany). MDA-MB-231 cells were kindly provided by Dr. Pierpaolo Moscariello (Max-Planck-Institute for Polymer Research, Mainz, Germany) and cultured in Gibco™ DMEM (low glucose, pyruvate) medium supplemented with 10 % FCS. Cell lines were split at subconfluence and incubated at 37 °C in a humidified atmosphere in the presence of 5 % CO₂.

Whole blood bags from healthy donors were purchased from the local Blood Transfusion Center (University Medical Center Mainz, Germany) in 500 mL CompoFlex® blood bags (Fresenius Kabi, Bad Homburg, Germany) with CPD-1 anticoagulant and stored at room temperature for a maximum of three days. Informed consent was obtained from the donors as usual in clinical blood donation guidelines.

4.2. Immobilization of biotinylated antibodies on streptavidin coupled magnetic microbeads

Dynabeads™ MyOne™ Streptavidin T1 superparamagnetic beads were tumor-specifically coated with biotinylated monoclonal mouse anti-human EpCAM (CD326; 20 µg/mL) antibody 1B7. EpCAM antibody was immobilized on the bead surface with an extended incubation time of 1 h. After immobilization, a saturated biotin/PBS solution was added for 30 min with gentle rotation of the tube to block free streptavidin binding sites and prevent clumping. After an additional washing step, anti-EpCAM magnetic beads (herein abbreviated as “beads”) were stored in PBS/0.1 % BSA at 4 °C for several weeks.

4.3. Bead sedimentation test

Different solutions of PBS, 0.125, 0.05 and 0.01 % polysaccharide transfer buffer (TB, subject to confidentiality), 23, 50 and 100 % glycerol and 23 % glycerol/5 % mannitol were produced. An amount of 5×10^9 /mL 1 µm beads were added to 1 mL test solution in a

reaction tube, respectively. The visual sedimentation was observed over the course of 30 min.

4.4. Spike-in experiments and automated CTCelect single cell isolation of tumor cells

Spike-in experiments and automated CTCelect assays were performed as described in [9]. Cell recovery rates were determined using fluorescence microscopy. CFSE staining was conducted as directed in the CellTrace™ CFSE Cell Proliferation kit manual.

4.5. Immunostaining of pre-enriched samples

Immunomagnetically enriched samples were stained with monoclonal antibody EpCAM (1B7)-, CD144-, CD84-, CD63-PE eBioscience™ antibody (1:30) to label epithelial cells and with nuclear dye Hoechst33342 (1:1000) for 10 min at room temperature. Washing steps were performed in a magnetic separator. Stained samples were processed in the microfluidic chip of the CTCelect device or measured using the Accuri C6 flow cytometer (BD Biosciences, Franklin Lakes, NJ, USA).

4.6. Nucleic acid extraction and single cell RT-qPCR of isolated tumor cells

To confirm cancer-relevant mRNAs in cell bulks and in single cell isolates, two-step and one-step real time quantitative PCR (RT-qPCR) was performed. β -actin (RPLP0) served as housekeeping RNA control. RNA was extracted from dispensed droplets immediately after CTCelect isolation using 2x or 10x guanidine salt-free lysis buffer (LB; 1:1 to the droplet volume/1:9 in pooled samples) or transferred in purification columns using either the RNeasy Micro kit or AllPrep DNA/mRNA Nano kit (both QIAGEN, Hilden, DE) by following the manuals of the manufacturer. Elution was performed at the lowest volume possible to maintain highest RNA concentrations. For two-step protocols, total RNA was reverse transcribed into cDNA with the SensiFAST™ cDNA Synthesis kit (Meridian Bioscience, Luckenwalde, Germany) and qPCR was conducted using 5 μ L cDNA and QuantiFast SYBR Green RT-PCR kit (QIAGEN, Hilden, DE) in a 96 well cycler (BioRad CFX96 Touch Real-Time PCR Detection System, Feldkirchen, Germany). One-step qPCR was performed by means of the SensiFAST™ Probe No-ROX One-Step kit (Meridian Bioscience, Luckenwalde, Germany) whereas reverse transcription was extended to 20 min and extension time was set to 10 s. BreastCancer Detect Adnatest (QIAGEN, Hilden, Germany)

primers were added as described in the manual. Threshold cycle values (C_T) were obtained. Primers are available in the Supplementary Materials (see Table S1) and were designed with Primer-BLAST (National Institutes of Health, Bethesda, MD, USA; <https://www.ncbi.nlm.nih.gov/tools/primer-blast/> accessed on 29 July 2022). Primer sequences of the Adnatest are non-disclosed by QIAGEN.

4.7. Gel electrophoresis and Bioanalyzer

To analyze PCR product sizes, gel electrophoresis and automated electrophoresis using the Bioanalyzer (Agilent Technologies) was performed. For gel electrophoresis, we used a 2 % agarose gel in tris-acetate-EDTA buffer. DNA was diluted 1:1 in DEPC H₂O, added 1:5 6x Orange G loading dye per sample and run for 45 min at 100 V. Ladders were used at 5 μ L (100 bp DNA Ladder, puC19 Ladder, both Carl Roth, Karlsruhe, Germany). Gels were displayed in the Fujifilm LAS-3000 Luminescent Image Analyzer. Automated electrophoresis in the Bioanalyzer was performed using the Agilent DNA 1000 kit as indicated in the manual.

4.8. Statistical analyses

Each experiment was repeated as indicated in the text, figures or legends. CTCelect data were collected from the output files of the software and further analyzed using Microsoft Excel 2016. Data are depicted as means with SD, and statistical analysis was done using GraphPad PRISM 8.2.0 for Windows (GraphPad Software, San Diego, CA, USA, www.graphpad.com). The p values of the statistical tests given in the respective figures were reported as not significant (ns) when $P^{ns} > 0.05$ and as significant when * $p \leq 0.05$.

3 Discussion and Conclusions

This section discusses the main achievements, conclusions and some of the blind spots of the conducted studies and delineates perspective on future research. As for the primary goal of this work, a single cell isolation by means of automated immunomagnetic enrichment and antibody-based fluorescence detection in a chip-based microfluidic system and the molecular biological characterization of these cells was realized.

3.1 Summary

The first step was to outline all the bottlenecks and determining factors of the overall isolation process and to sight previous works for room of improvement. With manual enrichment, we developed a suitable CTC model system to establish the protocol for squamous cell carcinoma and breast cancer. Using this model, reproducible performance of 1 μm tosyl-activated, hydrophobic magnetic beads was demonstrated resulting in high cell recovery rates for both the existing prototype enrichment device IsoMAG and CTCelect (see Chapter 2.1 and 2.2). In parallel, white blood cell contamination was quantified via FACS analysis. EpCAM-based enrichment led to a bycatch of ~ 1200 WBCs as similarly described for CellSearch[®]. Nonetheless, the comparably low total number of 10^3 WBCs after enrichment (compared to 10^7 WBCs/mL in healthy adults) enabled immunofluorescent assessment of the patient isolates and marker-based distinction between potential CTCs and WBCs [60].

Subsequently, we showed that both IsoMAG and CTCelect are applicable for HNSCC patient samples and characterized isolated CTCs by immunostaining using a panel of tumor markers (see Chapter 2.1, Figure 5 and 2.2, Figure 6). For example, it was possible to isolate 74 to 93 potential epithelial-like CTCs from patients suffering from different HNC subtypes (hypo- and oropharynx cancers with lymph node metastasis). Beyond that, CTCelect enabled automated dispensing of single circulating tumor cells from HNSCC patient samples and qPCR-based confirmation of tumor-related biomarkers. In fact, there is growing interest in singularizing pre-enriched rare cells like CTCs to decrease signal-to-noise ratio for downstream molecular analysis, e.g. to distinguish between hormone receptor-associated tumor subtypes. For this purpose, we developed a simplified qPCR protocol for single cells without RNA purification targeting cancer subtype-relevant transcripts, published in the third paper (see Chapter 2.3). During the research, several setbacks were faced. Most of them were resolved or discussed in the respective publications and in-depth error analysis and optimizations were a

centerpiece in this work. One of the biggest hurdles was bringing together macro- and microfluidics in a very complex fluid like whole blood. A standard blood sample comprises 7.5 mL of blood. The successive washing steps had to be reduced stepwise in such a way that an enriched fluid reduced to 300 to 500 μ L was available before microfluidic processing in the chip. This circumstance always involves a certain risk of losing sample fluid, and thus target cells.

On a further note, the experiments performed so far are based only on EpCAM expression. In Chapter 2.2 and 2.3, we highlighted and discussed the risks and drawbacks of enrichment and detection using EpCAM antibodies alone. Meaningful variation of capture antibodies should be investigated in the future. This also feeds into the lack of diagnostic or prognostic significance of the pilot experiments with patient material from HNC patients performed here. Our very early results included a total of only five HNC samples from whole blood. Although our technologies demonstrated that cancer is associated with the presence of CTCs in 100 % of the samples tested, the study is too small to derive any direct added value. In addition, no breast cancer samples could be analyzed so far. Another consideration was that for clinical application, a higher degree of parallelization of the platform would be attractive. Regarding this problem, engineering adjustments to other liquid biopsy platforms in-house concerning tube sizes and multi-sample holders already exist [61]. Concerning the microfluidic fluorescence-based detection, a major issue was that magnetic beads exhibit a certain autofluorescence signal, especially in the red spectrum, overlapping with PE-staining. We showed this overlap in the third publication (see Chapter 2.3, Figure 4). As a possible solution, we implemented a gating function for the cytometer subunit of CTCelect to selectively dispense cells instead of autofluorescent objects.

In summary, this work was intended to profoundly characterize the CTC isolation platforms developed at the institute in terms of biological validation, microfluidic handling, assay conception and downstream analysis. In the end, we were able to confirm automated immunomagnetic enrichment using IsoMAG and single cell isolation using CTCelect of potential CTCs from head and neck cancer patient samples. To this end, various cancer-relevant nucleic acid and immunostaining detection methods were devised during this work and published accordingly as listed below:

- a) PanCK-PE immunostaining of enriched potential CTCs from HNSCC patient blood using IsoMAG (paper 1).
- b) EpCAM-PE and Integrin-PE immunostaining of dispensed single potential CTCs from HNSCC patient blood using CTCelect (paper 2).
- c) EpCAM, Stratifin and Integrin mRNA detection from dispensed single potential CTCs from HNSCC patient blood using CTCelect (paper 2).
- d) EpCAM, GA733-2, Muc-1, PGR, ESR, CXCR4 and Her-2 mRNA detection method development from cultured and dispensed single breast cancer cells using CTCelect (paper 3).

3.2 Advantages of CTC Analysis

To a predominant extent, the advantages of CTC analysis compared to invasive diagnostics and other biomarkers in blood-based liquid biopsies were emphasized in this work.

CTCs are systemic tumor components and hence are of high clinical value. A benefit of isolating CTCs is that cells are complete organizational structures that include all information on a cellular, RNA and DNA level and are not highly diluted in the blood like cell free tumor DNA. This opens up a broad range of downstream research on proteomics, methylation, mutagenomics and drug tests. Interestingly, Next Generation Sequencing (NGS) of captured CTCs from patients with unknown primary tumors could even be used to identify tissue-specific genes and pin down the tumor origin [62].

The CTC count was established as independent prognostic marker with reasonable evidence for progression-free and overall survival. Consequently, the working group Gynecological Oncology AGO-Mamma of the German Cancer Society (DKG) added CTC analysis as prognostic and early detection marker for therapy resistance in metastatic breast cancer to their guidelines [63]. In fact, CTC dynamics indicate possible success or resistance already a few weeks after therapy initiation, similar to the effects in circulating tumor DNA levels. For example, Yu and colleagues impressively displayed CTC dynamics between disease progression and treatment response using longitudinal monitoring of EMT features in CTCs from a patient with lobular breast cancer, who was serially sampled during treatment with pathway inhibitors and chemotherapy [64]. For CTC enrichment and characterization, the researchers used the very advanced herringbone CTC-chip technology developed by Stott et al. in 2010 which combines physical enrichment due to microstructuring and biochemical capture using antibody immobilization in the inner chip walls [11]. However, this technology does not support tumor cell recovery for further transcriptomic analysis or tumor cell culture.

This is due to the permanent trapping, fixation and permeabilization of the cells in the chip to realize intracellular staining, such as for cytokeratins. Similar disadvantages of other isolation methods were discussed in the above presented publications (i.e. see Chapter 2.2, Table 2).

Although CTCelect did not necessarily enable cell recovery rates as high as in other platforms, it is aiming for viable single cell dispensing and does not require fixation. This feature holds enormous potential for single cell studies and CTC culture. Diverse studies revealed that precise cell line selection and patient stratification in cancer drug approval is crucial for the clinical trial success rate. In detail, 97 % of oncology clinical trials fail to receive approval. This is mainly due to toxic off-target effects, misinterpreted mechanisms of action or diseased-healthy comparisons and simply the wrong selection of patients [65]. Recently, the FDA approved the first PI3K inhibitor alpelisib for ESR⁺ metastatic breast cancer with activating PIK3CA mutations. The companion diagnostic PCR test to detect the PIK3CA mutation in a tissue and/or a liquid biopsy was also FDA-approved [66]. Surprisingly, studies revealed potential cell line-specific PI3K α inhibitor resistance mechanisms even though the cells carried the PIK3CA mutation [67]. These findings underline that a mutation only is not always the adequate biomarker for a successful therapy. Besides that, inter- and intratumoral heterogeneity might lead to different mutational hotspots. The isolation of viable tumor cells using platforms like CTCelect and their cultivation into so-called tumoroids offer new possibilities for fast personalized drug screening to avoid patient- and metastasis-dependent resistances. Anderle et al. identified individual treatment responses and therapeutic vulnerabilities in ovarian cancer using patient-derived microtumors grown from tumor cell single suspensions [68]. Comparable findings were made for the treatment response of patient-derived organoid models in metastatic gastrointestinal cancers [69]. Generally speaking, in 100 % of cases, if a drug didn't work on a single cells-derived patient's organoid, then it didn't have effect on the patient. And in almost 90 % of cases, if a drug did work on the organoid, then it also worked in the patient [70]. Tumoroids can be cultured from a single cell suspension from one (liquid) biopsy within a short generation time of a few weeks. These impressive possibilities were not within the scope of the results presented here and only inadequately discussed in the respective publications but will be subject to research in the future. As a first step, the enrichment of patient-derived tumor cells using IsoMAG and the dispensing of intact single cells using CTCelect without fixation, presented in these studies here, indicate that tumoroid cultivation is feasible.

From an economic perspective, the oncology therapeutic market is still by far the leading area based on sales with 145 billion USD in 2019 [71]. It has to be mentioned that from 10,000 potential drug compounds, only one will make it to FDA approval that goes into this

sales number [72]. As explained above, new techniques to pre-test pharmacological efficiency of potential cancer therapeutics on patient-derived tumoroids could help to accelerate this process. In *BioProcess International*, GlobalData analyst Nadia McLurcan stated that it is widely recognized that not all drugs have effects on all patients. Of all drugs, the least effective (such as those for cancer) are the most expensive and the ones with the most harmful side effects. Companion diagnostics (i.e. CTC analysis supported by the CTCelect technology) can assist to predict how patients will respond to treatment, allowing the most balanced dose from the start, while also reducing overall costs by reserving expensive therapies for populations who will really respond to them [73]. The industry is reacting to the emerging understanding of personalized medicine. In fact, the global CTCs market size was estimated at 8.4 billion USD in 2020 and is expected to grow at a compound annual growth rate of 11.7 % from 2021 to 2027 to reach 18.3 billion USD by 2027 [74].

Another advantage of including CTC analysis in early marker diagnostics is the increased sensitivity. As already mentioned in the introduction, CTCs were detectable in COPD patients before lung cancer outbreak [16]. Other studies also report early-stage accuracy, low risks and high sensitivity of CTC diagnostics superior to those based on tissue biopsy and X-rays [75]. This also applies to neck level lymph node biopsies in head and neck cancer for example. In reality, 50 to 80 % of HNSCC and HNC patients are diagnosed when lymph node metastases are already detectable, resulting in a poor overall prognosis and little curative chances. Another 13 % of patients even exhibit distant metastases upon first diagnosis [76,77]. However, before the primary tumor or micrometastases are visible via imaging technologies, there still is a small time frame for early CTC diagnostics before the development or detectability of locoregional metastases (Figure 8).

In addition, a certain risk of overlooking single malignant cells or even cell populations in paraffin-embedded lymph node tissue sections from histopathology always remains. In this case, enzymatic or mechanical dissociation using tissue grinders, as for example described by Scheuermann et al. [80], could be of assistance in producing single cell suspensions from tissue biopsies. Single malignant cells can then be detected in these cell suspensions with the aid of optomicrofluidic devices such as CTCelect, which opens up a complete new application field for the platform of high resolution biopsy and *in vitro* personalized therapeutics testing. A conceivable diagnostic model would not be to replace the classical histopathological findings but rather to additionally extend the imaging techniques with single cell analyses from the dissociated tissue. In this way, the overall resolution of the diagnostics would increase and the tumor cells found could be examined more closely or tested for drug response.

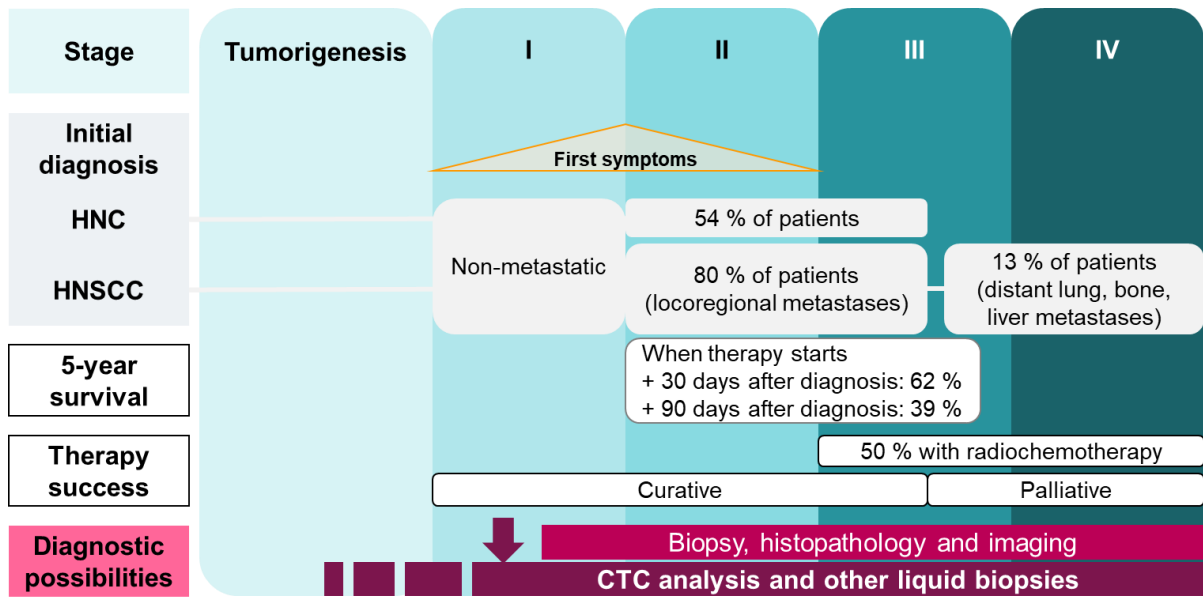


Figure 8: Tumor staging, HNC metrics and diagnostic possibilities.

About 50 to 80 % of patients with HNSCC and HNC in general are often diagnosed when they already have locoregional metastases and receive a poor overall prognosis. Curative chances decrease at this point. However, before the original tumor or micrometastases are detectable via imaging technologies, CTC analysis from a blood sample can already take place as indicated with the purple arrow (source: own graphic, references: [76–79]).

3.3 Innovation Management

According to an innovation management study on CTCelect by Fleßa et al. from 2020, the innovation process goes through various phases: from the product idea, development, approval, reimbursement to market launch. Up to now, the first 3 phases are predominantly seen as a technical problem, while the last two phases are reserved to economics. Efficient innovation management, on the other hand, requires the use of business management and health economics elements from the very beginning in the sense of an integrative development [81]. Indeed, we have observed that it takes great efforts to cross the threshold to clinical application, which requires involvement of economic thought processes from the start. A decisive factor, especially in the health insurance system in the German market, is the question of reimbursement for liquid biopsy as outlined in Figure 9, which in turn must be considered early on and adequately supported by clinical data.

The establishment of new technologies depends on government health authorities and the reimbursement policies of insurers because if a molecular assay (for example CTC analysis) cannot be refunded, few patients will get it [73]. Hence, larger patient sample studies are required to enhance trust for investments and our studies here can only cover the first steps of placing the platform technology in routine lab work. Despite the high Technology

Readiness Level of the systems, we certainly addressed basic research to seek proof-of-concept and characterize the strengths and weaknesses of the inventions.

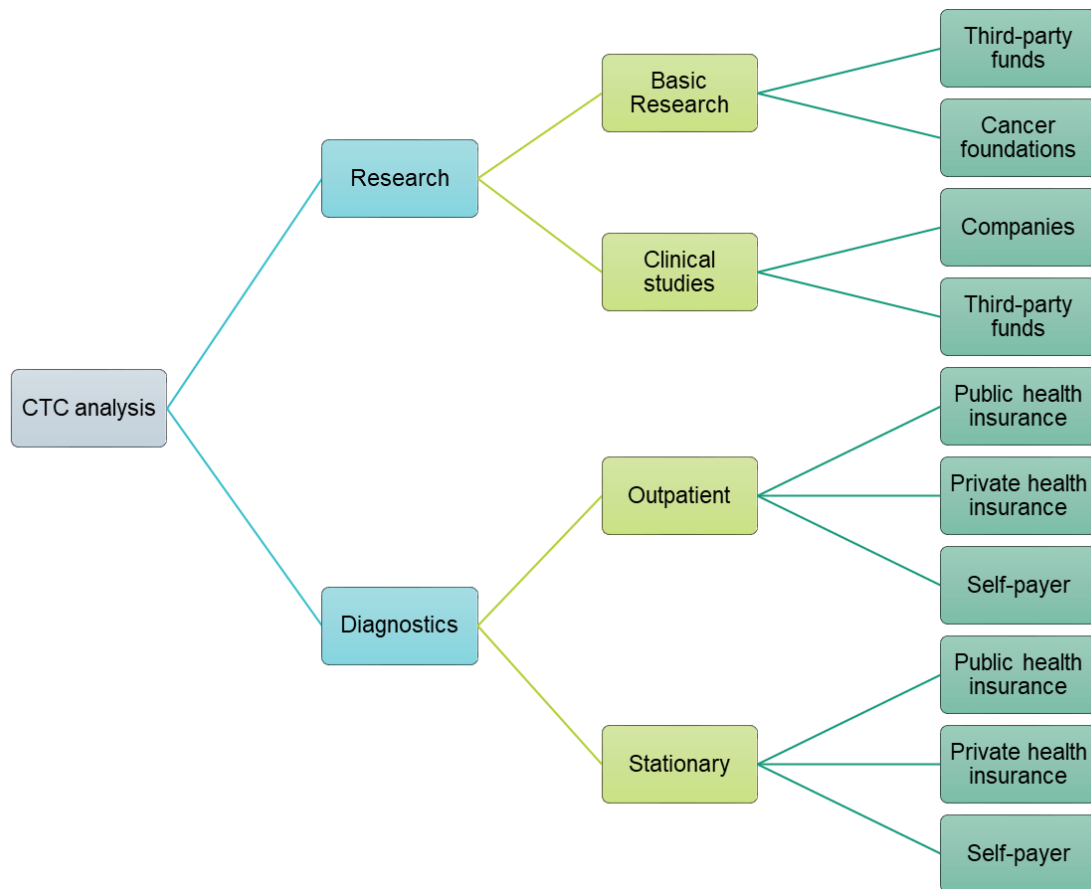


Figure 9: Market segments for CTC analysis.

The funding and reimbursement of CTC analysis has to be differentiated into market segments. As a research tool, funding for basic research and clinical studies is provided by third-party funds, foundations or companies seeking approval for their technologies. IVD certified CTC analysis platforms are financed by the public and private health insurances depending on their recommendations or by self-payers (modified, adapted from [81]).

3.4 Future Perspectives

Taking a look into the clinic, therapy decisions for i.e. metastatic breast cancer are still broadly made on primary tumor and lymph node biopsy. As explained in Chapter 2.3, hormone receptor positive patients receive endocrine therapy, HER-2 positive tumors are targeted using anti-HER-2 therapy and TNBC is eligible only for chemotherapy. Harbeck et al. impressively reviewed that different types of advanced mBC are more or less likely to metastasize at certain sites in the body. In reality, there is however a clear overlap in tissues at risk of metastasis by completely different cancer subtypes [82]. Liquid biopsy will help unravel the molecular mechanisms underlying these metastatic preferences and also predict potential therapies that could not be foreseen by primary tumor biopsy.

While in the past, therapy decisions were exclusively derived from patient history, medical imaging and histopathology of primary and secondary tumor tissue to monitor therapy response, it has nowadays been extended to molecular analysis of DNA mutation profiles from ctDNA and CTCs in the so-called Molecular Tumor Boards. It would be highly desirable to add 3D CTC cultures and biomarker identifications for personalized medicine to molecular analyses in future tumor treatment guidelines to predict individual drug response or resistance. As an example of a pioneering exploratory Early Phase I study, researchers at the University Hospital Basel have investigated since 2020 whether the cardiac glycoside digoxin is able to disrupt CTC clusters in advanced or metastatic breast cancer patients. Blood samples are drawn to isolate tumor cell clusters and measure CTC cluster size changes [83]. CTC clusters are considered relatively new biomarkers that carry 20- to 100-fold greater metastatic potential than single CTCs and their study has only recently been brought into the light [84]. With little modifications to the chip dimensions of CTCelect, CTC cluster isolation could also be feasible. Preliminary experiments already showed that cluster enrichment from cell culture using IsoMAG is possible. Furthermore, approval of oncologica predominantly fails in Phase II at success rates of only 24.6 %, with “insufficient efficacy” being the reasons for failure in 48 % of these cases. A lack of effect of active compounds in CTCs, independent of the primary tumor, could be a major driver for the lack of overall response to therapy in the patient. To overcome this obstacle, Garcia-Villa et al. showed, for example, if a platinum-based chemotherapy response is present in patient-derived CTCs [85]. In the future, multi-omic multi-analyte liquid biopsy approaches will become more and more important to address these topics (Figure 10).

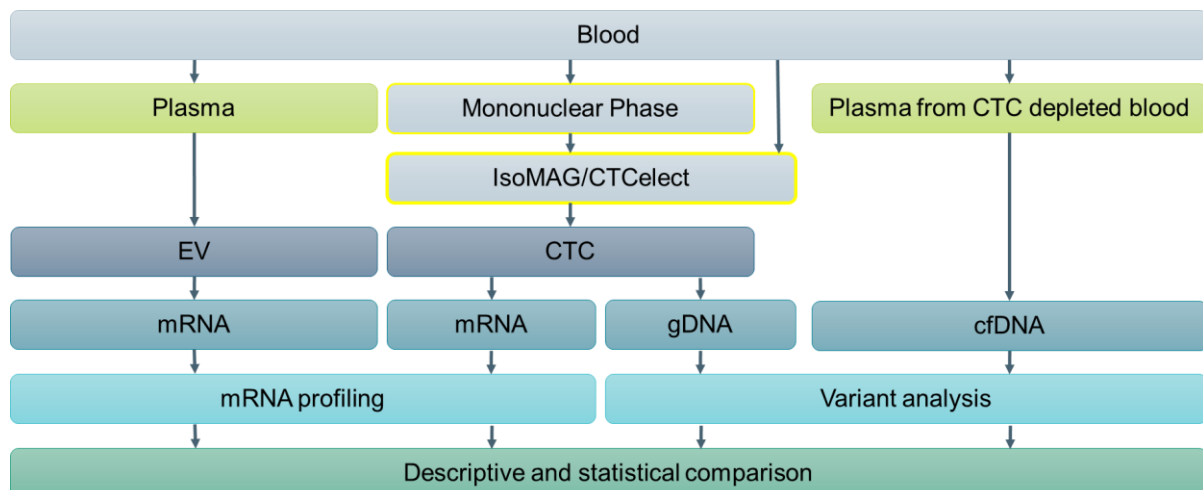


Figure 10: Evaluation of multiple Liquid biopsy analytes In Metastatic breast cancer patients All from one blood sample (ELIMA) study design and possible contribution of CTC isolation platforms.

EV mRNA, CTC mRNA, CTC gDNA, and cfDNA were isolated from blood and mRNA profiling or variant profiling resulted in comparable data sets for comprehensive integration. Integrative statistical analyses performed included the analysis of the individual analytes and their prognostic value. As indicated in yellow, CTC isolation

devices such as CTCelect could be of use to separate CTCs from the rest of the blood components or from the mononuclear cell phase to contribute to these kind of multi-faceted studies (modified, adapted from [86]).

This means that individual blood fractions, such as plasma, CTCs and CTC-depleted plasma, are first obtained from a minimized volume of the starting material, whole blood. Biomarkers such as mRNA and gDNA from CTCs, extracellular vesicles and cfDNA can then be extracted from the individual fractions from the same samples. In the 2021 landmark “ELIMA” study (*Evaluation of multiple Liquid biopsy analytes In Metastatic breast cancer patients All from one blood sample*), this approach increased the number of patients with actionable signals in all analytes to over 95 % [86]. The established ELIMA score that weighs the contribution of each analyte to the overall survival had significant prognostic value compared to the single analytes. Large-scale endeavors such as these are indicative that high-resolution comprehensive liquid biopsy can provide far more insight into individual cancers than just CTC counts in prognostic approaches such as CellSearch®. Our literature searches revealed that increasing incidence of CTCs is indeed associated with worsened prognosis and progressive tumor staging in many studies. However, considering the sometimes earlier or later occurrence of CTCs, a comprehensive view of the individual case must always be taken. In 2016, Andree et al. described CellSearch® as the still-remaining gold standard for CTC enumeration but the researchers also highlighted the prevalence of difficulties in assigning objects as CTCs using their software and in comparing CTC isolation technologies due to the lack of a uniform CTC definition [57].

To date, randomized outcome studies in particular are missing to legally establish the benefit of the addition of liquid biopsies in tumor diagnosis and follow-up. It should not be forgotten that the apparently expensive diagnostic costs still represent only a tiny fraction of the overall therapy costs. Contrary to this paradox, the trend must be towards giving comprehensive diagnostics their rightful importance, so that immense costs of a simply wrong therapy can be prevented in advance. As sequencing becomes more affordable, new research fields in transcriptomics, genomics and methylation profiling will emerge and terms like the “exome” or “multi-omics” will become more fashionable to improve early detection and facilitate personalized cancer diagnostics and therapy. CTC isolation platforms such as CTCelect or IsoMAG that indeed separate tumor cells from other blood components will prospectively be able to contribute to these multi-omic multi-analyte pipelines in an automated manner.

4 Appendix

A. Acknowledgements

B. Publication notice

Stiefel, J.; Baßler, M.; Wittek, J. et Freese, C. Automated immunomagnetic enrichment and optomicrofluidic detection to isolate breast cancer cells: A proof-of-concept towards PoC therapeutic decision-making. *Magnetochemistry* 2022; 8(9): 99. <https://doi.org/10.3390/magnetochemistry8090099>

Stiefel, J.; Freese, C.; Sriram, A.; Alebrand, S.; Srinivas, N.; Sproll, C. et al. Characterization of a novel microfluidic platform for the isolation of rare single cells to enable CTC analysis from head and neck squamous cell carcinoma patients. *Eng Life Sci.* 2022; 22: 391– 406. <https://doi.org/10.1002/elsc.202100133>

Gribko, A.‡; Stiefel, J.‡; Liebetanz, L.; Nagel, S.M.; Künzel, J.; Wandrey, M. et al. IsoMAG—An Automated System for the Immunomagnetic Isolation of Squamous Cell Carcinoma-Derived Circulating Tumor Cells. *Diagnostics* 2021; 11, 2040. <https://doi.org/10.3390/diagnostics11112040>; (‡contributed equally).

Non-scientific publications and unpublished work:

Alebrand, S.; Freese, C.; Stiefel, J.; Wehler, T.; Raem, A. M.; Baßler, M. Automatisierte Isolation zirkulierender Tumorzellen für die Liquid Biopsy. In: *Immunoassays: Ergänzende Methoden, Troubleshooting, regulatorische Anforderungen*; Raem, A.; Rauch, P., Eds., 2. Auflage 2023; *Springer Spektrum*: Berlin, ISBN 9783662626702. *Accepted for publication.*

Stiefel, J. et Freese, C. Tropfen für Tropfen gegen Krebs. *Laborpraxis* 2022. <https://www.laborpraxis.vogel.de/tropfen-fuer-tropfen-gegen-krebs-a-1093245/> [latest access: 2022-04-19]

Stiefel, J. Vollautomatisierte Isolation von zirkulierenden Tumorzellen aus Blutproben: Optimierung des CTCelect-Gesamtprozesses. Fraunhofer IMM Mainz; Johannes Gutenberg University Mainz. *Master thesis* 2019 (*unpublished*).

C. Abbreviations

μ CS	Microfluidic fluorescence-activated cell sorting
a.u.	Arbitrary unit
Ab	Antibody
BSA	Bovine serum albumin
CD45	Cluster differentiation 45 antigen
cfDNA	Cell free DNA
CFSE	Carboxyfluorescein succinimidyl ester
COPD	Chronic obstructive pulmonary disease
C_t	Threshold cycle
CT	Computer tomography
CTC	Circulating tumor cell
ctDNA	Circulating tumor DNA
CXCR4	C-X-C motif chemokine receptor 4
d	Day(s)
DMEM	Dulbecco's Modified Eagle Medium
DTC	Disseminated tumor cell
EDTA	Ethylenediaminetetraacetate
EMT	Epithelial-mesenchymal transition
EpCAM	Epithelial cell adhesion molecule
ESR	Estrogen receptor
EV	Extracellular vesicle
FACS	Fluorescence-activated cell sorting
FCS	Fetal calf serum
FDA	Food and Drug Administration
HER-2	Human epidermal growth factor receptor 2
HNC	Head and neck cancer
HNSCC	Head and neck squamous cell carcinoma
HPV	Human papilloma virus
IMS	Immunomagnetic separation
mBC	Metastatic breast cancer
MCF-7	Michigan Cancer Foundation 7
MET	Mesenchymal-epithelial transition
NCBI	National Center for Biotechnology Information

PBMC	Peripheral blood mononuclear cells
PBS	Phosphate buffered saline
PE	Phycoerythrin
pEMT	Partial/post-EMT
PET scan	Positron emission tomography
PR	Progesterone receptor
pTNM staging	Histopathologic tumor-nodes-metastasis staging
RT-qPCR	Real time quantitative polymerase chain reaction
SCL-1	Squamous cancer line 1
SPEC	Single photon emission computed tomography
TNBC	Triple-negative breast cancer
USD	U.S. dollars
WBC	White blood cell

D. Supplements and References of the Publications

This section presents the supplements and references of the publications discussed in this dissertation as originally published.

The copyright of the original publications is held by the respective copyright holders/authors.

The documents are available online at:

(1) <https://www.mdpi.com/article/10.3390/diagnostics11112040/s1>

(2) <https://doi.org/10.1002/elsc.202100133>

(3) https://mdpi-res.com/d_attachment/magnetochemistry/magnetochemistry-0800099/article_deploy/magnetochemistry-08-00099s001.zip?version=1662479136

Supplement (1)

IsoMAG – an automated system for the immunomagnetic isolation of squamous cell carcinoma-derived circulating tumor cells

Alena Gribko ^{1,†}, Janis Stiefel ^{2,†}, Lana Liebetanz ², Sophie Madeleine Nagel ¹, Julian Künzel ³, Madita Wandrey ¹, Jan Hagemann ¹, Roland H. Stauber ¹, Christian Freese ^{2,*} and Désirée Gül ^{1,*}

¹ Department of Otorhinolaryngology/ENT University Medical Center Mainz, Langenbeckstr. 1, 55131 Mainz, Germany

² Fraunhofer Institute for Microengineering and Microsystems IMM, Carl-Zeiss-Str. 18-20, 55129 Mainz, Germany

³ Department of Otorhinolaryngology, University Hospital Regensburg, Franz-Josef-Strauß-Allee 11, 93053 Regensburg, Germany

* Correspondence: Christian.freese@imm.fraunhofer.de; guel@uni-mainz.de

† Contributed equally

Tables

Table S1. Detailed protocol of IsoMAG isolation procedure

No.	Program section	Chapter title	Carousel: position	Magnet: position	Flowrate [ml/min]	Duration [s]
1	Initialization	Home position	Position 1	Position home	40	
2		to pipette position				
3		Taking pipette				
4		Pipette up				
5		to carousel position				
6	Blood sample	to blood sample position				
7		Blood sample mixing			10	1800
8		Aspirate blood			10	
9		Aspirate to extra position				
10		Aspirate to carousel position				
11		Waiting				5
12		magnet pos 1		Position 1		200
13		magnet pos 2		Position 2		400

4 Appendix

14		waste blood			1	
15	Washing buffer 1 5ml	pipette up/ change to position 2	Position 2	Position home		
16		wash buffer mixing			10	600
17		wash buffer				
18		Aspirate			10	
19		Aspirate to extra position				
20		cone mixing			10	60
21		Aspirate buffer			10	
22		Aspirate to carousel position				
23		magnet pos 1		Position 1		200
24		magnet pos 2		Position 2		400
25		waste buffer			1	
26	Washing buffer 2 5ml	pipette up/change to position 3	Position 3	Position home		
27		wash buffer mixing			10	600
28		wash buffer				
29		Aspirate			10	
30		Aspirate to extra position				
31		cone mixing			10	60
32		Aspirate buffer			10	
33		Aspirate to carousel position				
34		magnet pos 1		Position 1		200
35		magnet pos 2		Position 2		400
36		waste buffer			1	
37	Washing buffer 3 4ml	pipette up/change to position 4	Position 4	Position home		
38		4ml wash buffer mixing			10	600
39		wash buffer				
40		Aspirate			10	
41		Aspirate to extra position				
42		cone mixing			10	60
43		Aspirate buffer			10	
44		Aspirate to carousel position				

4 Appendix

45		magnet pos 1	Position 1	200
46		waste buffer	1	
47		waiting		200
48		waste buffer 2	1	
49	Washing buffer 4 1ml	pipette up/change position 5	Position 5 Position home	
50		wash buffer mixing	10	300
51		wash buffer		
52		Aspirate	5	
53		Aspirate to carousel position		
54		pipette up		
55		eppi dialog		1
56		dispense liquid	5	
57		Home position + removing falcons and pipette		

Figures

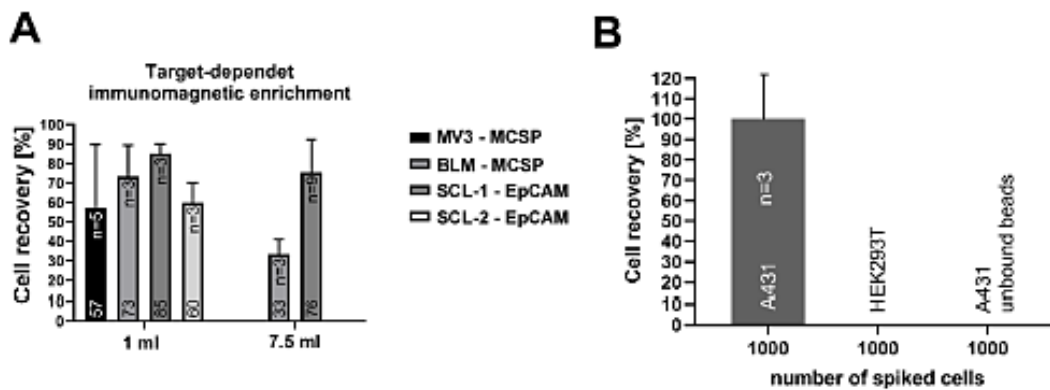


Figure S1. Recovery rates of different cancer cell lines during protocol establishment. **A.** Melanoma and carcinoma single cells were recovered from 1 and 7.5 mL culture medium. 20 CFSE labeled single cell were spiked in 1 or 7.5 mL respectively and manually enriched using a magnetic separator. Dynabeads MyOne Streptavidin T1 beads were coated with 20 $\mu\text{g}/\text{mL}$ biotinylated monoclonal mouse anti-human melanoma-associated chondroitin sulfate proteoglycan (MCSP) antibody EP-1 (Miltenyi Biotec) for melanoma cells MV3 and BLM or biotinylated monoclonal mouse anti-human EpCAM (CD326) antibody 1B7 for squamous cell carcinoma cells SCL-1 and SCL-2. **B.** A431 cells (EpCAM-positive) and HEK293T cells (negative control) were spiked into 7.5 mL culture medium and enriched as described in A.

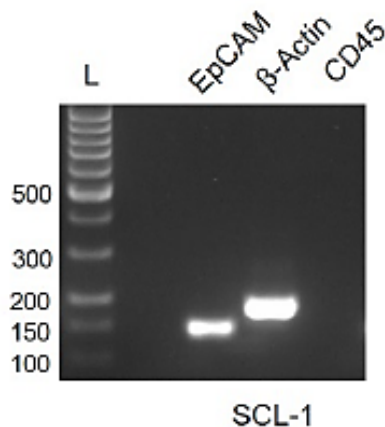


Figure S2. Gel electrophoresis of EpCAM RT-qPCR products (136 bp) from SCL-1 single cell RNA. Total single cell RNA was isolated using RNeasy Micro Kit (QIAGEN) with a downscaled protocol spiking one cell in lysis buffer and reverse-transcribed in cDNA with Sensifast cDNA synthesis Kit (Bioline). qPCR was performed with Quantifast qPCR Kit (QIAGEN). β -Actin (176 bp) served as positive control and leukocyte marker CD45 (159 bp) was used as negative control. Primers were designed with Primer-BLAST (National Institutes of Health; <https://www.ncbi.nlm.nih.gov/tools/primer-blast/>).

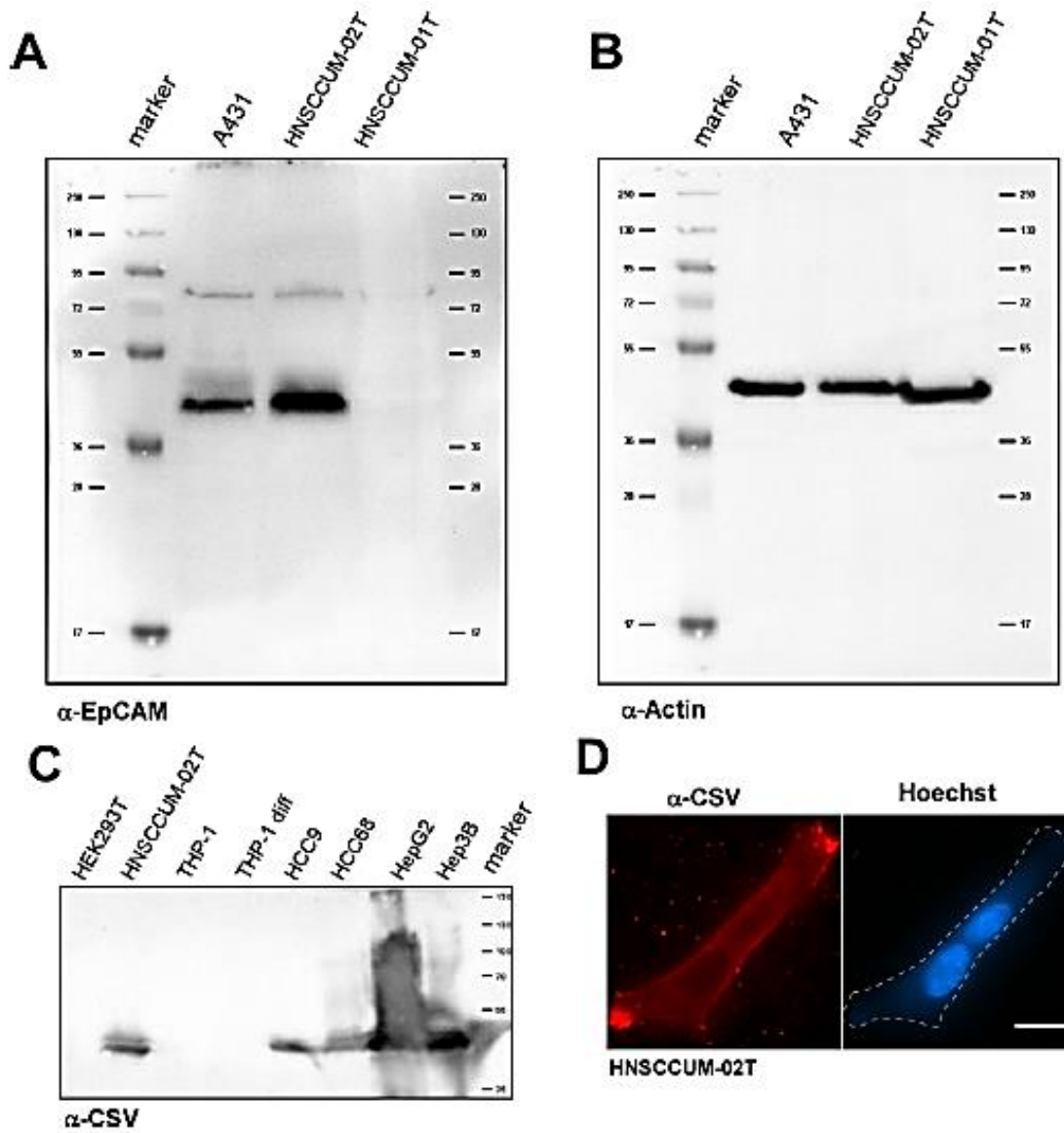


Figure S3. Expression of EpCAM protein (A, B) and CSV (C, D) in HNSCCUM-02T. Expression of EpCAM protein in whole cell lysates was visualized using α -CD326 purified Ab (44 kDa, eBioscience #14-9326) and α -Actin Ab (42 kDa, Sigma #A2066) served as loading control (B). Expression of CSV protein was visualized using α -cell surface vimentin Ab (50 kDa, Abnova, 17121-84-1) by Western Blot of whole cell lysates (C) and immunofluorescence staining of HNSCCUM-02T cells (D). Nuclei were stained with Hoechst. Scale bar, 10 μ m.

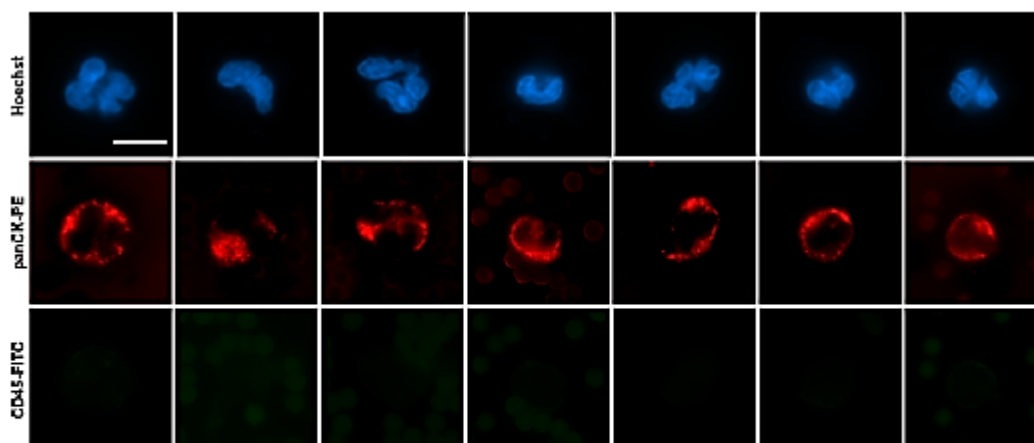


Figure S4. Potential circulating tumor cells (CTCs) could be enriched from whole blood of a HNSCC patient using EpCAM and CSV beads. 7.5 mL of patient blood was mixed with EpCAM- and CSV-coupled T1 beads (1:1) and placed into the IsoMAG unit for automated enrichment of CTCs. For cell counting, enriched cells were stained with Hoechst dye, cytokeratin (panCK-PE), and CD45-FITC antibodies and quantified by fluorescence microscopy. [Hoechst+/CD45-/panCK+] cells were classified as potential CTCs. Scale bar, 10 μm .

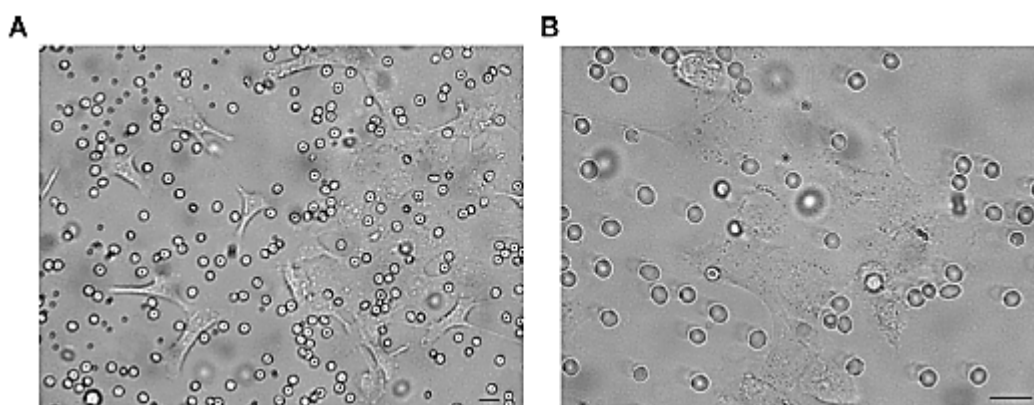


Figure S5. Brightfield microscopic images (20-fold (A) and 40-fold (B) magnification) of HNSCCUM-02T cells which were cultivated after immunomagnetic isolation using the Dynabeads™ FlowComp™ Flexi Kit (Invitrogen). 35 HNSCCUM-02T cells were spiked into 7.5ml blood of healthy donor, and manually isolated using EpCAM beads as described in Materials and Methods section. Additionally, after repeated magnetic separation and washing steps cells were re-suspended in 1ml release buffer and incubated for 10min on ice. The supernatant was centrifuged (350xg, 10min), and the cell pellet was resuspended in a mixture of fresh and pre-conditioned medium (1/3 to 2/3). Cells were seeded in collagen slides (#80802, ibidi GmbH, Gräfelfing, Germany), and imaged 7 days after seeding. Scale bars, 20 μm .

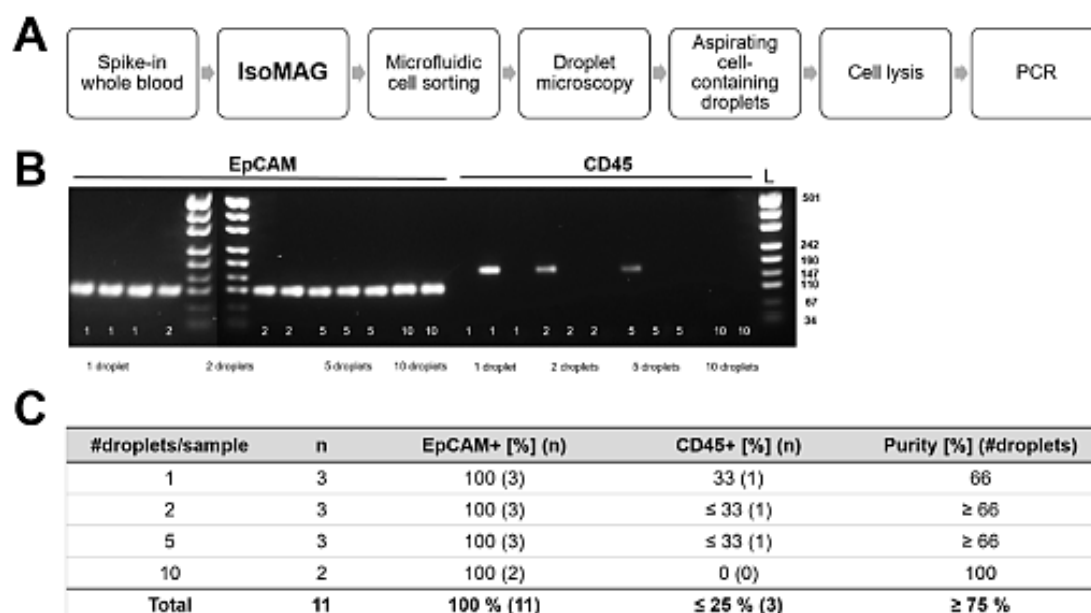


Figure S6. Establishment of CTCselect unit improves purity of isolated tumor cells from whole blood. **A.** Workflow of cell analysis including IsoMAG isolation unit, microfluidic cell sorting, and downstream PCR analysis. CFSE stained tumor cells (MCF-7) were spiked in 7.5 mL whole blood from a healthy donor. Immunomagnetic pre-enrichment using IsoMAG reduced WBC concentration by 10,000-fold compared to whole blood enabling microfluidic cell sorting. We used an in-house developed cell sorting unit consisting of a microfluidic chip for hydrodynamic sample focusing and a 480 nm laser with two silicon photomultiplier-supported fluorescence detectors to dispense single cells in single droplets. By establishing appropriate flow conditions and droplet sizes in chip-based microfluidic systems, the arithmetical probability of dispensing one WBC with a cancer cell in the same droplet is 10 %. Droplets containing a fluorescent tumor cell were identified under the fluorescence microscope and pooled in samples of 1, 2, 5 ($n=3$) and 10 ($n=2$) droplets. Samples were lysed for 15 min at 4 °C using a guanidine salt-free lysis buffer for direct one-step RT-PCR with the SensiFAST™ SYBR No-ROX One-Step Kit (Bioline) according to the manual. **B.** RT-PCR products were analyzed by means of gel electrophoresis. Leukocyte marker CD45 (159 bp) was targeted to detect WBCs in the droplets. EpCAM transcript (136 bp) served as positive control for tumor cells. Primers were designed with Primer-BLAST (National Institutes of Health; <https://www.ncbi.nlm.nih.gov/tools/primer-blast/>). **C.** WBC contamination was quantified as the ratio between samples positive for CD45 and EpCAM. Depending on the sample size, only 0-33 % (mean ≤ 25 %) of the samples were CD45+. Consequently, a purity of at least 75 % was determined and the feasibility of downstream PCR analysis after automated immunomagnetic enrichment and cell sorting was confirmed.

Supplement (2)

Characterization of a novel microfluidic platform for the isolation of rare single cells to enable CTC analysis from head and neck squamous cell carcinoma patients

Janis Stiefel, Ashwin Sriram, Christian Freese, Sabine Alebrand, Nalini Srinivas, Christoph Sproll, Madita Wandrey, Désirée Gül, Jan Hagemann, Jürgen C. Becker, Michael Baßler

Wiley *Engineering in Life Sciences*, 2021.

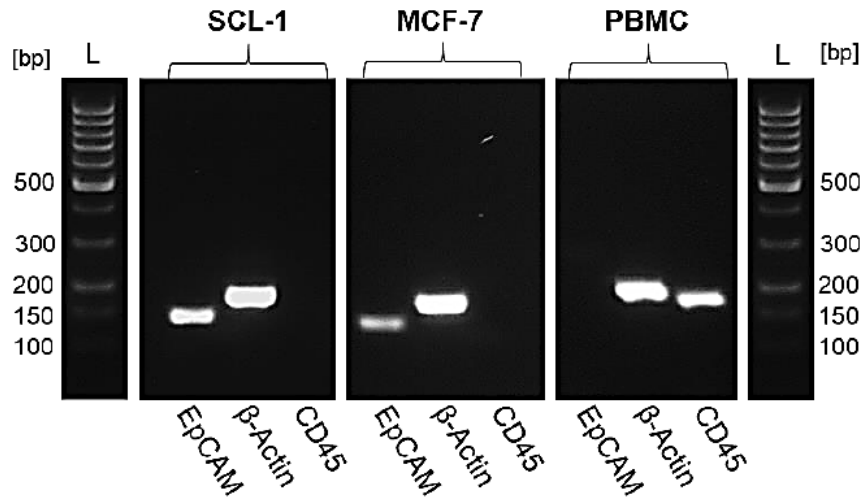


Figure S1: Gel electrophoresis of RT-qPCR products from single cell RNA to confirm EpCAM transcripts in the SCL-1 and MCF-7 cell line. Total single cell RNA was isolated using RNeasy Micro Kit (QIAGEN) with an adapted protocol lysing one cell. cDNA was synthesized with Sensifast cDNA synthesis Kit (Bioline). qPCR was performed with Quantifast qPCR Kit (QIAGEN). EpCAM product was expected at a size of 136 bp. β -Actin (176 bp) served as reference transcript. RT-qPCR towards leukocyte marker CD45 (159 bp) of one peripheral blood mononuclear cell RNA from a healthy donor was used as negative control. Primers were designed with Primer-BLAST (National Institutes of Health; <https://www.ncbi.nlm.nih.gov/tools/primer-blast/>).

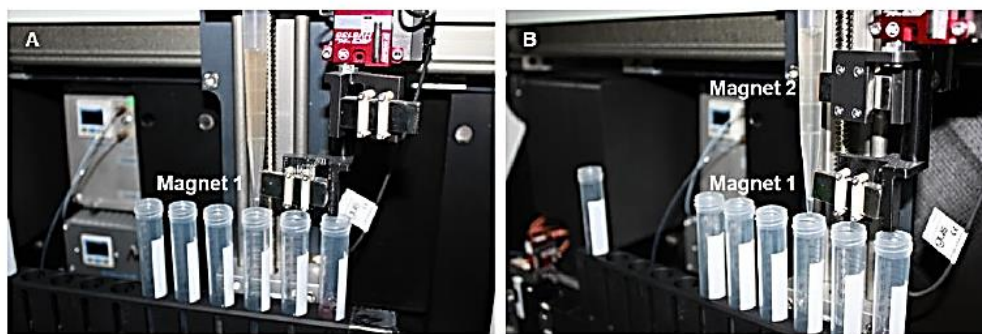


Figure S2: Automated enrichment in the CTCelect device. A) After each washing step, bead-cell pellets were captured in the 10 mL pipet tip by placing magnet 1 on one side of the pipet tip. B) When washing in larger volumes (5 mL), immunomagnetic enrichment was additionally performed using the upper magnet 2.

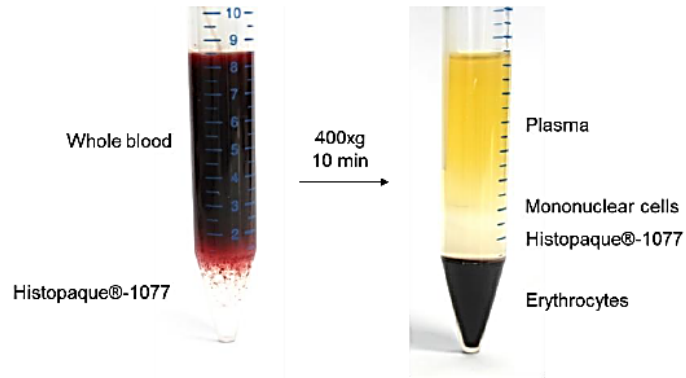


Figure S3: Buffy coat of peripheral blood mononuclear cells from a healthy donor. 1 mL Histopaque®-1077 (Merck, Darmstadt, DE) was coated with 7.5 mL whole blood and centrifuged for 10 min at 400xg. The plasma was discarded. The PBMC phase was collected, resuspended 1:1 in PBS and centrifuged for 5 min at 400xg. The cell pellet was resuspended in 1 mL PBS for further experiments.

Supplement (3)

Automated immunomagnetic enrichment and optomicrofluidic detection to isolate breast cancer cells: A proof-of-concept towards PoC therapeutic decision-making

Janis Stiefel ^{1,*}, Michael Baßler ¹, Jörn Wittek ¹ and Christian Freese ¹

¹ Fraunhofer Institute for Microengineering and Microsystems IMM, Mainz, Germany

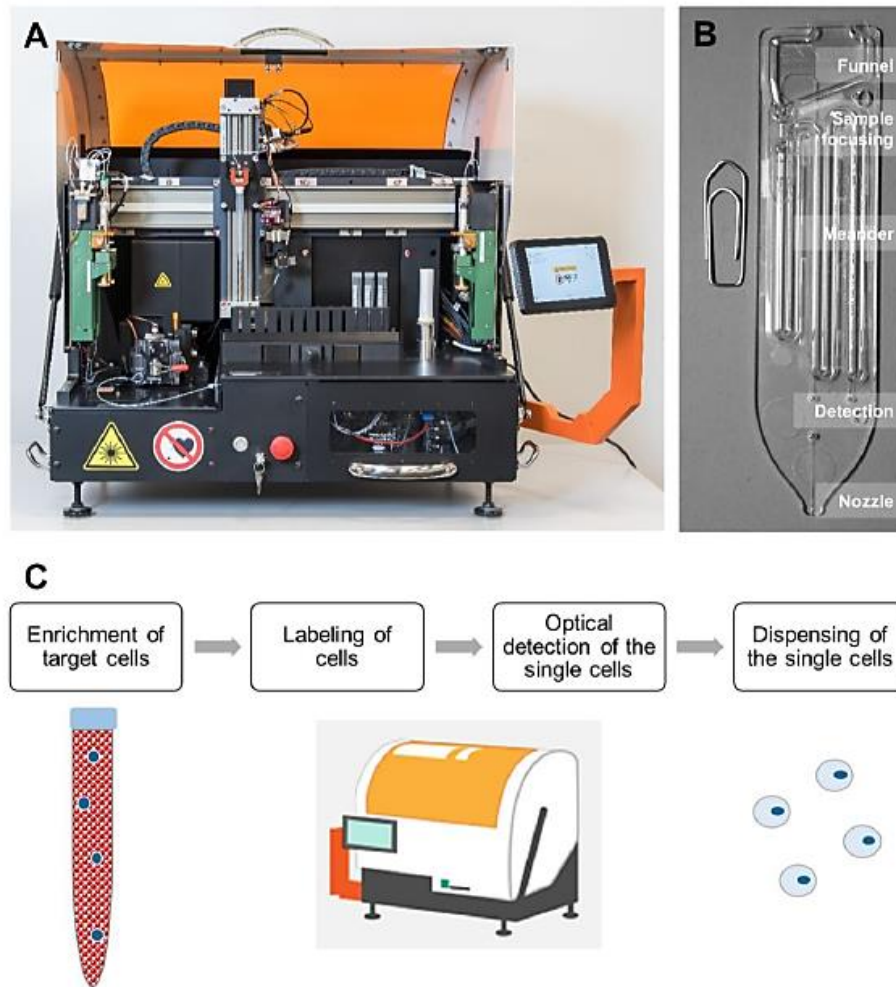


Figure S1: CTCelect system, microfluidic chip and process conception. A) The benchtop device consists of an immunomagnetic enrichment module (right-sided) and a microfluidic fluorescence-activated cell sorting (μ CS) subunit (left-sided). The fully-automated isolation process is user-controlled via touchscreen. Sample handling and transfer is managed by a pipetting robot. B) The CTCelect chip is placed in the chip holder of the cell sorting subunit and disposed after isolation. The chip consists of a reservoir funnel for the cell suspension, a hydrodynamic focusing channel, a detection zone and a nozzle for cell dispensing. C) CTCelect concept for single cell dispensing from 7.5 mL samples (from Stiefel et al. *Eng Life Sci.* 2022; 22: 391– 406. <https://doi.org/10.1002/elsc.202100133> [9]).

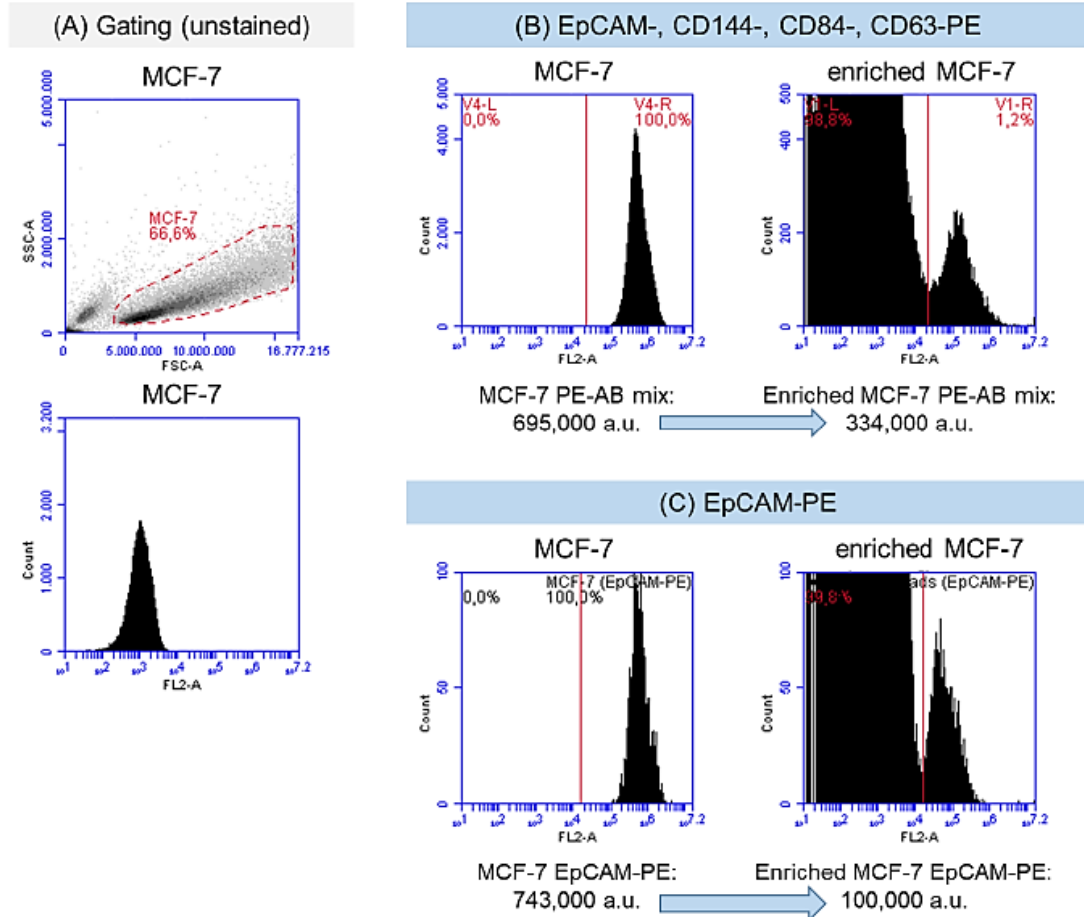


Figure S2: Flow cytometry of PE-antibody (AB) stained MCF-7 cells with or without beads enrichment. MCF-7 cells were enriched with EpCAM-coupled immunomagnetic beads for 10 minutes. Unbound and enriched cells were then stained with either EpCAM-, CD144-, CD84-, CD63-PE (B) or only EpCAM-PE (C) antibody solution (1:30) alternated with several washing steps. Fluorescence intensity in the FL2 channel was measured using the flow cytometer. Events of unbound cells were gated to an unstained MCF-7 population from a previous measurement (A). Beads were detected as a large overlapping population at $FL2 < 10^4$ a.u.

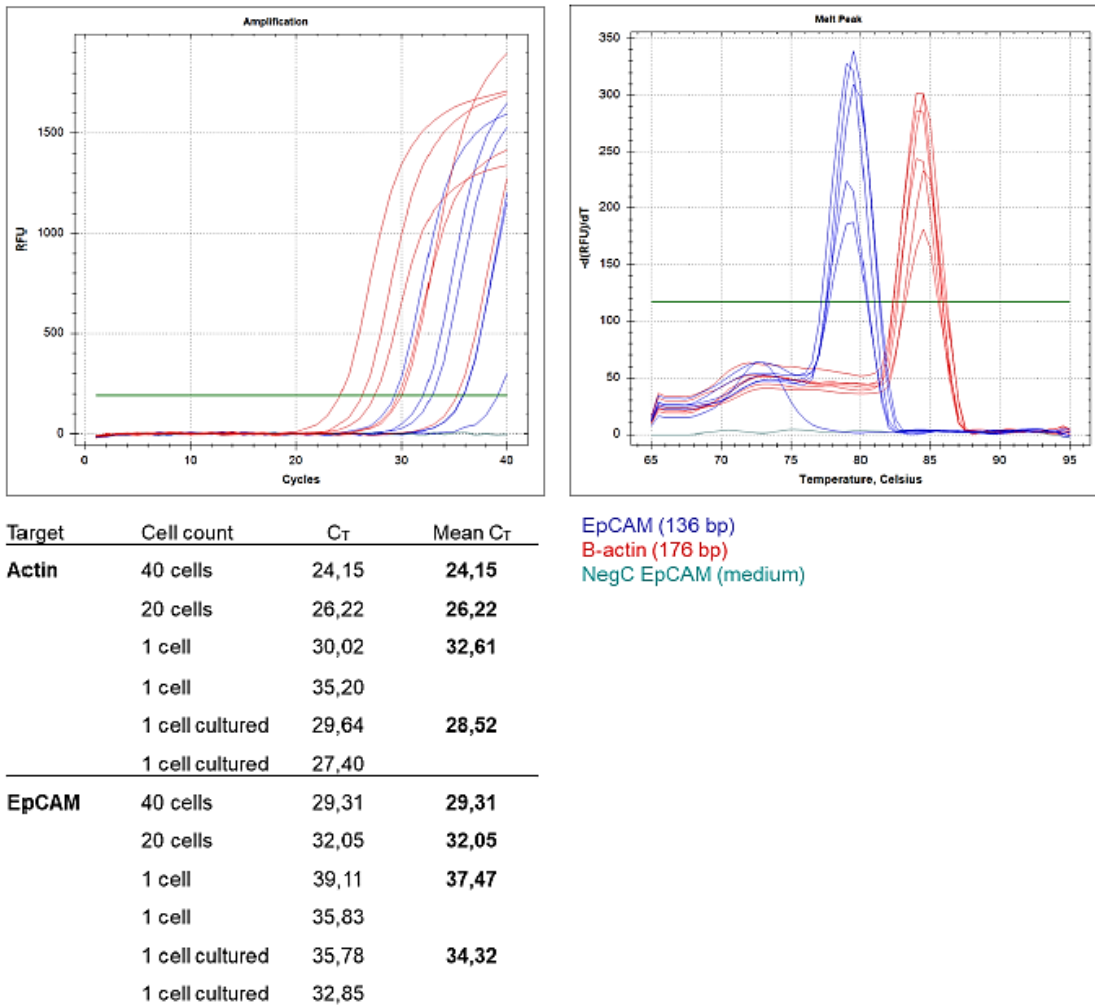


Figure S3: qPCR and melt curve analysis from RNA of one, 20 and 40 MCF-7 single cells targeting EpCAM and β -actin. Two-step qPCR was performed with RNeasy Micro RNA isolation kit (QIAGEN) to confirm fluorescence signals at low cell numbers. Therefore, we picked single cells from a cell suspension in a petri dish and directly lysed one, 20 and 40 cells per spin column. We observed an increase in relative fluorescence intensity in clear correlation with the cell number for both EpCAM and β -actin expression. Seeded single cells (“cultured”) from a 96 well plate served as a control.

Table T1: Primer Sequences.

Name	Gene (human), mRNA	Product length [bp]	Sequence (5'-3')
Aktin_for	β-actin ACTB	176	ATT GCC GAC AGG ATG CAG AA
Aktin_rev			GGG CCG GAC TCG TCA TAC TC
EpCAM_for	Epithelial cell adhesion molecule	136	CCG CAG CTC AGG AAG AAT GT
EpCAM_rev			CAT TTG GCA GCC AGC TTT GA
PGR_for	Progesterone transcr. V1	194	GTCTACCCGCCCTATCTCAAC
PGR_rev			TAGTTGTGCTGCCCTTCCATT
ESR1_for	Estrogen transcr. V1	129	TGGGAATGATGAAAGGTGGGA
ESR1_rev			GGTTGGCAGCTCTCATGTCT
HER2_for	HER-2/NEU (ERBB2) transcr. V1	108	CCGGAGCCGCAGTGAG
HER2_rev			CTGTGCCGGTGCACACTT
CD45_for	CD45; PTPRC transcr. V1	159	ACCAGGAATGGATGTCGCTA
CD45_rev			TGGGGCCTGTAAAAGTGCC
CXCR4_for	C-X-C motif chemokine receptor 4	60	CTGTGAGCAGAGGGTCCAG
CXCR4_rev			ATGAATGTCCACCTCGCTT





References (1)

1. Kunzel, J.; Gribko, A.; Lu, Q.; Stauber, R.H.; Wunsch, D. Nanomedical detection and downstream analysis of circulating tumor cells in head and neck patients. *Biol. Chem.* **2019**, *400*, 1465–1479. [CrossRef] [PubMed]
2. Gül, D.; Habtemichael, N.; Dietrich, D.; Dietrich, J.; Gößwein, D.; Khamis, A.; Deuss, E.; Künzel, J.; Schneider, G.; Strieth, S.; et al. Identification of cytokeratin24 as a tumor suppressor for the management of head and neck cancer. *Biol. Chem.* **2021**. [CrossRef] [PubMed]
3. Siemer, S.; Fauth, T.; Scholz, P.; Al-Zamel, Y.; Khamis, A.; Gül, D.; Freudelsperger, L.; Wollenberg, B.; Becker, S.; Stauber, R.H.; et al. Profiling Cisplatin Resistance in Head and Neck Cancer: A Critical Role of the VRAC Ion Channel for Chemoresistance. *Cancers* **2021**, *13*, 4831. [CrossRef]
4. Beltz, A.; Gosswein, D.; Zimmer, S.; Limburg, I.; Wunsch, D.; Gribko, A.; Deichelbohrer, M.; Hagemann, J.; Stauber, R.H.; Kunzel, J. Staging of oropharyngeal squamous cell carcinoma of the head and neck: Prognostic features and power of the 8th edition of the UICC staging manual. *Eur. J. Surg. Oncol.* **2019**, *45*, 1046–1053. [CrossRef] [PubMed]
5. Kiweler, N.; Wunsch, D.; Wirth, M.; Mahendrarajah, N.; Schneider, G.; Stauber, R.H.; Brenner, W.; Butter, F.; Kramer, O.H. Histone deacetylase inhibitors dysregulate DNA repair proteins and antagonize metastasis-associated processes. *J. Cancer Res. Clin. Oncol.* **2020**, *146*, 343–356. [CrossRef]
6. Hu, Y.; Yu, X.; Xu, G.; Liu, S. Metastasis: An early event in cancer progression. *J. Cancer Res. Clin. Oncol.* **2017**, *143*, 745–757. [CrossRef] [PubMed]
7. Park, S.-Y.; Nam, J.-S. The force awakens: Metastatic dormant cancer cells. *Exp. Mol. Med.* **2020**, *52*, 569–581. [CrossRef]
8. Ashworth, T.R. A case of cancer in which cells similar to those in the tumours were seen in the blood after death. *Australas. Med. J.* **1869**, *14*, 146–147.
9. Murray, N.P.; Albarran, V.; Perez, G.; Villalon, R.; Ruiz, A. Secondary Circulating Tumor Cells (CTCs) but not Primary CTCs are Associated with the Clinico-Pathological Parameters in Chilean Patients With Colo-Rectal Cancer. *Asian Pac. J. Cancer Prev.* **2015**, *16*, 4745–4749. [CrossRef] [PubMed]
10. Wendel, M.; Bazhenova, L.; Boshuizen, R.; Kolatkar, A.; Honnatti, M.; Cho, E.H.; Marrinucci, D.; Sandhu, A.; Perricone, A.; Thistlethwaite, P.; et al. Fluid biopsy for circulating tumor cell identification in patients with early-and late-stage non-small cell lung cancer: A glimpse into lung cancer biology. *Phys. Biol.* **2012**, *9*, 016005. [CrossRef]
11. Engel, H.; Kleespies, C.; Friedrich, J.; Breidenbach, M.; Kallenborn, A.; Schondorf, T.; Kolhagen, H.; Mallmann, P. Detection of circulating tumour cells in patients with breast or ovarian cancer by molecular cytogenetics. *Br. J. Cancer* **1999**, *81*, 1165–1173. [CrossRef]
12. Jaeger, B.A.; Jueckstock, J.; Andergassen, U.; Salmen, J.; Schochter, F.; Fink, V.; Alunni-Fabroni, M.; Rezai, M.; Beck, T.; Beckmann, M.W.; et al. Evaluation of two different analytical methods for circulating tumor cell detection in peripheral blood of patients with primary breast cancer. *Biomed. Res. Int.* **2014**, *2014*, 491459. [CrossRef] [PubMed]
13. Mocellin, S.; Hoon, D.; Ambrosi, A.; Nitti, D.; Rossi, C.R. The prognostic value of circulating tumor cells in patients with melanoma: A systematic review and meta-analysis. *Clin. Cancer Res.* **2006**, *12*, 4605–4613. [CrossRef] [PubMed]
14. de Bono, J.S.; Scher, H.I.; Montgomery, R.B.; Parker, C.; Miller, M.C.; Tissing, H.; Doyle, G.V.; Terstappen, L.W.; Pienta, K.J.; Raghavan, D. Circulating tumor cells predict survival benefit from treatment in metastatic castration-resistant prostate cancer. *Clin. Cancer Res.* **2008**, *14*, 6302–6309. [CrossRef]
15. Zhou, S.; Wang, L.; Zhang, W.; Liu, F.; Zhang, Y.; Jiang, B.; Wang, J.; Yuan, H. Circulating Tumor Cells Correlate With Prognosis in Head and Neck Squamous Cell Carcinoma. *Technol. Cancer Res. Treat.* **2021**, *20*, 1533033821990037. [CrossRef]
16. Kulasinghe, A.; Perry, C.; Jovanovic, L.; Nelson, C.; Punyadeera, C. Circulating tumour cells in metastatic head and neck cancers. *Int. J. Cancer* **2015**, *136*, 2515–2523. [CrossRef]
17. Muller, V.; Stahmann, N.; Riethdorf, S.; Rau, T.; Zabel, T.; Goetz, A.; Janicke, F.; Pantel, K. Circulating tumor cells in breast cancer: Correlation to bone marrow micrometastases, heterogeneous response to systemic therapy and low proliferative activity. *Clin. Cancer Res.* **2005**, *11*, 3678–3685. [CrossRef]
18. Weller, P.; Nel, I.; Hassenkamp, P.; Gauler, T.; Schlueter, A.; Lang, S.; Dountsop, P.; Hoffmann, A.C.; Lehnerdt, G. Detection of circulating tumor cell subpopulations in patients with head and neck squamous cell carcinoma (HNSCC). *PLoS ONE* **2014**, *9*, e113706. [CrossRef] [PubMed]
19. Pantel, K.; Alix-Panabieres, C. Circulating tumour cells in cancer patients: Challenges and perspectives. *Trends Mol. Med.* **2010**, *16*, 398–406. [CrossRef]
20. Pérez-Barríos, C.; Nieto-Alcalado, I.; Torrente, M.; Jiménez-Sánchez, C.; Calvo, V.; Gutierrez-Sanz, L.; Palka, M.; Donoso-Navarro, E.; Provencio, M.; Romero, A. Comparison of methods for circulating cell-free DNA isolation using blood from cancer patients: Impact on biomarker testing. *Transl. Lung Cancer Res.* **2016**, *5*, 665–672. [CrossRef] [PubMed]
21. Cristofanilli, M.; Broglio, K.R.; Guarneri, V.; Jackson, S.; Fritsche, H.A.; Islam, R.; Dawood, S.; Reuben, J.M.; Kau, S.W.; Lara, J.M.; et al. Circulating tumor cells in metastatic breast cancer: Biologic staging beyond tumor burden. *Clin. Breast Cancer* **2007**, *7*, 471–479. [CrossRef]
22. Tinhofer, I.; Staudte, S. Circulating tumor cells as biomarkers in head and neck cancer: Recent advances and future outlook. *Expert Rev. Mol. Diagn.* **2018**, *18*, 897–906. [CrossRef] [PubMed]
23. Satelli, A.; Mitra, A.; Brownlee, Z.; Xia, X.; Bellister, S.; Overman, M.J.; Kopetz, S.; Ellis, L.M.; Meng, Q.H.; Li, S. Epithelial-mesenchymal transitioned circulating tumor cells capture for detecting tumor progression. *Clin. Cancer Res.* **2015**, *21*, 899–906. [CrossRef] [PubMed]
24. Reisbeck, M.; Richter, L.; Helou, M.J.; Arlinghaus, S.; Anton, B.; van Dommelen, I.; Nitzsche, M.; Baßler, M.; Kappes, B.; Friedrich, O.; et al. Hybrid integration of scalable mechanical and magnetophoretic focusing for magnetic flow cytometry. *Biosens. Bioelectron.* **2018**, *109*, 98–108. [CrossRef]
25. Gribko, A.; Kunzel, J.; Wunsch, D.; Lu, Q.; Nagel, S.M.; Knauer, S.K.; Stauber, R.H.; Ding, G.B. Is small smarter? Nanomaterial-based detection and elimination of circulating tumor cells: Current knowledge and perspectives. *Int. J. Nanomed.* **2019**, *14*, 4187–4209. [CrossRef]
26. Siemer, S.; Wunsch, D.; Khamis, A.; Lu, Q.; Scherberich, A.; Filippi, M.; Krafft, M.P.; Hagemann, J.; Weiss, C.; Ding, G.B.; et al. Nano Meets Micro-Translational Nanotechnology in Medicine: Nano-Based Applications for Early Tumor Detection and Therapy. *Nanomaterials* **2020**, *10*, 383. [CrossRef]

27. Rauscher, H.; Sokull-Kluttgen, B.; Stamm, H. The European Commission's recommendation on the definition of nanomaterial makes an impact. *Nanotoxicology* **2013**, *7*, 1195–1197. [CrossRef]
28. Shashni, B.; Ariyasu, S.; Takeda, R.; Suzuki, T.; Shiina, S.; Akimoto, K.; Maeda, T.; Aikawa, N.; Abe, R.; Osaki, T.; et al. Size-Based Differentiation of Cancer and Normal Cells by a Particle Size Analyzer Assisted by a Cell-Recognition PC Software. *Biol. Pharm. Bull.* **2018**, *41*, 487–503. [CrossRef]
29. Nichols, A.C.; Lowes, L.E.; Szeto, C.C.; Basmaji, J.; Dhaliwal, S.; Chapeskie, C.; Todorovic, B.; Read, N.; Venkatesan, V.; Hammond, A.; et al. Detection of circulating tumor cells in advanced head and neck cancer using the CellSearch system. *Head Neck* **2012**, *34*, 1440–1444. [CrossRef]
30. Riethdorf, S.; Fritsche, H.; Muller, V.; Rau, T.; Schindlbeck, C.; Rack, B.; Janni, W.; Coith, C.; Beck, K.; Janicke, F.; et al. Detection of circulating tumor cells in peripheral blood of patients with metastatic breast cancer: A validation study of the CellSearch system. *Clin. Cancer Res.* **2007**, *13*, 920–928. [CrossRef] [PubMed]
31. Riethdorf, S.; O'Flaherty, L.; Hille, C.; Pantel, K. Clinical applications of the CellSearch platform in cancer patients. *Adv. Drug Deliv. Rev.* **2018**, *125*, 102–121. [CrossRef]
32. Obayashi, K.; Akatsuka, J.; Endo, Y.; Takeda, H.; Hayashi, T.; Toyama, Y.; Suzuki, Y.; Hamasaki, T.; Kimura, G.; Ohnaga, T.; et al. Initial detection of circulating tumor cells from metastatic prostate cancer patients with a novel small device. *Prostate Int.* **2019**, *7*, 131–138. [CrossRef]
33. Boukamp, P.; Tilgen, W.; Dzarlieva, R.T.; Breitkreutz, D.; Haag, D.; Riehl, R.K.; Bohnert, A.; Fusenig, N.E. Phenotypic and genotypic characteristics of a cell line from a squamous cell carcinoma of human skin. *J. Natl. Cancer Inst.* **1982**, *68*, 415–427.
34. Welkoborsky, H.J.; Jacob, R.; Riazimand, S.H.; Bernauer, H.S.; Mann, W.J. Molecular biologic characteristics of seven new cell lines of squamous cell carcinomas of the head and neck and comparison to fresh tumor tissue. *Oncology* **2003**, *65*, 60–71. [CrossRef]
35. Gribko, A.; Hahlbrock, A.; Strieth, S.; Becker, S.; Hagemann, J.; Deichelbohrer, M.; Hildebrandt, A.; Habtemichael, N.; Wunsch, D. Disease-relevant signalling-pathways in head and neck cancer: Taspase1's proteolytic activity fine-tunes TFIIA function. *Sci. Rep.* **2017**, *7*, 14937. [CrossRef] [PubMed]
36. Goesswein, D.; Habtemichael, N.; Gerhold-Ay, A.; Mazur, J.; Wunsch, D.; Knauer, S.K.; Kunzel, J.; Matthias, C.; Strieth, S.; Stauber, R.H. Expressional analysis of disease-relevant signalling-pathways in primary tumours and metastasis of head and neck cancers. *Sci. Rep.* **2018**, *8*, 7326. [CrossRef]
37. Wunsch, D.; Hahlbrock, A.; Heiselmayer, C.; Backer, S.; Heun, P.; Goesswein, D.; Stocker, W.; Schirmeister, T.; Schneider, G.; Kramer, O.H.; et al. Fly versus man: Evolutionary impairment of nucleolar targeting affects the degradome of *Drosophila*'s Taspase1. *FASEB J.* **2015**, *29*, 1973–1985. [CrossRef] [PubMed]
38. Deuss, E.; Gosswein, D.; Gul, D.; Zimmer, S.; Foersch, S.; Eger, C.S.; Limburg, I.; Stauber, R.H.; Kunzel, J. Growth Factor Receptor Expression in Oropharyngeal Squamous Cell Cancer: Her1-4 and c-Met in Conjunction with the Clinical Features and Human Papillomavirus (p16) Status. *Cancers* **2020**, *12*, 3358. [CrossRef] [PubMed]
39. Barak, V.; Goike, H.; Panaretakis, K.W.; Einarsson, R. Clinical utility of cytokeratins as tumor markers. *Clin. Biochem.* **2004**, *37*, 529–540. [CrossRef]
40. Foddai, A.; Elliott, C.T.; Grant, I.R. Maximizing capture efficiency and specificity of magnetic separation for *Mycobacterium avium* subsp. *paratuberculosis* cells. *Appl. Environ. Microbiol.* **2010**, *76*, 7550–7558. [CrossRef] [PubMed]
41. Foddai, A.C.G.; Grant, I.R. A novel one-day phage-based test for rapid detection and enumeration of viable *Mycobacterium avium* subsp. *paratuberculosis* in cows' milk. *Appl. Microbiol. Biotechnol.* **2020**, *104*, 9399–9412. [CrossRef] [PubMed]
42. Siemer, S.; Westmeier, D.; Barz, M.; Eckrich, J.; Wunsch, D.; Seckert, C.; Thyssen, C.; Schilling, O.; Hasenberg, M.; Pang, C.; et al. Biomolecule-corona formation confers resistance of bacteria to nanoparticle-induced killing: Implications for the design of improved nanoantibiotics. *Biomaterials* **2018**, *192*, 551–559. [CrossRef] [PubMed]
43. Hussain, T.; Gellrich, D.; Siemer, S.; Reichel, C.A.; Eckrich, J.; Dietrich, D.; Knauer, S.K.; Stauber, R.H.; Strieth, S. TNF-alpha-Inhibition Improves the Biocompatibility of Porous Polyethylene Implants In Vivo. *Tissue Eng. Regen. Med.* **2021**, *18*, 297–303. [CrossRef]
44. Westmeier, D.; Siemer, S.; Vallet, C.; Steinmann, J.; Docter, D.; Buer, J.; Knauer, S.K.; Stauber, R.H. Boosting nanotoxicity to combat multidrug-resistant bacteria in pathophysiological environments. *Nanoscale Adv.* **2020**, *2*, 5428–5440. [CrossRef]
45. Stauber, R.H.; Siemer, S.; Becker, S.; Ding, G.B.; Strieth, S.; Knauer, S.K. Small Meets Smaller: Effects of Nanomaterials on Microbial Biology, Pathology, and Ecology. *ACS Nano* **2018**, *12*, 6351–6359. [CrossRef]
46. Stauber, R.H.; Westmeier, D.; Wandrey, M.; Becker, S.; Docter, D.; Ding, G.B.; Thines, E.; Knauer, S.K.; Siemer, S. Mechanisms of nanotoxicity—Biomolecule coronas protect pathological fungi against nanoparticle-based eradication. *Nanotoxicology* **2020**, *14*, 1157–1174. [CrossRef]
47. Steuwerts, A.M.; Kraan, J.; Bolt-de Vries, J.; van der Spoel, P.; Mostert, B.; Martens, J.W.; Gratama, J.W.; Sleijfer, S.; Foekens, J.A. Molecular characterization of circulating tumor cells in large quantities of contaminating leukocytes by a multiplex real-time PCR. *Breast Cancer Res. Treat.* **2009**, *118*, 455–468. [CrossRef]
48. Chudziak, J.; Burt, D.J.; Mohan, S.; Rothwell, D.G.; Mesquita, B.; Antonello, J.; Dalby, S.; Ayub, M.; Priest, L.; Carter, L.; et al. Clinical evaluation of a novel microfluidic device for epitope-independent enrichment of circulating tumour cells in patients with small cell lung cancer. *Analyst* **2016**, *141*, 669–678. [CrossRef]
49. Ciccio, M.; Bravo-Santano, N.; Davis, A.; Lewis, J.; Malcolm, R.; Pailhes-Jimenez, A.S. Mesenchymal markers: The new avenue for circulating tumor cells detection. In Proceedings of the ANGLE plc AACR 2021, Virtual Meeting, 9–14 April 2021.
50. Grover, P.K.; Cummins, A.G.; Price, T.J.; Roberts-Thomson, I.C.; Hardingham, J.E. Circulating tumour cells: The evolving concept and the inadequacy of their enrichment by EpCAM-based methodology for basic and clinical cancer research. *Ann. Oncol.* **2014**, *25*, 1506–1516. [CrossRef]
51. Grisanti, S.; Almic, C.; Consoli, F.; Buglione, M.; Verardi, R.; Bolzoni-Villaret, A.; Bianchetti, A.; Ciccicarese, C.; Mangoni, M.; Ferrari, L.; et al. Circulating tumor cells in patients with recurrent or metastatic head and neck carcinoma: Prognostic and predictive significance. *PLoS ONE* **2014**, *9*, e103918. [CrossRef]
52. Menarini Silicon Biosystems Inc. Available online: https://documents.cellsearchctc.com/pdf/e631600006/e631600006_EN.pdf (accessed on 10 October 2021).

References (2)

ORCID

Janis Stiefel  <https://orcid.org/0000-0002-1166-4326>
 Christian Freese  <https://orcid.org/0000-0001-8411-1573>
 Nalini Srinivas  <https://orcid.org/0000-0002-6899-0800>
 Désirée Gül  <https://orcid.org/0000-0002-2446-5756>
 Jan Hagemann  <https://orcid.org/0000-0002-9846-7850>
 Jürgen C. Becker  <https://orcid.org/0000-0001-9183-653X>
 Michael Baßler  <https://orcid.org/0000-0003-3911-2897>

References

- Alix-Panabières C, Schwarzenbach H, Pantel K, Circulating tumor cells and circulating tumor DNA. *Annu Rev Med* 2012, 63, 199–215, <https://doi.org/10.1146/annurev-med-062310-094219>.
- Nolé F, Munzone E, Zorzino L, Minchella I et al., Variation of circulating tumor cell levels during treatment of metastatic breast cancer: prognostic and therapeutic implications. *Ann Oncol Offic J Euro Soc Medi Oncol* 2008, 19, 891–897, <https://doi.org/10.1093/annonc/mdm558>.
- Mentis A-FA, Grivas PD, Dardiotis E, Romas NA et al., Circulating tumor cells as Trojan Horse for understanding, preventing, and treating cancer: a critical appraisal. *Cell Mole Life Sci CMLS* 2020, 77, 3671–3690, <https://doi.org/10.1007/s00018-020-03529-4>.
- Reduzzi C, Vismara M, Gerratana L, Silvestri M et al., The curious phenomenon of dual-positive circulating cells: Longtime overlooked tumor cells. *Semin Cancer Biol* 2020, 60, 344–350, <https://doi.org/10.1016/j.semcancer.2019.10.008>.
- Lei KF, A Review on Microdevices for Isolating Circulating Tumor Cells. *Micromachines* 2020, 11, <https://doi.org/10.3390/mi11050531>.
- Rawal S, Yang YP, Cote R, Agarwal A, Identification and quantitation of circulating tumor cells. *Annu Rev Anal Chem (Palo Alto, Calif.)* 2017, 10, 321–343, <https://doi.org/10.1146/annurev-anchem-061516-045405>.
- Ferreira MM, Ramani VC, Jeffrey SS, Circulating tumor cell technologies†. *Mole Oncol* 2016, 10, 374–394, <https://doi.org/10.1016/j.molonc.2016.01.007>.
- Hayes DF, Cristofanilli M, Budd GT, Ellis MJ et al., Circulating tumor cells at each follow-up time point during therapy of metastatic breast cancer patients predict progression-free and overall survival. *Clinical cancer research an official journal of the Am Assoc Canc Res* 2006, 12, 4218–4224, <https://doi.org/10.1158/1078-0432.CCR-05-2821>.
- Cohen SJ, Punt CJA, Iannotti N, Saidman BH et al., Relationship of circulating tumor cells to tumor response, progression-free survival, and overall survival in patients with metastatic colorectal cancer. *J Clin Oncol Offic J Am Soc Clin Oncol* 2008, 26, 3213–3221, <https://doi.org/10.1200/JCO.2007.15.8923>.
- Bono JS, Scher HI, Montgomery RB, Parker C et al., Circulating tumor cells predict survival benefit from treatment in metastatic castration-resistant prostate cancer. *Clin Canc Res an Offic J Am Assoc Canc Res* 2008, 14, 6302–6309, <https://doi.org/10.1158/1078-0432.CCR-08-0872>.
- Vokes EE, Agrawal N, Seiwert TY, HPV-Associated head and neck cancer. *J Natl Cancer Inst* 2015, 107, djv344, <https://doi.org/10.1093/jnci/djv344>.
- Economopoulou P, Bree R, Kotsantis I, Psyrris A, Diagnostic tumor markers in head and neck squamous cell carcinoma (HNSCC) in the clinical setting. *Front Oncol* 2019, 9, <https://doi.org/10.3389/fonc.2019.00827>.
- Bree R, Deurloo EE, Snow GB, Leemans CR, Screening for distant metastases in patients with head and neck cancer. *Laryngoscope* 2000, 110, 397–401, <https://doi.org/10.1097/00005537-200003000-00012>.
- Siegel R, Naishadham D, Jemal A, Cancer statistics, 2012. *CA Cancer J Clin* 2012, 62, 10–29, <https://doi.org/10.3322/caac.20138>.
- Boukamp P, Tilgen W, Dzarlieva RT, Breitkreutz D et al., Phenotypic and genotypic characteristics of a cell line from a squamous cell carcinoma of human skin. *J Natl Cancer Inst* 1982, 68, 415–427.
- Bulfoni M, Gerratana L, Ben FD, Marzinotto S et al., In patients with metastatic breast cancer the identification of circulating tumor cells in epithelial-to-mesenchymal transition is associated with a poor prognosis. *Breast Cancer Res* 2016, 18, 1–15, <https://doi.org/10.1186/s13058-016-0687-3>.
- Chudziak J, Burt DJ, Mohan S, Rothwell DG et al., Clinical evaluation of a novel microfluidic device for epitope-independent enrichment of circulating tumour cells in patients with small cell lung cancer. *Analyst* 2016, 141, 669–678, <https://doi.org/10.1039/c5an02156a>.
- Gribko A, Stiefel J, Liebetanz L, Nagel SM et al., IsoMAG-An Automated System for the Immunomagnetic Isolation of Squamous Cell Carcinoma-Derived Circulating Tumor Cells. *Diagnostics (Basel, Switzerland)* 2021, 11, <https://doi.org/10.3390/diagnostics11112040>.
- Lee W, Tseng P, Di Carlo D, *Microtechnology for Cell Manipulation and Sorting*, SPRINGER, 2018.
- Plyavin YA, Blum EY, Magnetic parameters of blood cells and high gradient paramagnetic and diamagnetic phoresis. *Magneto-hydrodynamics* 1983, 19, 349–359.
- Candas-Green D, Xie B, Huang J, Fan M et al., Dual blockade of CD47 and HER2 eliminates radioresistant breast cancer cells. *Nat Commun*, 11, 1–15, <https://doi.org/10.1038/s41467-020-18245-7>.
- Liu R, Wei H, Gao P, Yu H et al., CD47 promotes ovarian cancer progression by inhibiting macrophage phagocytosis. *Oncotarget* 2017, 8, 39021–39032, DOI: 10.18632/oncotarget.16547.
- Scheiermann C, Frenette PS, Hidalgo A, Regulation of leucocyte homeostasis in the circulation. *Cardiovasc Res* 2015, 107, 340–351, <https://doi.org/10.1093/cvr/cvv099>.
- Nelep C, Eberhardt J, Automated rare single cell picking with the ALS celllector™. *Cytometry* 2018, 93, 1267–1270, <https://doi.org/10.1002/cyto.a.23568>.
- Alebrand S, Freese C, Schunck T, Bassler M, Zirkulierende Tumorzellen - voll automatisierte Vereinzelung aus Blut. *Biospektrum* 2017, 23, 766–768, <https://doi.org/10.1007/s12268-017-0869-2>.
- Mouliere F, Chandrananda D, Piskorz AM, Moore EK et al., Enhanced detection of circulating tumor DNA by fragment size analysis. *Sci Transl Med* 2018, 10, <https://doi.org/10.1126/scitranslmed.aat4921>.
- Shaw JA, Guttery DS, Hills A, Fernandez-Garcia D et al., Mutation Analysis of Cell-Free DNA and Single Circulating Tumor Cells in Metastatic Breast Cancer Patients with High Circulating Tumor Cell Counts. *Clinical cancer research an official journal of the Am Assoc Cancer Research* 2017, 23, 88–96, <https://doi.org/10.1158/1078-0432.CCR-16-0825>.

28. Cho J-K, Lee GJ, Kim H-D, Moon UY *et al.*, Differential impact of circulating tumor cells on disease recurrence and survivals in patients with head and neck squamous cell carcinomas: an updated meta-analysis. *PLoS One* 2018, 13, e0203758, <https://doi.org/10.1371/journal.pone.0203758>.
29. Alix-Panabières C, Pantel K, Clinical Applications of Circulating tumor cells and circulating tumor DNA as liquid biopsy. *Cancer Discov* 2016, 6, 479–491, <https://doi.org/10.1158/2159-8290.CD-15-1483>.

References (3)

1. Strati, A.; Nikolaou, M.; Georgoulas, V.; Lianidou, E.S. RNA-Based CTC Analysis Provides Prognostic Information in Metastatic Breast Cancer. *Diagnostics* **2021**, *11*, 513. [CrossRef] [PubMed]
2. Jin, L.; Zhao, W.; Zhang, J.; Chen, W.; Xie, T.; Wang, L.; Fan, W.; Xie, S.; Shen, J.; Zheng, H.; et al. Evaluation of the diagnostic value of circulating tumor cells with CytoSorter@CTC capture system in patients with breast cancer. *Cancer Med.* **2020**, *9*, 1638–1647. [CrossRef] [PubMed]
3. Hofman, P. Detecting Resistance to Therapeutic ALK Inhibitors in Tumor Tissue and Liquid Biopsy Markers: An Update to a Clinical Routine Practice. *Cells* **2021**, *10*, 168. [CrossRef] [PubMed]
4. Alix-Panabières, C.; Schwarzenbach, H.; Pantel, K. Circulating tumor cells and circulating tumor DNA. *Annu. Rev. Med.* **2012**, *63*, 199–215. [CrossRef] [PubMed]
5. Robert Koch Institute; The Association of Population-Based Cancer Registries in Germany. *Cancer in Germany 2017/2018*; Robert Koch Institute: Berlin, Germany, 2022; pp. 86–89. Available online: https://www.krebsdaten.de/Krebs/EN/Content/Publications/Cancer_in_Germany/cancer_chapters_2017_2018/cancer_c50.pdf?__blob=publicationFile (accessed on 28 July 2022).
6. Zhang, Y.; Lv, Y.; Niu, Y.; Su, H.; Feng, A. Role of Circulating Tumor Cell (CTC) Monitoring in Evaluating Prognosis of Triple-Negative Breast Cancer Patients in China. *Med. Sci. Monit.* **2017**, *23*, 3071–3079. [CrossRef] [PubMed]
7. Yadav, B.S.; Chanana, P.; Jhamb, S. Biomarkers in triple negative breast cancer: A review. *World J. Clin. Oncol.* **2015**, *6*, 252–263. [CrossRef] [PubMed]
8. Gelmon, K.; Dent, R.; Mackey, J.R.; Laing, K.; McLeod, D.; Verma, S. Targeting triple-negative breast cancer: Optimising therapeutic outcomes. *Ann. Oncol.* **2012**, *23*, 2223–2234. [CrossRef] [PubMed]
9. Stiefel, J.; Freese, C.; Sriram, A.; Alebrand, S.; Srinivas, N.; Sproll, C.; Wandrey, M.; Gül, D.; Hagemann, J.; Becker, J.C.; et al. Characterization of a novel microfluidic platform for the isolation of rare single cells to enable CTC analysis from head and neck squamous cell carcinoma patients. *Eng. Life Sci.* **2022**, *22*, 391–406. [CrossRef] [PubMed]
10. Gribko, A.; Stiefel, J.; Liebetanz, L.; Nagel, S.M.; Künzel, J.; Wandrey, M.; Hagemann, J.; Stauber, R.H.; Freese, C.; Gül, D. IsoMAG—An Automated System for the Immunomagnetic Isolation of Squamous Cell Carcinoma-Derived Circulating Tumor Cells. *Diagnostics* **2021**, *11*, 2040. [CrossRef] [PubMed]
11. Yaron, J.R.; Ziegler, C.P.; Tran, T.H.; Glenn, H.L.; Meldrum, D.R. A convenient, optimized pipeline for isolation, fluorescence microscopy and molecular analysis of live single cells. *Biol. Proced. Online* **2014**, *16*, 9. [CrossRef] [PubMed]
12. Hespeler, D.; Knoth, D.; Keck, C.M.; Müller, R.H.; Pyo, S.M. smartPearls® for dermal bioavailability enhancement—Long-term stabilization of suspensions by viscoelasticity. *Int. J. Pharm.* **2019**, *562*, 293–302. [CrossRef] [PubMed]
13. Felderhof, B.U. Sedimentation of spheres at small Reynolds number. *J. Chem. Phys.* **2005**, *122*, 214905. [CrossRef] [PubMed]
14. Macías García, B.; Ortega Ferrusola, C.; Aparicio, I.M.; Miró-Morán, A.; Morillo Rodríguez, A.; Gallardo Bolaños, J.M.; González Fernández, L.; Balao da Silva, C.M.; Rodríguez Martínez, H.; Tapia, J.A.; et al. Toxicity of glycerol for the stallion spermatozoa: Effects on membrane integrity and cytoskeleton, lipid peroxidation and mitochondrial membrane potential. *Theriogenology* **2012**, *77*, 1280–1289. [CrossRef] [PubMed]
15. Andree, K.C.; van Dalum, G.; Terstappen, L.W.M.M. Challenges in circulating tumor cell detection by the CellSearch system. *Mol. Oncol.* **2016**, *10*, 395–407. [CrossRef] [PubMed]
16. Roth, S.; Hadass, O.; Cohen, M.; Verbarq, J.; Wilsey, J.; Danielli, A. Improving the Sensitivity of Fluorescence-Based Immunoassays by Photobleaching the Autofluorescence of Magnetic Beads. *Small* **2019**, *15*, e1803751. [CrossRef] [PubMed]
17. Ruiz-Rodríguez, A.J.; Molina-Vallejo, M.P.; Aznar-Peralta, I.; González Puga, C.; Cañas García, I.; González, E.; Lorente, J.A.; Serrano, M.J.; Garrido-Navas, M.C. Deep Phenotypic Characterisation of CTCs by Combination of Microfluidic Isolation (IsoFlux) and Imaging Flow Cytometry (ImageStream). *Cancers* **2021**, *13*, 6386. [CrossRef] [PubMed]
18. Horwitz, K.B.; Costlow, M.E.; McGuire, W.L. MCF-7: A human breast cancer cell line with estrogen, androgen, progesterone, and glucocorticoid receptors. *Steroids* **1975**, *26*, 785–795. [CrossRef]
19. Bacus, S.S.; Kiguchi, K.; Chin, D.; King, C.R.; Huberman, E. Differentiation of cultured human breast cancer cells (AU-565 and MCF-7) associated with loss of cell surface HER-2/neu antigen. *Mol. Carcinog.* **1990**, *3*, 350–362. [CrossRef] [PubMed]
20. Alix-Panabières, C.; Pantel, K. Liquid Biopsy: From Discovery to Clinical Application. *Cancer Discov.* **2021**, *11*, 858–873. [CrossRef] [PubMed]
21. Papadopoulou, E.; Tsoulos, N.; Tsantikidi, K.; Metaxa-Mariatou, V.; Stamou, P.E.; Kladi-Skandali, A.; Kapeni, E.; Tsaousis, G.; Penteroudakis, G.; Petrakis, D.; et al. Clinical feasibility of NGS liquid biopsy analysis in NSCLC patients. *PLoS ONE* **2019**, *14*, e0226853. [CrossRef] [PubMed]

5 References

1. Boyle, J. Molecular biology of the cell, 5th edition by B. Alberts, A. Johnson, J. Lewis, M. Raff, K. Roberts, and P. Walter. *Biochem. Mol. Biol. Educ.* **2008**, *36*, 317–318, doi:10.1002/bmb.20192.
2. Paget, S. The distribution of secondary growths in cancer of the breast. 1889. *Cancer Metastasis Rev.* **1989**, *8*, 98–101.
3. Fidler, I.J. The pathogenesis of cancer metastasis: the 'seed and soil' hypothesis revisited. *Nat. Rev. Cancer* **2003**, *3*, 453–458, doi:10.1038/nrc1098.
4. Christofori, G. New signals from the invasive front. *Nature* **2006**, *441*, 444–450, doi:10.1038/nature04872.
5. ROMSDAHL, M.M.; POTTER, J.F.; MALMGREN, R.A.; CHU, E.W.; BRINDLEY, C.O.; SMITH, R.R. A clinical study of circulating tumor cells in malignant melanoma. *Surg. Gynecol. Obstet.* **1960**, *111*, 675–681.
6. Wagener, C.; Müller, O. *Molekulare Onkologie*; Georg Thieme Verlag: Stuttgart, 2010, ISBN 9783131035134.
7. Joosse, S.A.; Gorges, T.M.; Pantel, K. Biology, detection, and clinical implications of circulating tumor cells. *EMBO Mol. Med.* **2014**, *7*, 1–11, doi:10.15252/emmm.201303698.
8. Qiu, B.; Wei, W.; Zhu, J.; Fu, G.; Lu, D. EMT induced by loss of LKB1 promotes migration and invasion of liver cancer cells through ZEB1-induced YAP signaling. *Oncol. Lett.* **2018**, *16*, 6465–6471, doi:10.3892/ol.2018.9445.
9. Etienne-Manneville, S. Polarity proteins in migration and invasion. *Oncogene* **2008**, *27*, 6970–6980, doi:10.1038/onc.2008.347.
10. HARTKOPF, A.D.; WAGNER, P.; WALLWIENER, D.; FEHM, T.; ROTHMUND, R. Changing Levels of Circulating Tumor Cells in Monitoring Chemotherapy Response in Patients with Metastatic Breast Cancer. *Anticancer Research* **2011**, *31*, 979–984.
11. Stott, S.L.; Lee, R.J.; Nagrath, S.; Yu, M.; Miyamoto, D.T.; Ulkus, L.; Inserra, E.J.; Ulman, M.; Springer, S.; Nakamura, Z.; et al. Isolation and Characterization of

- Circulating Tumor Cells from Patients with Localized and Metastatic Prostate Cancer. *Sci. Transl. Med.* **2010**, *2*, 25ra23, doi:10.1126/scitranslmed.3000403.
12. Castro-Giner, F.; Aceto, N. Tracking cancer progression: from circulating tumor cells to metastasis. *Genome Med* **2020**, *12*, 1–12, doi:10.1186/s13073-020-00728-3.
 13. Stewart, C.A.; Gay, C.M.; Xi, Y.; Sivajothi, S.; Sivakamasundari, V.; Fujimoto, J.; Bolisetty, M.; Hartsfield, P.M.; Balasubramanian, V.; Chalisehar, M.D.; et al. Single-cell analyses reveal increased intratumoral heterogeneity after the onset of therapy resistance in small-cell lung cancer. *Nat. Cancer* **2020**, *1*, 423–436, doi:10.1038/s43018-019-0020-z.
 14. Kim, M.-Y.; Oskarsson, T.; Acharyya, S.; Nguyen, D.X.; Zhang, X.H.-F.; Norton, L.; Massagué, J. Tumor self-seeding by circulating cancer cells. *Cell* **2009**, *139*, 1315–1326, doi:10.1016/j.cell.2009.11.025.
 15. Uhr, J.W.; Pantel, K. Controversies in clinical cancer dormancy. *Proc. Natl. Acad. Sci. U. S. A.* **2011**, *108*, 12396–12400, doi:10.1073/pnas.1106613108.
 16. Ilie, M.; Hofman, V.; Long-Mira, E.; Selva, E.; Vignaud, J.-M.; Padovani, B.; Mouroux, J.; Marquette, C.-H.; Hofman, P. “Sentinel” Circulating Tumor Cells Allow Early Diagnosis of Lung Cancer in Patients with Chronic Obstructive Pulmonary Disease. *PLoS One* **2014**, *9*, doi:10.1371/journal.pone.0111597.
 17. Nolé, F.; Munzone, E.; Zorzino, L.; Minchella, I.; Salvatici, M.; Botteri, E.; Medici, M.; Verri, E.; Adamoli, L.; Rotmensz, N.; et al. Variation of circulating tumor cell levels during treatment of metastatic breast cancer: prognostic and therapeutic implications. *Ann. Oncol.* **2008**, *19*, 891–897, doi:10.1093/annonc/mdm558.
 18. Ferlito, A.; Shaha, A.R.; Silver, C.E.; Rinaldo, A.; Mondin, V. Incidence and sites of distant metastases from head and neck cancer. *ORL J. Otorhinolaryngol. Relat. Spec.* **2001**, *63*, 202–207, doi:10.1159/000055740.
 19. Haddad, R.I.; Shin, D.M. Recent advances in head and neck cancer. *N. Engl. J. Med.* **2008**, *359*, 1143–1154, doi:10.1056/NEJMra0707975.
 20. Economopoulou, P.; Bree, R. de; Kotsantis, I.; Psyrris, A. Diagnostic Tumor Markers in Head and Neck Squamous Cell Carcinoma (HNSCC) in the Clinical Setting. *Front. Oncol.* **2019**, *9*, 827, doi:10.3389/fonc.2019.00827.
 21. Mahieu, R.; Maar, J.S. de; Nieuwenhuis, E.R.; Deckers, R.; Moonen, C.; Alic, L.; Haken, B. ten; Keizer, B. de; Bree, R. de. New Developments in Imaging for Sentinel Lymph

- Node Biopsy in Early-Stage Oral Cavity Squamous Cell Carcinoma. *Cancers (Basel)* **2020**, *12*, doi:10.3390/cancers12103055.
22. Siegel, R.; Naishadham, D.; Jemal, A. Cancer statistics, 2012. *CA Cancer J. Clin.* **2012**, *62*, 10–29, doi:10.3322/caac.20138.
23. Hu, Y.; Yu, X.; Xu, G.; Liu, S. Metastasis: an early event in cancer progression. *J. Cancer Res. Clin. Oncol.* **2017**, *143*, 745–757, doi:10.1007/s00432-016-2279-0.
24. Robert Koch Institute (ed.) and the Association of Population-based Cancer Registries in Germany. Cancer in Germany 2017/ 2018. Available online: https://www.krebsdaten.de/Krebs/EN/Content/Publications/Cancer_in_Germany/cancer_chapters_2017_2018/cancer_c50.pdf?__blob=publicationFile (accessed on 28 July 2022).
25. Zhang, Y.; Lv, Y.; Niu, Y.; Su, H.; Feng, A. Role of Circulating Tumor Cell (CTC) Monitoring in Evaluating Prognosis of Triple-Negative Breast Cancer Patients in China. *Med. Sci. Monit.* **2017**, *23*, 3071–3079, doi:10.12659/msm.902637.
26. Yadav, B.S.; Chanana, P.; Jhamb, S. Biomarkers in triple negative breast cancer: A review. *World J. Clin. Oncol.* **2015**, *6*, 252–263, doi:10.5306/wjco.v6.i6.252.
27. Gelmon, K.; Dent, R.; Mackey, J.R.; Laing, K.; McLeod, D.; Verma, S. Targeting triple-negative breast cancer: optimising therapeutic outcomes. *Ann. Oncol.* **2012**, *23*, 2223–2234, doi:10.1093/annonc/mds067.
28. Carkaci, S.; Macapinlac, H.A.; Cristofanilli, M.; Mawlawi, O.; Rohren, E.; Gonzalez Angulo, A.M.; Dawood, S.; Resetskova, E.; Le-Petross, H.T.; Yang, W.-T. Retrospective study of 18F-FDG PET/CT in the diagnosis of inflammatory breast cancer: preliminary data. *J. Nucl. Med.* **2009**, *50*, 231–238, doi:10.2967/jnumed.108.056010.
29. American College of Surgeons. Breast Cancer Staging. Available online: <https://www.facs.org/for-patients/home-skills-for-patients/breast-cancer-surgery/breast-cancer-types/breast-cancer-staging/> (accessed on 5 October 2022).
30. Gold, B.; Cankovic, M.; Furtado, L.V.; Meier, F.; Gocke, C.D. Do circulating tumor cells, exosomes, and circulating tumor nucleic acids have clinical utility? A report of the association for molecular pathology. *J. Mol. Diagn.* **2015**, *17*, 209–224, doi:10.1016/j.jmoldx.2015.02.001.
31. Santarpia, M.; Liguori, A.; D’Aveni, A.; Karachaliou, N.; Gonzalez-Cao, M.; Daffinà, M.G.; Lazzari, C.; Altavilla, G.; Rosell, R. Liquid biopsy for lung cancer early detection. *J. Thorac. Dis.* **2018**, *10*, S882–97, doi:10.21037/jtd.2018.03.81.

32. Huang, Z.; Chen, Y.; Hang, W.; Gao, Y.; Lin, L.; Li, D.Y.; Xing, J.; Yan, X. Holistic metabonomic profiling of urine affords potential early diagnosis for bladder and kidney cancers. *Metabolomics* **2013**, *9*, 119–129, doi:10.1007/s11306-012-0433-5.
33. Carrola, J.; Rocha, C.M.; Barros, A.S.; Gil, A.M.; Goodfellow, B.J.; Carreira, I.M.; Bernardo, J.; Gomes, A.; Sousa, V.; Carvalho, L.; et al. Metabolic signatures of lung cancer in biofluids: NMR-based metabonomics of urine. *J. Proteome Res.* **2011**, *10*, 221–230, doi:10.1021/pr100899x.
34. Sack, U. *Zelluläre Diagnostik und Therapie*; De Gruyter, 2015, ISBN 9783110344066.
35. Zhang, X.; Yuan, X.; Shi, H.; Wu, L.; Qian, H.; Xu, W. Exosomes in cancer: small particle, big player. *J. Hematol. Oncol.* **2015**, *8*, 83, doi:10.1186/s13045-015-0181-x.
36. Cazzoli, R.; Buttitta, F.; Di Nicola, M.; Malatesta, S.; Marchetti, A.; Pass, H.I. MicroRNAs derived from circulating exosomes as non-invasive biomarkers for screening and diagnose lung cancer. *J. Thorac. Oncol.* **2013**, *8*, 1156–1162, doi:10.1097/JTO.0b013e318299ac32.
37. Yakimchuk, K. Exosomes: isolation methods and specific markers. *MATER METHODS* **2015**, *5*, doi:10.13070/mm.en.5.1450.
38. Leon, S.A.; Shapiro, B.; Sklaroff, D.M.; Yaros, M.J. Free DNA in the serum of cancer patients and the effect of therapy. *Cancer Res.* **1977**, *37*, 646–650.
39. Siravegna, G.; Marsoni, S.; Siena, S.; Bardelli, A. Integrating liquid biopsies into the management of cancer. *Nat. Rev. Clin. Oncol.* **2017**, *14*, 531–548, doi:10.1038/nrclinonc.2017.14.
40. Dahl, E.; Jung, A.; Fassunke, J.; Hummel, M.; Penzel, R.; Dietmaier, W.; Laßmann, S. Chancen und Risiken der blutbasierten molekularpathologischen Analytik zirkulierender Tumorzellen (CTC) und zellfreier DNA (cfDNA) in der personalisierten Krebstherapie: Eine Stellungnahme des Arbeitskreises "Liquid Biopsy" der AG Molekularpathologie in der Deutschen Gesellschaft für Pathologie (DGP). *Pathologe* **2015**, *36*, 92–97, doi:10.1007/s00292-014-2069-x.
41. Fernandez-Cuesta, L.; Perdomo, S.; Avogbe, P.H.; Leblay, N.; Delhomme, T.M.; Gaborieau, V.; Abedi-Ardekani, B.; Chanudet, E.; Olivier, M.; Zaridze, D.; et al. Identification of Circulating Tumor DNA for the Early Detection of Small-cell Lung Cancer. *EBioMedicine* **2016**, *10*, 117–123, doi:10.1016/j.ebiom.2016.06.032.

42. Fontanilles, M.; Duran-Peña, A.; Idbaih, A. Liquid Biopsy in Primary Brain Tumors: Looking for Stardust! *Curr. Neurol. Neurosci. Rep.* **2018**, *18*, 13, doi:10.1007/s11910-018-0820-z.
43. Negishi, R.; Yamakawa, H.; Kobayashi, T.; Horikawa, M.; Shimoyama, T.; Koizumi, F.; Sawada, T.; Oboki, K.; Omuro, Y.; Funasaka, C.; et al. Transcriptomic profiling of single circulating tumor cells provides insight into human metastatic gastric cancer. *Commun Biol*, *5*, 1–12, doi:10.1038/s42003-021-02937-x.
44. Millner, L.M.; Linder, M.W.; Valdes, R. Circulating Tumor Cells: A Review of Present Methods and the Need to Identify Heterogeneous Phenotypes. *Ann. Clin. Lab. Sci.* **2013**, *43*, 295–304.
45. Alix-Panabières, C.; Pantel, K. Circulating tumor cells: liquid biopsy of cancer. *Clin. Chem.* **2013**, *59*, 110–118, doi:10.1373/clinchem.2012.194258.
46. Harouaka, R.A.; Nisic, M.; Zheng, S.-Y. Circulating tumor cell enrichment based on physical properties. *J. Lab. Autom.* **2013**, *18*, 455–468, doi:10.1177/2211068213494391.
47. Alix-Panabières, C.; Pantel, K. Challenges in circulating tumour cell research. *Nat Rev Cancer* **2014**, *14*, 623–631, doi:10.1038/nrc3820.
48. Litvinov, S.V.; Velders, M.P.; Bakker, H.A.; Fleuren, G.J.; Warnaar, S.O. Ep-CAM: a human epithelial antigen is a homophilic cell-cell adhesion molecule. *J. Cell Biol.* **1994**, *125*, 437–446, doi:10.1083/jcb.125.2.437.
49. Armstrong, A.; Eck, S.L. EpCAM: A new therapeutic target for an old cancer antigen. *Cancer Biol. Ther.* **2003**, *2*, 320–326, doi:10.4161/cbt.2.4.451.
50. Yap, T.A.; Lorente, D.; Omlin, A.; Olmos, D.; Bono, J.S. de. Circulating tumor cells: a multifunctional biomarker. *Clin. Cancer Res.* **2014**, *20*, 2553–2568, doi:10.1158/1078-0432.CCR-13-2664.
51. Pecot, C.V.; Bischoff, F.Z.; Mayer, J.A.; Wong, K.L.; Pham, T.; Bottsford-Miller, J.; Stone, R.L.; Lin, Y.G.; Jaladurgam, P.; Roh, J.W.; et al. A novel platform for detection of CK+ and CK– CTCs. *Cancer Discov.* **2011**, *1*, 580–586, doi:10.1158/2159-8290.CD-11-0215.
52. Esmailsabzali, H.; Beischlag, T.V.; Cox, M.E.; Parameswaran, A.M.; Park, E.J. Detection and isolation of circulating tumor cells: principles and methods. *Biotechnol. Adv.* **2013**, *31*, 1063–1084, doi:10.1016/j.biotechadv.2013.08.016.

53. Illumina Inc. Illumina @ a Glance Fact Sheet. Available online: <https://www.illumina.com/content/dam/illumina-marketing/documents/company/illumina-at-a-glance.pdf> (accessed on 6 October 2022).
54. The Scientist. 2020 Top 10 Innovations. Available online: <https://www.the-scientist.com/features/2020-top-10-innovations-68176> (accessed on 6 October 2022).
55. Burklund, A.; Tadimety, A.; Nie, Y.; Hao, N.; Zhang, J.X.J. Advances in diagnostic microfluidics. *Adv. Clin. Chem.* **2020**, *95*, 1–72, doi:10.1016/bs.acc.2019.08.001.
56. Fisher, R.; Pusztai, L.; Swanton, C. Cancer heterogeneity: implications for targeted therapeutics. *Br. J. Cancer* **2013**, *108*, 479–485, doi:10.1038/bjc.2012.581.
57. Andree, K.C.; van Dalum, G.; Terstappen, L.W.M.M. Challenges in circulating tumor cell detection by the CellSearch system. *Mol. Oncol.* **2016**, *10*, 395–407, doi:10.1016/j.molonc.2015.12.002.
58. Hong, X.; Roh, W.; Sullivan, R.J.; Wong, K.H.K.; Wittner, B.S.; Guo, H.; Dubash, T.D.; Sade-Feldman, M.; Wesley, B.; Horwitz, E.; et al. The lipogenic regulator SREBF2 induces Transferrin in circulating melanoma cells and suppresses ferroptosis. *Cancer Discov.* **2020**, *11*, 678–695, doi:10.1158/2159-8290.CD-19-1500.
59. Xiao, Z.; Dai, Z.; Locasale, J.W. Metabolic landscape of the tumor microenvironment at single cell resolution. *Nat. Commun.* **2019**, *10*, doi:10.1038/s41467-019-11738-0.
60. Gribko, A.; Stiefel, J.; Liebetanz, L.; Nagel, S.M.; Künzel, J.; Wandrey, M.; Hagemann, J.; Stauber, R.H.; Freese, C.; Gül, D. IsoMAG-An Automated System for the Immunomagnetic Isolation of Squamous Cell Carcinoma-Derived Circulating Tumor Cells. *Diagnostics (Basel)* **2021**, *11*, doi:10.3390/diagnostics11112040.
61. Allelein, S.; Aerchlimann, K.; Rösch, G.; Khajehamiri, R.; Kölsch, A.; Freese, C.; Kuhlmeier, D. Prostate-Specific Membrane Antigen (PSMA)-Positive Extracellular Vesicles in Urine-A Potential Liquid Biopsy Strategy for Prostate Cancer Diagnosis? *Cancers (Basel)* **2022**, *14*, doi:10.3390/cancers14122987.
62. Ruan, H.; Zhou, Y.; Shen, J.; Zhai, Y.; Xu, Y.; Pi, L.; Huang, R.; Chen, K.; Li, X.; Ma, W.; et al. Circulating tumor cell characterization of lung cancer brain metastases in the cerebrospinal fluid through single-cell transcriptome analysis. *Clin. Transl. Med.* **2020**, *10*, doi:10.1002/ctm2.246.
63. Gynecological Oncology AGO-Mamma of the German Cancer Society. Guidelines/Recommendations: Prognostic and Predictive Factors. Available online: <https://www.ago-online.de/fileadmin/ago->

- online/downloads/_leitlinien/kommission_mamma/2022/englisch/Einzeldateien/AGO_2022E_05_Prognostic_and_predictive_faktors.pdf.
64. Yu, M.; Bardia, A.; Wittner, B.S.; Stott, S.L.; Smas, M.E.; Ting, D.T.; Isakoff, S.J.; Ciciliano, J.C.; Wells, M.N.; Shah, A.M.; et al. Circulating breast tumor cells exhibit dynamic changes in epithelial and mesenchymal composition. *Science* **2013**, *339*, 580–584, doi:10.1126/science.1228522.
 65. Wong, C.H.; Siah, K.W.; Lo, A.W. Estimation of clinical trial success rates and related parameters. *Biostatistics (Oxford, England)* **2019**, *20*, 273, doi:10.1093/biostatistics/kxx069.
 66. U.S. Food and Drug Administration. FDA approves first PI3K inhibitor for breast cancer. Available online: <https://www.fda.gov/news-events/press-announcements/fda-approves-first-pi3k-inhibitor-breast-cancer> (accessed on 7 October 2022).
 67. Zañudo, J.G.T.; Mao, P.; Alcon, C.; Kowalski, K.; Johnson, G.N.; Xu, G.; Baselga, J.; Scaltriti, M.; Letai, A.; Montero, J.; et al. Cell line-specific network models of ER+ breast cancer identify potential PI3K α inhibitor resistance mechanisms and drug combinations. *Cancer Res.* **2021**, *81*, 4603, doi:10.1158/0008-5472.CAN-21-1208.
 68. Anderle, N.; Koch, A.; Gierke, B.; Keller, A.-L.; Staebler, A.; Hartkopf, A.; Brucker, S.Y.; Pawlak, M.; Schenke-Layland, K.; Schmees, C. A Platform of Patient-Derived Microtumors Identifies Individual Treatment Responses and Therapeutic Vulnerabilities in Ovarian Cancer. *Cancers (Basel)* **2022**, *14*, doi:10.3390/cancers14122895.
 69. Vlachogiannis, G.; Hedayat, S.; Vatsiou, A.; Jamin, Y.; Fernández-Mateos, J.; Khan, K.; Lampis, A.; Eason, K.; Huntingford, I.; Burke, R.; et al. Patient-derived organoids model treatment response of metastatic gastrointestinal cancers. *Science* **2018**, *359*, 920–926, doi:10.1126/science.aao2774.
 70. The Scientist. Tumor Organoids Predict How Well Patients Respond to Cancer Drugs. Available online: <https://www.the-scientist.com/news-opinion/tumor-organoids-predict-how-well-patients-respond-to-cancer-drugs-30086> (accessed on 7 October 2022).
 71. Statista. Leading 10 therapeutic areas worldwide by sales in 2019. Available online: <https://www.statista.com/statistics/407971/projected-revenue-of-top-therapeutic-areas-worldwide/> (accessed on 14 October 2022).
 72. U.S. Food and Drug Administration. FDA CASE STUDY: DRUG APPROVAL—BRINGING A NEW DRUG TO THE MARKET. Available online: <https://www.fda.gov/media/94428/download> (accessed on 18 October 2022).

73. BioProcess International. Oncology Companion Diagnostics Market Will Approach US\$414 million by 2023 **2017**, 15.
74. Grand View Research Inc. Circulating Tumor Cells Market Size, Share & Trends Analysis Report By Technology, By Application (Clinical, Research), By Product, By Specimen (Bone Marrow, Blood), By Region, And Segment Forecasts, 2021 - 2027: (Healthcare). Report ID: 978-1-68038-287-7.
75. Maharjan, N.; Thapa, N.; Tu, J. Blood-based Biomarkers for Early Diagnosis of Lung Cancer: A Review Article. *JNMA J. Nepal Med. Assoc.* **2020**, *58*, 519–524, doi:10.31729/jnma.5023.
76. Vermorken, J.B.; Specenier, P. Optimal treatment for recurrent/metastatic head and neck cancer. *Ann. Oncol.* **2010**, *21 Suppl 7*, vii252-61, doi:10.1093/annonc/mdq453.
77. Mohanti, B.K.; Nachiappan, P.; Pandey, R.M.; Sharma, A.; Bahadur, S.; Thakar, A. Analysis of 2167 head and neck cancer patients' management, treatment compliance and outcomes from a regional cancer centre, Delhi, India. *J. Laryngol. Otol.* **2007**, *121*, 49–56, doi:10.1017/S0022215106002751.
78. Grisanti, S.; Almici, C.; Consoli, F.; Buglione, M.; Verardi, R.; Bolzoni-Villaret, A.; Bianchetti, A.; Ciccarese, C.; Mangoni, M.; Ferrari, L.; et al. Circulating tumor cells in patients with recurrent or metastatic head and neck carcinoma: prognostic and predictive significance. *PLoS One* **2014**, *9*, e103918, doi:10.1371/journal.pone.0103918.
79. Polesel, J.; Furlan, C.; Birri, S.; Giacomarra, V.; Vaccher, E.; Grando, G.; Gobitti, C.; Navarria, F.; Schioppa, O.; Minatel, E.; et al. The impact of time to treatment initiation on survival from head and neck cancer in north-eastern Italy. *Oral Oncol.* **2017**, *67*, 175–182, doi:10.1016/j.oraloncology.2017.02.009.
80. Scheuermann, S.; Schäfer, A.; Langejürgen, J.; Reis, C. A step towards enzyme-free tissue dissociation. *Current Directions in Biomedical Engineering* **2019**, *5*, 545–548, doi:10.1515/cdbme-2019-0137.
81. Fleßa, S.; Aichinger, H.; Bratan, T. Innovationsmanagement diagnostischer Geräte am Beispiel der Detektion zirkulierender Tumorzellen. *Gesundheitsökonomie & Qualitätsmanagement* **2021**, *26*, 30–39, doi:10.1055/a-1139-6968.
82. Harbeck, N.; Penault-Llorca, F.; Cortes, J.; Gnant, M.; Houssami, N.; Poortmans, P.; Ruddy, K.; Tsang, J.; Cardoso, F. Breast cancer. *Nat. Rev. Dis. Primers* **2019**, *5*, 66, doi:10.1038/s41572-019-0111-2.

83. Breast Cancer Center, University Hospital Basel. Digoxin Induced Dissolution of CTC Clusters. ClinicalTrials.gov Identifier: NCT03928210. Available online: <https://clinicaltrials.gov/ct2/show/NCT03928210> (accessed on 18 October 2022).
84. Schuster, E.; Taftaf, R.; Reduzzi, C.; Albert, M.K.; Romero-Calvo, I.; Liu, H. Better together: circulating tumor cell clustering in metastatic cancer. *Trends Cancer* **2021**, *7*, 1020–1032, doi:10.1016/j.trecan.2021.07.001.
85. Garcia-Villa, A.; Balasubramanian, P.; Miller, B.L.; Lustberg, M.B.; Ramaswamy, B.; Chalmers, J.J. Assessment of γ -H2AX levels in circulating tumor cells from patients receiving chemotherapy. *Front. Oncol.* **2012**, *2*, 128, doi:10.3389/fonc.2012.00128.
86. Keup, C.; Suryaprakash, V.; Hauch, S.; Storbeck, M.; Hahn, P.; Sprenger-Haussels, M.; Kolberg, H.-C.; Tewes, M.; Hoffmann, O.; Kimmig, R.; et al. Integrative statistical analyses of multiple liquid biopsy analytes in metastatic breast cancer. *Genome Med* **2021**, *13*, 1–14, doi:10.1186/s13073-021-00902-1.

6 Curriculum Vitae

